THESIS

TOWARDS IMPROVED UNDERSTANDING AND OPTIMIZATION OF THE INTERNAL HYDRAULICS OF CHLORINE CONTACT TANKS

Submitted by

Zachary H Taylor

Department of Civil and Environmental Engineering

In partial fulfillment of the requirements

For the Degree of Master of Science

Colorado State University

Fort Collins, Colorado

Spring 2012

Master's Committee:

Advisor: S. Karan Venayagamoorthy

Brian Bledsoe
Ellen Wohl

ABSTRACT

TOWARDS IMPROVED UNDERSTANDING AND OPTIMIZATION OF THE INTERNAL HYDRAULICS OF CHLORINE CONTACT TANKS

The research presented in this thesis focuses on utilizing computational fluid dynamics (CFD) to further the understanding of the internal flow dynamics in chlorine contact tanks. In particular, we aim to address the following two critical questions: (1) for a given footprint of a serpentine chlorine contact tank with a fixed inlet configuration, how does the hydraulic efficiency of the tank depend on the configuration of internal baffles?, and (2) for water storage tanks modified for use as chlorine contact tanks, can inlet conditions be modified such that near plug flow conditions are induced close to the inlet and throughout the rest of the tank? Key design parameters were identified and parametrically tested for each of these design problems.

For the serpentine baffle tanks, a benchmark contact tank geometry based on a scaled model of the Embsay chlorine contact tank in Yorkshire, England was used for validation and then subsequently modified by varying both the number and length of baffles. In order to define guidelines for hydraulically efficient baffle tanks, a parametric study consisting of forty high-resolution 3-D simulations of different tank configurations were performed to quantify the efficiency of the scaled contact tank as a function of the dimensional relationships between the inlet width, channel width, tank width, tank length, and baffle opening lengths. The simulations tested the hydraulic efficiencies of the different tank configurations. Hydraulic efficiency was quantified by the baffle factor (*BF*). We found that the most efficient tank had a *BF* of 0.71, and that hydraulic

efficiency was optimized in this tank by maximizing the length to width ratio in baffle chambers and by minimizing flow separation through the tank, which was achieved by setting equal dimensions to the inlet width, channel width, and baffle opening length. A new contact tank geometry was then developed by applying the dimensional relationships that were shown by the parametric study to optimize *BF*, and by modifying the baffle geometries to minimize flow separation around baffle tips. The new contact tank design had a *BF* of 0.78, which represents a 10% improvement in hydraulic efficiency compared to the Embsay contact tank.

In the study of inlet modifications for cylindrical storage tanks, inlet diffusers and inlet manifolds were developed and modeled. Experimental flow through curves (FTCs) of a benchmark storage tank used as a contact tank were used to validate the CFD model that was utilized in the study. Thirty-seven modified inlet configurations using two representative flow rates were modeled. The inlet manifolds improved *BF* significantly, whereas the inlet diffuser had insignificant effects. The key design parameters identified for the inlet manifold were the number of inlets and the height of the inlet(s) in the tank. The inlet manifold designed with 16 inlets with the inlet height set at 10 percent of the tank height improved the *BF* of the storage tank from 0.16 to 0.51. This 220 percent increase in *BF* represents a major improvement in hydraulic efficiency for such cylindrical contact tanks that are widely used by small water treatment systems.

ACKNOWLEDGEMENTS

I want to thank my family and especially my parents, Ted and Gretchen Taylor, for their encouragement and support of my education. This thesis represents a major milestone in my formal education, and would not have been possible without their help. Tremendous credit also goes to my fiancée, Maryam Kling, whose enthusiasm for challenges encouraged me to attend graduate school and whose support and understanding carried me through its trials.

I would like to deeply express my gratitude to my advisor, Dr. Karan Venayagamoorthy, for his guidance during my graduate studies and research. His enthusiasm for teaching and pushing the envelope of our understanding of the world inspired me to study fluid mechanics. I would also like to acknowledge my committee members, Dr. Brian Bledsoe and Dr. Ellen Wohl, for their support.

I would like to thank Jordan Wilson and Qing Xu, whose research of the problem of disinfection efficiency provided the foundation upon which my research was built. I would also like to thank my research group, Simon Schaad, Ben Mater, Cole Davis, Fahrid Karimpur, Hyeyun Ku, and Taylor Barnett, for their technical and moral support during the writing of this thesis.

Finally, I would like to acknowledge the Colorado Department of Public Health and Environment (CDPHE) Water Quality Division, USA (Program Engineers: Tyson Ingles, Melanie Criswell, and Gordon Whittaker) for their support of this project.

TABLE OF CONTENTS

CHAPTER 1. INTRODUCTION

1.1 Background

In the United States, water quality regulations are developed and administered by the United States Environmental Protection Agency (US EPA). In most states, the regulations set by the US EPA are enforced by state regulatory agencies that have been given primacy by the US EPA (US EPA, 1998). In the state of Colorado, the Colorado Department of Public Health and Environment (CDPHE) has primacy to enforce US EPA regulations.

CDPHE regulates water treatment with regards to microbiological contaminants according to the regulations set in the Long Term 1 Enhanced Surface Water Treatment Rule (LT1ESWTR) *Disinfection Profiling and Disinfection Technical Guidance Manual* (US EPA, 2003). These regulations set minimum levels of disinfection according to the *CT* methodology where the product of *CT* must meet a minimum level and where *C* represents disinfectant concentration, and *T* represents contact time between contaminants and disinfectants (Davis and Cornwell, 2008). *T* can be increased through the use of contact tanks, which have a theoretical detention time (*TDT*) of *V/Q*, where *V* is the tank volume and *Q* is the flow rate. The *TDT* calculation assumes plug flow, where there is no flow separation and every water particle or contaminant passing through the tank is in the tank for the same amount of time.

Short circuiting and dead zones in contact tanks cause non-uniform contact times. In order to ensure that contaminants are disinfected before entering the water distribution system, the characteristic contact time used in calculations to determine the appropriate disinfectant concentration is set as T_{10}, which is the time it takes for 10% of a given

concentration released at the inlet of the contact tank to reach the outlet. Hydraulic efficiency is commonly quantified by baffle factor (*BF*), which is calculated as T_{10}/TDT. The purpose of the research done in this thesis was to develop design methods to maximize T_{10} in a given contact tank by attempting to eliminate short circuiting and dead zones. The research was done, in part, to satisfy sections of the third and fourth phases of a four phase project for the Water Quality Division of CDPHE.

The first and second phases of the CDPHE project involved validating computational fluid dynamics (CFD) techniques for modeling contact tanks and proposing several pre-engineered contact tank designs for use by small water treatment systems in Colorado. The third phase of the project involved the actual design as well as physical and CFD modeling of pre-engineered contact tanks. The fourth phase of the project is ongoing, and entails using CFD models to develop modifications that can be cheaply implemented to increase T_{10} in existing contact tanks.

The first phase of the project was primarily completed by Qing Xu for her Master's thesis titled *Internal Hydraulics of Baffled Disinfection Contact Tanks Using Computational Fluid Dynamics*. The second phase and the first half of the third phase of the project were completed by Jordan Wilson in his Master's thesis titled *Evaluation of Flow and Scalar Transport Characteristics of Small Public Water Disinfection Systems Using Computational Fluid Dynamics*. The completion of the remainder of the third phase and the beginning of the fourth phase are represented by the work presented in this thesis.

1.2 Objectives

The main objective of this thesis is to determine the design parameters of chlorine contact tanks that will optimize disinfection efficiency. Plug flow, where longitudinal velocity profiles are relatively uniform, represents the ideal flow condition for disinfection. Two categories of contact tanks will be evaluated. First, serpentine contact tanks, whose hydraulic efficiency is primarily controlled by inlet conditions, length to width ratios of baffle chambers, and baffle configurations, were analyzed using a parametric study designed to isolate the effects of baffle and inlet configurations. Second, modified storage tanks, whose hydraulic efficiency is controlled by the length to width ratio of the tank and the inlet and outlet configurations, were analyzed using a parametric study of inlet configurations that are designed to induce near plug flow as close as possible to the inlet location. All modeling associated with this study was performed using 3-D CFD techniques that were validated with physical models.

1.3 New Contributions

The significant new research contributions presented in this thesis include:

- The development of guidelines for serpentine contact tank design that optimize hydraulic efficiency utilizing dimensional relationships between inlet width, channel width, tank length, baffle opening length, and number of baffles in a tank built on a fixed footprint.
- A new design for a serpentine baffle tank utilizing a standard footprint and inlet conditions that, in addition to following the design guidelines presented in this thesis, introduces a new baffle geometry that minimizes flow separation around baffle tips and increases *BF* by 10%.

- Findings that indicate that in vertical storage tanks with inlet manifolds designed with appropriate horizontal spacing and inlet height, *BF* is linearly related to the inlet area for tanks designed with practical numbers and sizes of inlets.
- The design of an inlet manifold that was shown to increase *BF* in a modified storage tank by 220%. This inlet manifold induced flow patterns in the modified storage tank that were 81% as hydraulically efficient as the flow patterns modeled in an idealized tank with the physically impossible condition of a perfectly uniform inlet velocity across the direction of flow in the tank.

1.4 Research Publications

Chapter 3 of this thesis contains portions of a paper by Taylor *et al.* titled *Hydraulic Efficiency of Baffled Disinfection Contact Tanks* that has been submitted to the ASCE *Journal of Environmental Engineering*.

The research presented in Chapter 4 is being prepared for submission to the ASCE *Journal of Hydraulic Engineering*.

An abstract and paper titled, *Computational Modeling of Baffle Disinfection Tanks*, has been accepted and will be presented at the Environmental Water Resources Institute (EWRI) World Environmental and Water Resources Congress, May 20-24, 2012.

1.5 Organization of Work

Chapter 2 provides a literature review of current water treatment disinfection protocols in the United States and explains the CFD techniques used in the modeling of the contact tanks in this thesis. The discussion of the disinfection protocols includes an explanation of the chlorination process and a description of the different categories of

disinfection contact tanks. The CFD techniques introduced include CFD methods, turbulence models, wall treatments, and commercial CFD software.

Chapter 3 presents a parametric study of serpentine baffle tank configurations with variable numbers of baffles and variable baffle opening lengths. Chapter 4 describes an analysis of modified inlet configurations for storage tanks used as chlorine contact tanks. An inlet manifold that is shown to increase efficiency by over 200% is introduced. Chapter 5 provides recommendations for further research and presents the conclusions of the work presented. Appendix I shows the user-defined function for diffusivity used by the FLUENT models.

CHAPTER 2. LITERATURE REVIEW

2.1 Water Treatment

In the United States, water treatment systems are designed to control physical, chemical, microbiological, and radiological characteristics of water. Physical characteristics include temperature, color, turbidity, taste, and odor, and often are related to the appearance of water. Chemical characteristics are related to the hardness and softness of water. Radiological substances can be found in water whose source has been contaminated by radiological substances. Microbiological contaminants in water are largely responsible for water-borne illness in the United States and around the world (Davis and Cornwell, 2008). The focus of this thesis is on the deactivation of microbiological contaminants from drinking water.

The United States Environmental Protection Agency (US EPA) sets standards for naturally-occurring and man-made contaminants in drinking water provided by public water systems as authorized by the Safe Drinking Water Act (SDWA) of 1974 (US EPA, 2004). US EPA enforces the removal of primary contaminants through the National Primary Drinking Water Regulations (NPDWR), which list contaminants and their maximum contaminant level (MCL) (US EPA, 2009). The two primary microbiological contaminants listed in the NPDWR are giardia and cryptosporidium (US EPA, 2009). Between 1980 and 1996, there were over 430,000 cases of waterborne illness caused by these contaminants (Davis and Cornwell, 2008).

The US EPA sets standards for contaminant levels in water, but primary enforcement of the standards can be assumed by states or Indian Tribes if they meet certain requirements (US EPA, 1998). When a state or Indian Tribe desires to enforce

the water quality standards set by the EPA and they meet the requirements of the EPA, they are given primacy. Wyoming and the District of Columbia are the only places in the United States without primacy. In these two locations, water quality regulations are enforced directly by the EPA.

The research in this thesis was done in part for the Colorado Department of Public Health and Environment (CDPHE), which has primacy in the state of Colorado. CDPHE regulates the contaminant levels in water supplied by public water systems in Colorado according to the Colorado Primary Drinking Water Regulations (CPDWR), which meet or surpass the NPDWR regulations in terms of MCL. Disinfection of water is accomplished through the removal of cysts, viruses, and bacteria, and chlorination is a common method of disinfection.

2.1.1 Chlorination

Chlorination is the most common form of disinfection used in the United States (Davis and Cornwell, 2008). There are many different ways water can be chlorinated, but for the purposes of the work in this thesis, the methodology of the *CT* concept will suffice to describe the basic way in which all chlorination processes disinfect water. Through a process which is still not completely understood, when chlorine in solution comes in contact with microbial contaminants, it kills them over time. The rate of this process is dependent on the concentration of chlorine, the pH of the water, and the temperature of the water. The *CT* concept describes the level of inactivation of contaminants that can be achieved when a certain disinfectant concentration (*C*) is in contact with contaminants for a given length of time (*T*). *CT* represents the product of disinfectant concentration and contact time and indicates the level of inactivation

achieved in water treatment. The empirical equation for *CT* (Davis and Cornwell, 2008) is given as

$$CT = 0.9847C^{0.1758}pH^{2.7519}temp^{-0.1467}, \quad (1)$$

where C = disinfection concentration, T = contact time, pH = pH of the water being treated, and *temp* = temperature of the water being treated (°*C*).

Water system operators use tables developed by the EPA (using Eq. (1) and safety factors) to determine the *CT* required for the water source being treated (Davis and Cornwell, 2008). Tables for *CT* at different log-inactivation levels, pH values, and temperatures can be found in the LT1ESWTR *Disinfection Profiling and Disinfection Technical Guidance Manual*. Log-inactivation level is a measure of the reduction in contaminant levels achieved in disinfection, and is calculated as

$$Log\ inactivation\ level = log\left(\frac{influent\ concentration}{effluent\ concentration}\right). \quad (2)$$

A common requirement for inactivation is 4-log, which requires that 99.99% of contaminants be removed (Davis and Cornwell, 2008). *CT* measured in a water system must be greater than the *CT* required by the EPA by at least the number of log-inactivations required. The measured *CT* is the product of the measured disinfectant concentration and the characteristic contact time of the contact tank. The characteristic contact time, T_{10}, is the amount of time it takes for the first 10% of a concentration of disinfectant released at the tank inlet to reach the tank outlet. Contact tanks are used at the end of water systems to increase the level of inactivation of contaminants by increasing the amount of time contaminants are in contact with disinfectants before entering the distribution system.

2.1.2 Contact Tanks

The purpose of contact tanks is to maximize the contact time of disinfection so that high levels of disinfection can occur at low disinfectant concentrations. Ideal contact tanks cause plug flow, where every particle of water traveling through the tank spends the same amount of time in the tank. Theoretical detention time (*TDT*) represents the contact time of a tank with plug flow conditions. *TDT* is calculated as the ratio of the tank volume to the flow rate. The hydraulic efficiency of contact tanks is quantified by baffle factor (*BF*), which is calculated as T_{10}/TDT (US EPA, 2003). If two tanks have identical *TDT*, but one tank has a higher *BF*, the tank with higher *BF* will require a lower chlorine dose for the same level of disinfection. High *BF* is desirable because water systems that use lower chlorine doses and still meet required inactivation levels reduce their expenditures on chlorine and reduce the production of disinfection by products (DBPs). DBPs are regulated as primary contaminants by the EPA (US EPA, 1999).

*BF*s of contact tanks are assessed in several manners. The most thorough and costly method involves full-scale tracer studies on existing tanks. Small water systems often cannot afford to perform tracer studies and instead use empirical relationships to estimate *BF* based on tank characteristics. *BF*s that are assigned to tanks solely based on tank characteristics according to LT1ESWTR are shown in Table 1. Although the table provides fairly detailed descriptions of the baffling in the tank, assigning a *BF* without performing tracer studies or CFD modeling involves a high error margin and can often lead to over-disinfection and high DBP risk.

Table 1. Baffling classification according to US EPA (2003)

Baffling Condition	T_{10}/T	Baffling Description
Unbaffled (mixed flow)	0.1	None, agitated basin, very low length to width ratio, high inlet and outlet flow velocities.
Poor	0.3	Single or multiple unbaffled inlets and outlets, no intra-basin baffles.
Average	0.5	Baffled inlet or outlet with some intra-basin baffles.
Superior	0.7	Perforated inlet baffle, serpentine or perforated intra-basin baffles, outlet weir or perforated launders.
Perfect (plug flow)	1.0	Very high length to width ratio (pipeline flow), perforated inlet, outlet, and intra-basin baffles.

The most recently developed method for determining the *BF* in contact tanks utilizes CFD. CFD tracer (scalar transport) studies can be used to estimate *BF* as long as proper validation is done. Shiono *et al.* (1991) performed physical tracer studies of a laboratory scale model of the Embsay chlorine contact tank in Yorkshire, England. The data from this study were used by Wang and Falconer (1998a), to validate the use of several turbulence closure schemes, and numerical methods to predict the 2-D velocity field in CFD models of the laboratory scale model. A similar study (Wang and Falconer 1998b) used the same methods to validate the use of CFD in predicting the scalar transport in a depth-averaged formulation (2-D) of the Embsay laboratory scale model.

The first validation of 3-D CFD modeling of baffled contact tanks was achieved by Khan *et al.* (2006). Their 3-D CFD model was computed using STAR-CD, which solved the Reynolds-averaged Navier-Stokes (RANS) equations and used the standard κ-ε turbulence closure model. They used a structured 3-D mesh and validated their model with a flow-through curve (FTC) and velocity profiles in several sections of the Embsay model tank.

3-D CFD models of contact tanks are advantageous because they give the user access to the 3-D velocity and other relevant flow fields, along with detailed information

about the transient scalar transport occurring in the tank. Physical tracer studies often only show the disinfectant concentration at the outlet, whereas CFD models can provide information about disinfectant concentrations at any position in the tank at any given time. This information is valuable in identifying areas in the tank in which the disinfectant is being inefficiently transported.

Until recently, CFD models of baffle tanks were un-validated and/or too computationally expensive for use with contact tanks. Advances in computer power and commercial CFD software, such as FLUENT, FLOW3D, and COMSOL, have made it feasible to model contact tanks, and to evaluate the effects of baffle modifications on the *BF* of contact tanks. Recent studies evaluating the effects of contact tank modifications have primarily considered three types of contact tanks: serpentine baffle tanks, pipe loops, and modified storage tanks.

2.1.2.1 Serpentine Contact Tanks

Serpentine contact tanks are generally used by large water systems. They are often constructed of concrete and have a plan form similar to the one modeled by Shiono *et al.* (1991), which is depicted in Figure 1. Khan *et al.* (2006) provided the first thorough validation of a commercial CFD code to solve the internal hydraulics and scalar transport in a contact tank using a 3-D RANS CFD model. Many recent studies have aimed to improve the *BF*s of serpentine contact tanks by using CFD models that are validated by tracer studies of existing tanks. These studies have shown dimensional relationships that influence the efficiency of the baffle tank. The key dimensional parameters that control hydraulic efficiency in serpentine contact tanks are: inlet width

(W_{inlet}), channel width (W_{ch}), baffle opening length (L_{bo}), and tank length (L_T), and tank width (W_T).

The work presented in Chapter 3 of this thesis illustrates the parametric study we performed to determine how the relationships of W_{inlet}/W_{ch}, W_{inlet}/L_{bo}, W_{ch}/L_{bo}, L_{bo}/L_T, and L_T/W_{ch} affect the hydraulic efficiency in serpentine baffle tanks. The studies we present in this literature review illustrate the CFD studies performed to define dimensional relationships that can be followed to optimize *BF* in baffled tanks. These studies have only addressed the dimensional relationships of L_T/W_{ch} and W_{ch}/L_{bo}, and as we will show, their parametric studies of these variables were incomplete. All of these papers show parametric studies of baffle tanks with a fixed footprint and varying numbers of baffles.

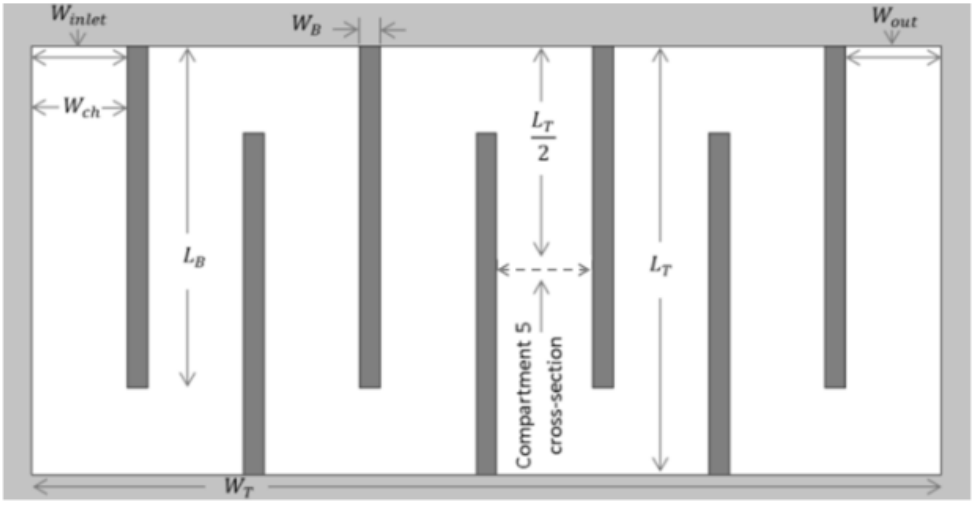

Figure 1. Plan form of the Embsay contact tank

Xu and Venayagamoorthy (2010) performed a 2-D RANS CFD study of the effect of baffle number on *BF* in a contact tank with the footprint of the scaled Embsay contact tank. The study modeled cases with 1, 2, 3, 4, 5, 6, 7, 8, 9, 10, and 11 baffles. Baffle length (L_B) and consequently, L_{bo}, were kept constant for each case. In cases where there were more than seven baffles, W_{inlet} was set equal to W_{ch}. In cases with seven baffles or

less, W_{inlet} was set to the inlet width used in the scaled Embsay contact tank from Shiono *et al.* (1991). This was the first study to model baffled tanks with inlet widths of different dimension than the channel width. The study found that the *BF* increased when the number of baffles was increased. This showed that *BF* is maximized when L_T/W_{ch} is maximized. The study did not mention or evaluate the effects of variable W_{inlet}, or the relationship of W_{inlet}/W_{ch}.

Amini *et al.* (2010) performed a parametric study of the number of baffles used in a 3-D RANS CFD model of the Embsay contact tank. One, three, five, seven, nine, and eleven baffles were tested in the study. The inlet and outlet widths were modified in each case so that the inlet width was the same as the channel width. This study showed that increasing the number of baffles increased the *BF*, and that the increase for each baffle added was diminishing. This study did not mention or consider the influence of altered inlet velocities on *BF*. To keep flow rate constant for each number of baffles, the inlet velocity was changed in each study. The inlet velocity was highest when the number of baffles was smallest, and vice versa. The only parameter evaluated in this study was L_T/W_{ch}.

Wenjun *et al.* (2007) performed 2-D CFD studies on serpentine baffle tanks to develop an empirical relationship between the median length of travel water takes in the contact tank to W_{ch}. In most work related to baffled contact tanks, the length to width ratio is taken as the width of the channel to the length of the *channel*. The total length of the baffle tank, if it is straightened, which is the parameter evaluated in the Wenjun *et al.* (2007) study, is irrelevant because the turns around the baffles interrupt the formation of fully developed flow. The contribution of this study is the observation that *BF* is best

when W_{ch}/L_{bo} =1. Their observation, however, is inconclusive because they did not isolate the effects of the relationship of W_{ch}/L_{bo} from the effects of W_{in}/L_{bo}, and it is not clear if they isolated the effects of L_T/W_{ch}. This study also presents a special case showing that the number of baffles in a tank is indirectly proportional to the *BF* because BF is decreased when the number of turns in the tank is increased. In this special case, L_T/W_{ch} was held constant as the number of baffles was varied, but the effects or dimensions of L_{bo} were not mentioned. Because L_{bo} was held constant in all cases tested in the study of Wenjun *et al.* (2007), the findings of their study are limited.

The work we present in this thesis provides new findings not found in the literature on the relationships of W_{inlet}/W_{ch}, W_{inlet}/L_{bo}, W_{ch}/L_{bo}, L_{bo}/L_T, and L_T/W_{ch} because our parametric study is the first of its kind to vary both the number of baffles and the length of the baffles.

2.1.2.2 Pipe Loops

Wilson and Venayagamoorthy (2010) validated the use of CFD to model the scalar transport in pipe loops. Pipe loops are some of the most efficient contact tank systems. The system modeled using CFD and physical tracer studies by Wilson and Venayagamoorthy (2010) had a *BF* greater than 0.9 at several flow rates.

Pipe loops are efficient because they have very long length to width ratios and they approximate plug flow in straight segments of pipe. Flow separation occurs at the bends in the pipe, but is minimal. Computational modeling of pipe loops is generally unnecessary because the high *BF* of pipe loops is well accepted by regulatory agencies such as the US EPA and CDPHE. The pipe loop tested by Wilson and Venayagamoorthy (2010) is shown in Figure 2.

Figure 2. Pipe loop (from Wilson and Venayagamoorthy, 2010)

2.1.2.3 Modified Storage Tanks

Many water systems use water storage tanks as contact tanks because the storage tanks can be bought cheaply from large manufacturers. These tanks have no baffles and inlet and outlet configurations that are not designed to induce plug flow. Unless tracer studies are performed, the US EPA assigns *BF*s of 0.1 to these storage tanks. Typically, only small water systems use these tanks, and they have to use high concentrations of disinfectants because of the low *BF*. Improving the *BF* of these tanks can be accomplished by linking them together in series, building baffles in the tanks, or by modifying the inlet configuration.

Wilson and Venayagamoorthy (2010) showed that pressurized cylindrical storage tanks connected in series have significantly higher *BF*s than single tanks; the tanks used had *BF*s on the order of 0.1 singly and 0.3 when three were linked in series. The tanks

tested in series by Wilson and Venayagamoorthy (2010) are shown in Figure 3(a). A study evaluating the *BF* of different numbers of tanks linked in series was done using CFD and verified with full-scale physical tracer studies.

Wilson and Venayagamoorthy (2011) modeled a 500 gallon storage tank using physical and CFD modeling. The *BF* of the tank was on the order of 0.1 for all flow rates. The 500 gallon tank, which is 6 feet tall, is shown in Figure 3(b).

(a) (b)

Figure 3. Modified storage tanks (from Wilson and Venayagamoorthy, 2011)

2.2 Computational Fluid Dynamics

Computational fluid dynamics (CFD) models have been thoroughly validated for the modeling of the internal hydraulics and scalar transport in baffled contact tanks and storage tanks modified to be contact tanks. The CFD softwares FLUENT and COMSOL were considered for use in this study. RANS equations were used, and two-equation

turbulence models were utilized for closure. Enhanced wall functions were set to ensure proper resolution of the inflated meshes generated for the study.

2.2.1 CFD Methods

CFD can be used to simulate or model fluid flow. There is a clear distinction between simulation and modeling; simulations solve the Navier-Stokes equations for the full flow field, whereas models solve the RANS equations. The three most common CFD methods are direct numerical simulation (DNS), large eddy simulation (LES), and RANS models. DNS is often used for academic research applications because it solves the smallest scales of fluid flow. Because DNS solves the smallest scales, it is also very computationally expensive and is not practical for use in simulations with high Reynolds number or a large domain (Pope, 2000).

LES is a combination of RANS models and DNS. Filters are used such that the full Navier-Stokes equations are solved for larger scale turbulent motions, but RANS models are used to solve the smaller scale turbulent motions. As computer processing technology advances, LES will become more and more practical for use in industry, but at this point it is still used primarily in research applications because of its computational costs. RANS models are the most commonly used CFD models for practical design and industrial applications. The RANS equations are derived by taking the time average of the Navier-Stokes equations, which introduces an artificial term that is called the Reynolds stress term. RANS methods are popular because they are less computationally expensive than DNS and LES models, but they require the addition of a turbulence model to represent the artificial Reynolds stresses (Pope, 2000).

2.2.2 Turbulence Models

Turbulence models are used in CFD codes to provide closure to the RANS equations by providing a solution to the Reynolds stresses. The Reynolds stresses can be modeled either by the turbulent viscosity hypothesis or by the modeled Reynolds stress transport equations (Pope, 2000). The turbulent viscosity hypothesis is valid assuming the modeled flow is in the category of simple shear flows (round jets, mixing layers, channel flows, and boundary layers). The flow in contact tanks meets this assumption, so turbulence models based on the turbulent viscosity hypothesis were used in this research.

There are many turbulence models based on the turbulent viscosity hypothesis, but the most common are the two-equation models. (For a more complete discussion of the turbulent viscosity hypothesis and turbulence models, please see Pope, 2000). The two-equation models used in this research were the κ-ε model and the κ-ω model, which are very commonly used and included in most commercial CFD programs. The κ-ε model solves the turbulent viscosity using the model transport equation for turbulent kinetic energy (κ) and the model transport equation for turbulent dissipation (ε). The turbulent viscosity is solved as

$$\nu_T = C_\mu \kappa^2 / \epsilon, \qquad (3)$$

where C_μ is a model constant (Pope, 2000). The κ-ω model is similar to the κ-ε model, in that it uses the model transport equation for turbulent kinetic energy (κ), but differs because the second equation solved, ω, represents the specific dissipation as κ / ε. For homogeneous turbulence, both models will have the same solution. For inhomogeneous turbulence, the models will have different solutions. The κ-ε model is suited for solving

free shear flows, whereas the κ-ω model is suited to solving boundary layer flows (ANSYS, Inc., 2011).

Commercial CFD software, such as ANSYS FLUENT, provides several versions of both the κ-ε and κ-ω models. The different versions of the models include the standard κ-ε, κ-ε RNG, κ-ε Realizable, κ-ω, and κ-ω SST, each of which has advantages for modeling applications of different types of flows.

2.2.2.1 κ-ε standard

The standard κ-ε model was proposed by Launder and Spalding (1972). It is accurate for a wide range of turbulent flows, but it is only valid in fully turbulent flows (ANSYS, Inc., 2011). In order to allow modeling of a wider variety of flows, such as flows that are not fully turbulent, several modified versions of the standard κ-ε model have been developed. The key differences in the model versions are: the method used to calculate turbulent viscosity, the turbulent Prandtl numbers used to predict turbulent diffusion, and the generation and destruction terms in the ε equation (ANSYS, Inc., 2011).

2.2.2.2 κ-ε RNG

The κ-ε RNG model is derived from the Navier-Stokes equations using a statistical technique called renormalization group theory (RNG). Because it is derived in a different manner, the κ-ε RNG model has different coefficients for the model transport equations than the standard κ-ε model. The key benefit of the RNG model over the standard model is that the RNG model accounts for low Reynolds number effects in non-fully turbulent flows through the use of an analytically derived formula for effective viscosity. The RNG model also accounts for the effects of swirl on turbulence and has an

extra term in the turbulent dissipation equation to account for rapid strain in flows. The standard κ-ε model uses a constant user-specified turbulent Prandtl number, whereas the RNG model specifies the turbulent Prandtl number with an analytical formula. These modifications to the standard κ-ε model make the RNG κ-ε model valid for wider array of flows (ANSYS Inc., 2011).

2.2.2.3 κ-ε Realizable

The realizable κ-ε model is, by definition, mathematically realizable in all cases. The standard and RNG κ-ε models contain mathematical anomalies in cases when the mean strain rate in the flow is very high. The realizable κ-ε model accounts for these anomalies by solving for C_μ, a model coefficient, based on the turbulence in the flow such that there are no mathematical anomalies and the equations are always realizable. The realizable model is validated to perform better than the other κ-ε models in cases with separated flows and flows with complex secondary flows. For other flow conditions, the realizable and RNG κ-ε models perform better than the standard κ-ε model, but it is not clear which model, RNG or realizable, performs better because the realizable model is relatively new (ANSYS, Inc., 2011).

2.2.2.4 κ-ω

The κ-ω model performs well in the boundary layer of flows, but does not perform well in turbulent free shear flows. This means that the κ-ω model does well close to walls in wall-bounded flows, but performs poorly far from the wall (ANSYS, Inc., 2011).

2.2.2.5 κ-ω SST

The *κ-ω* SST model combines the standard *κ-ω* model with a transformed *κ-ε* model so that flow can be accurately modeled in one simulation in areas with high or low Reynolds numbers and in the boundary or free shear layers. The results of each model are multiplied by a weighting factor dependent on the location in the flow, and the products of the models and their weighting functions are combined. The weighting function is set to 1 for the standard *κ-ω* model and zero for the transformed *κ-ε* model at the wall so that wall flows are modeled only using the *κ-ω* model. The opposite is done in the free shear layers so that only the transformed *κ-ε* model is used far from the wall (ANSYS, Inc., 2011).

2.2.1 Wall Functions

In wall bounded flows, the viscous boundary layer at the wall is the source for a large part of the turbulence in the flow because of the no-slip condition on the wall. Thus, it is important to accurately model the boundary layer in order to accurately model the turbulence. Close to the wall, viscous forces dominate the flow, and far from the wall turbulence dominates the flow. Distance from the wall is usually specified by the dimensionless wall unit, y^+, which is calculated as

$$y^+ = \frac{u_\tau y}{\nu}, \qquad (4)$$

where: u_τ = friction velocity $\equiv \sqrt{\tau_w/\rho}$, τ_w = wall shear stress, y = distance from the wall (dimensional), ρ = fluid density, and ν = kinematic viscosity of fluid (Pope, 2000).

In the flow close to the wall, there are several layers that are categorized based on dominant characteristics and wall y^+. In the viscous sublayer, $y^+<5$, viscous stresses dominate the Reynolds stresses. In the transition layer, $5 \leq y^+ \leq 50$, the viscous and

Reynolds stresses are both important. In the outer layer, $y^+ \geq 50$, Reynolds stresses are dominant (Pope, 2000). The purpose of wall functions is to calculate the shear stresses and turbulence close to the wall. The location of the first point in the mesh in relation to the wall, described as *y*, becomes very important in modeling, depending upon which type of wall function is used.

2.2.1.1 Standard Wall Function

Standard wall functions model the fully turbulent portion of the boundary layer, but do not model the viscous sublayer. A semi-empirical formula is used to calculate velocity and shear at the first point outside the viscous layer in the boundary layer so that turbulence models do not have to be modified for flow solutions close to the wall. The validity of standard wall functions is dependent on the location of the mesh point closest to the wall, which needs to satisfy $30 \leq y^+ \leq 60$. With standard wall functions, the accuracy of the solution is highly dependent on y^+ being in the correct range (ANSYS, Inc., 2011).

2.2.1.2 Enhanced Wall Function

Enhanced wall functions solve for the turbulence and shear generated at the wall with the first point assumed to be in the viscous sublayer of the wall boundary layer. This is convenient because it allows for high resolution meshes at the wall, whereas with the standard wall function the first mesh point needs to be outside of the viscous sublayer, which often leads to coarse meshes. The suggested range of y^+ for the enhanced wall function is $y^+ \leq 5$. Accuracy is dependent on the first point in the mesh being within the viscous sublayer, but the sensitivity of the solution of the enhanced wall function in regards to y^+ is less than that of the standard wall function (ANSYS, Inc., 2011). Mesh

generation techniques aimed at correctly placing the first point in the mesh will be discussed further in the model development sections of Chapters 3 and 4.

2.2.2 Commercial Software

There are many commercial CFD software packages. Some of the most common packages include COMSOL, FLUENT, FLOW-3D, and Open-Foam. Open-Foam is an open source code that is free to download. There is no graphical user interface for Open-Foam, so it is not a very user-friendly code. COMSOL, FLUENT, and FLOW 3-D all come with graphical user interfaces and are more user-friendly, but they require licenses that can be very expensive. At the time the research for this thesis was done, Colorado State University had licenses for COMSOL and FLUENT. Although FLOW 3-D has very good multi-phase modeling capabilities, it was not considered for use in this research because FLUENT and COMSOL were available and offered similar modeling capabilities. FLUENT and COMSOL were the commercial CFD software packages considered for this research.

2.2.2.1 COMSOL

COMSOL Multiphysics is a finite-element modeling program that has a CFD module for modeling fluid flow. COMSOL is very user-friendly because geometry generation, meshing, modeling, and post processing are all done in one program (COMSOL, 2010). The drawback of using COMSOL for modeling fluid flows is that finite element methods can be non-conservative in modeling fluid flow, whereas finite volume methods use the conservative form of the partial differential equations, and guarantee mass-conservation. COMSOL was not used for the research in this study because mass-conservation is not guaranteed by the finite-element method, and because

initial testing using COMSOL resulted in non-conservative and/or unstable results for scalar transport.

2.2.2.1 FLUENT

ANSYS FLUENT is a finite-volume CFD software. Model geometries can be imported into ANSYS FLUENT from CAD software, Solid Works, or ANSYS Mesh. ANSYS Workbench can be used to generate geometries and meshes and to perform post-processing. ANSYS Design Modeler and ANSYS Mesh are programs contained within ANSYS Design Modeler. ANSYS Design Modeler is used to develop model geometries. These model geometries can then be loaded into ANSYS Mesh to generate a mesh for the model. Once the mesh is generated and saved, it can be loaded into ANSYS FLUENT. This process is cumbersome compared to the one used in COMSOL because FLUENT requires the use of four separate programs to develop and run a CFD model, whereas an entire model can be developed and run from one window in one program using COMSOL. Although the development of CFD models in FLUENT is more cumbersome than in COMSOL, FLUENT was chosen as the CFD software for the research in this thesis because it uses the finite-volume method and guarantees mass-conservation.

CHAPTER 3. SERPENTINE BAFFLE TANKS

3.1 Introduction

Drinking water treatment in the United States is almost always done using disinfection with chlorine. Efficient chlorine contact tanks allow for thorough treatment of contaminants in water with the use of minimal concentrations of chlorine. Efficiency is quantified by the *BF* of the contact tank. The purpose of the following research has been to determine the characteristics of contact tanks with high *BF*s. Serpentine baffle tanks are often used in very large water systems, and they are the most practical and efficient tank design that is commonly used.

In this chapter of the thesis, the optimum configuration of serpentine baffle tanks will be investigated using CFD models of forty serpentine baffle tank configurations with the same footprint and very similar *TDT* in order to identify the characteristics of the tanks with the optimal *BF*. The validity of the use of CFD to model the internal hydraulics and scalar transport in baffled contact tanks has been thoroughly validated by Shiono *et al.* (1991), Shiono and Teixeira (2000), and Khan *et al.* (2006). Wang and Falconer (1998) demonstrated that validation of CFD models of contact tanks requires the reproduction of both the scalar transport, as shown by flow through curves (FTC), and internal hydraulics of the tank, as shown by velocity profiles. The scalar transport and internal hydraulics of the benchmark model for this study, a laboratory scale model of the Embsay Chlorine Contact Tank in West Yorkshire, England, were validated using data from physical models from Shiono *et al.* (1991).

The layout of this chapter is as follows: Section 3.2 will introduce the numerical methodology used in this study, Section 3.3 will present the CFD model and model

verification, Section 3.4 will introduce the parametric study, Section 3.5 will discuss the results of the parametric study, Section 3.6 introduces additional baffled contact tank models, and Section 3.7 discusses efficiency ratings of contact tanks.

An abstract and paper containing a portion of this chapter and titled *Computational Modeling of Baffled Disinfection Tanks* has been accepted to the 2012 ASCE-EWRI World Environmental & Water Resources Congress. Also, a significant portion of this chapter has been submitted to the ASCE *Journal of Environmental Engineering*.

3.2 Numerical Methodology

We employ the CFD software FLUENT, version 13.0, developed by FLUENT/ANSYS to perform highly resolved three-dimensional simulations. FLUENT is a finite-volume code that solves the Navier-Stokes equations. Finite-volume methods ensure both global and local conservation of mass and momentum, which are highly desirable properties for fluid flow simulations, particularly for scalar transport, as in the case of this study. Here, we use this code to solve the RANS equations and scalar transport equations on an unstructured tetrahedral mesh (Figure 4). The standard $\kappa-\varepsilon$ model (Launder and Spalding 1974) was chosen for the turbulence closure with standard empirical coefficients. The standard $\kappa-\varepsilon$ model was chosen because it has been validated to solve the velocity field in serpentine contact tanks (Khan *et al.* 2006).

The simulations were performed in two steps. First, the steady-state turbulent velocity field was calculated using the RANS equations with a first-order upwind solver. Enhanced wall-function boundary conditions were imposed on all walls and baffles. The water surface was treated with a symmetry boundary condition. Constant volume flow

rate, kinetic energy (κ) and kinetic energy dissipation rate (ε) were specified at the inlet, while the outlet was treated as a pressure outflow discharging to the atmosphere.

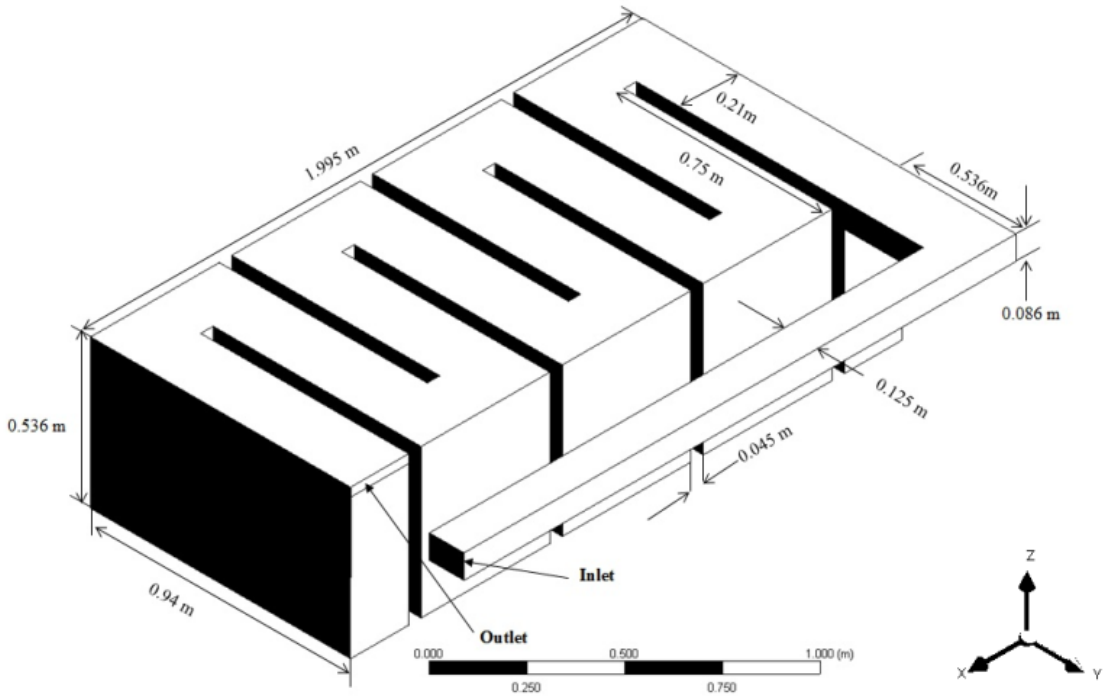

Figure 4. Benchmark geometry

Second, with the converged steady-state velocity field from the first step, the tracer concentration was calculated using the advection-diffusion equation given by

$$\frac{DC}{Dt} = \frac{\partial C}{\partial t} + \overline{U} \cdot \nabla C = \nabla \cdot \left(\left(\kappa + \frac{\nu_t}{Sc_t} \right) \nabla C \right), \qquad (5)$$

where C is the tracer concentration (e.g. chlorine), $\bar{U}$ is the steady state turbulent velocity field, κ is the molecular diffusivity of the tracer, which was set to the molecular diffusivity of water, and ν_t/Sc_t represents the turbulent scalar diffusivity, where ν_t is the turbulent eddy viscosity and Sc_t is the turbulent Schmidt number (Wilson and Venayagamoorthy, 2010). The sum of the molecular and turbulent scalar diffusivities was solved in FLUENT using a user-defined function, which is presented in Appendix I. The tracer was modeled as a conservative non-reactive scalar. Both $\bar{U}$ and ν_t were

obtained from the steady state solution of the momentum equations. The turbulent Schmidt number Sc_t was given as 0.7, a value widely accepted to be appropriate for neutrally stratified flow conditions (for a justification see, e.g., Venayagamoorthy and Stretch 2010).

The solutions of Eq. (5) were used to obtain the residence time distribution (RTD) curve at the outlet of the tank corresponding to a step tracer input at the inlet where the concentration was set as $C_o = C_{max} = 1$. The value of the scalar was monitored at the outlet as a flux. The variation of concentration at the outlet as a function of time provides the RTD curve of a step dose tracer input as shown in Figure 5, where the model time has been normalized by *TDT*. The differences in the RTDs of a tank with short circuiting and an ideal tank with plug flow are illustrated in Figure 5. The scalar transport in plug flow is illustrated by the jump from $C/C_o = 0$ to $C/C_o = 1$ at $t = TDT$. The slow increase in C/C_o for the tank with short-circuiting is shown in Figure 5. T_{10} is represented graphically in the RTD as the residence time when $C/C_o = 0.1$.

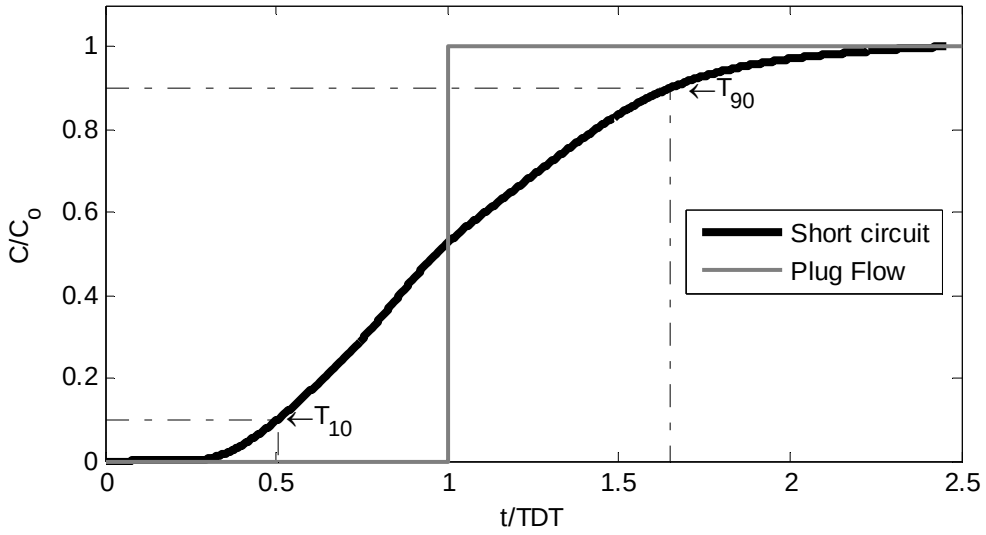

Figure 5. RTD curve at the outlet when the tracer is injected as a step dosage.

Flows through curves (FTCs) were also used to illustrate the hydraulics of the baffle tanks. The solutions of Eq. (5) are used to obtain the FTC at the outlet of the tank corresponding to a 15-second period where the inlet concentration was $C_o = C_{max} = 1$, followed by a period of $2.5TDT$ where the inlet concentration was $C_o = 0$. FTCs and RTD curves demonstrate the same physics in baffle tanks in different manners, much as a probability distribution function (PDF) and a cumulative distribution function (CDF) illustrate probabilities. When normalized by the inlet concentration, the FTC behaves like a PDF in that it will show the distribution of the concentration pulse released at the inlet over time at the outlet. The RTD behaves like a CDF in that it shows the amount of concentration accumulated in the tank over time. The FTC can be integrated to approximate the RTD curve as

$$\frac{1}{C_o * T_{release}} * \int_0^t FTC(t)dt \cong \frac{RTD(t)}{C_o}, \qquad (6)$$

where C_o is the inlet concentration and $T_{release}$ is the duration of the inlet pulse of the FTC.

Figure 6 shows a RTD curve generated using the un-baffled tank configuration in this study. Discretized data from the same configuration run with an FTC case have been numerically integrated using the trapezoidal rule and overlaid on the RTD curve to validate Eq. (6).

3.3 CFD Model Configuration and Verification

The Embsay Chlorine Contact Tank in West Yorkshire, England, has been the subject of a number of scaled physical and numerical studies, including but not limited to those of Shiono *et al.* (1991), Shiono and Teixeira (2000), and Khan *et al.* (2006).

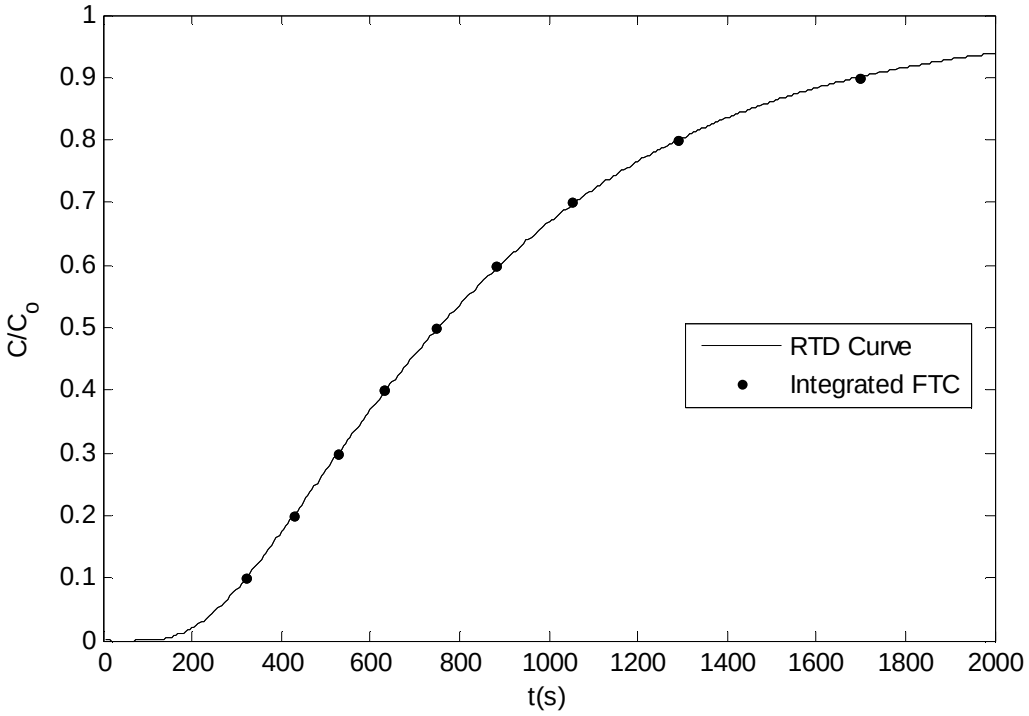

Figure 6. An integrated FTC approximates a RTD curve

In the article by Khan *et al.* (2006), a 3-D CFD model using the κ-ε turbulence model was presented and validated with physical model data of FTC and velocity profiles from Shiono *et al.* (1991). The experimental FTC and velocity data from the study of Shiono *et al.* (1991) were also used to validate the 3-D CFD model used in this study. The applicability of the κ-ε turbulence model to our study is shown by the validation of our model simulations with experimental results and the previous successful application of the κ-ε model by Khan *et al.* (2006).

3.3.1 Geometry

Figure 4 shows the footprint of the tank we employ in this study (the benchmark tank), which represents the main aspects of the seven baffle tank configuration used by Shiono *et al.* (1991). The tank is 1.995-m-long, 0.94-m-wide, and 0.6-m-deep. The inlet channel to the tank consists of two channels with a ninety degree bend in between. The

first inlet channel is 0.125 m wide and 0.086 m deep. The second inlet channel is 0.21 m wide and 0.086 m deep. The inlet opening between the inlet channel and the tank is 0.21 m wide and 0.086 m deep. Hereafter, the inlet opening will be referred to as the inlet, and the inlet channel will be referred to as the inlet channel. The inlet channel was included in the validation study to ensure that the flow conditions in the CFD model were the same as in the experiments done by Shiono *et al.* (1991). The inlet channel will be used on all model modifications in this study to ensure consistency. The outlet of the tank is 0.21 m wide and 0.031 m deep. Physical tracer studies were conducted by Shiono *et al.* (1991) with a continuous discharge of 1.17×10^{-3} m^3/s entering the tank, resulting in a mean water depth of 0.536 m and an initial mean cross-sectional velocity of 0.109 m/s at the inlet channel. The total detention time in the tank was 774 seconds. The flow rate used in all the CFD models in this study was the same flow rate used in the physical tracer studies.

In the experiments of Shiono *et al.* (1991), a weir was installed just upstream of the inlet opening. In the CFD models of Khan *et al.* (2006), the weir was included using a refined mesh near the weir and an empirical weir equation to define the water surface level upstream, across, and downstream of the weir. We have excluded the inlet weir from our models in order to avoid increased computational time due to mesh refinement at the inlet and to avoid numerical errors from empirical weir equations for water surface elevation. The mesh and time-step validations from this study show that any error from omitting the weir from our model is negligible.

In this study, we first validate our CFD model of the benchmark geometry with cross-sectional velocity plots and FTCs from Shiono *et al.* (1991), and then examine the

effects on *BF* of five geometric design parameters that will be introduced in Section 3.4 by modeling tanks with the footprint of the benchmark tank and geometries that represent forty different altered baffle configurations.

3.3.2 Mesh

The geometry and mesh files in this study were generated using ANSYS Workbench. The mesh of the benchmark geometry consists of 220,000 tetrahedral cells, and is shown in Figure 7. In order to verify that the mesh was appropriately sized, we used mesh adaptation based on y^+ values in FLUENT to increase the number of cells in the mesh to 500,000. We also used an un-adapted mesh with 1 million cells generated in Workbench by decreasing the minimum face size. Initial y^+ values from the benchmark mesh were acceptable for the enhanced wall functions used in FLUENT. Adapted y^+ values were approximately half the value of the initial values, which increased accuracy of the wall functions but did not affect scalar transport.

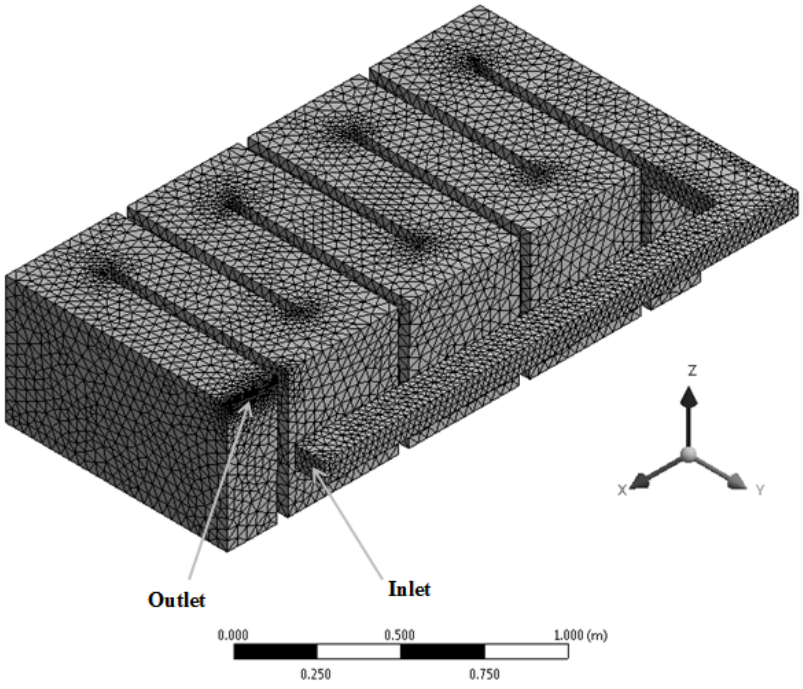

Figure 7. Benchmark mesh

The *BF*, RTD curve, and FTC curve of the model run with the adapted mesh were almost identical for the model run with the 200,000 cell mesh. Since there was no difference in accuracy caused by the small change in y+, adaption in FLUENT was deemed unnecessary. The FTCs for simulations run with both the benchmark mesh and the 1 million cell mesh and the FTC from Shiono *et al.* (1991) are almost identical to each other, again showing that the mesh with 220,000 cells is sufficient. Figure 8 shows the FTC curves generated with the different meshes and from the experimental data, where the concentration measured at the outlet is normalized by the maximum concentration measured at the outlet during the model run.

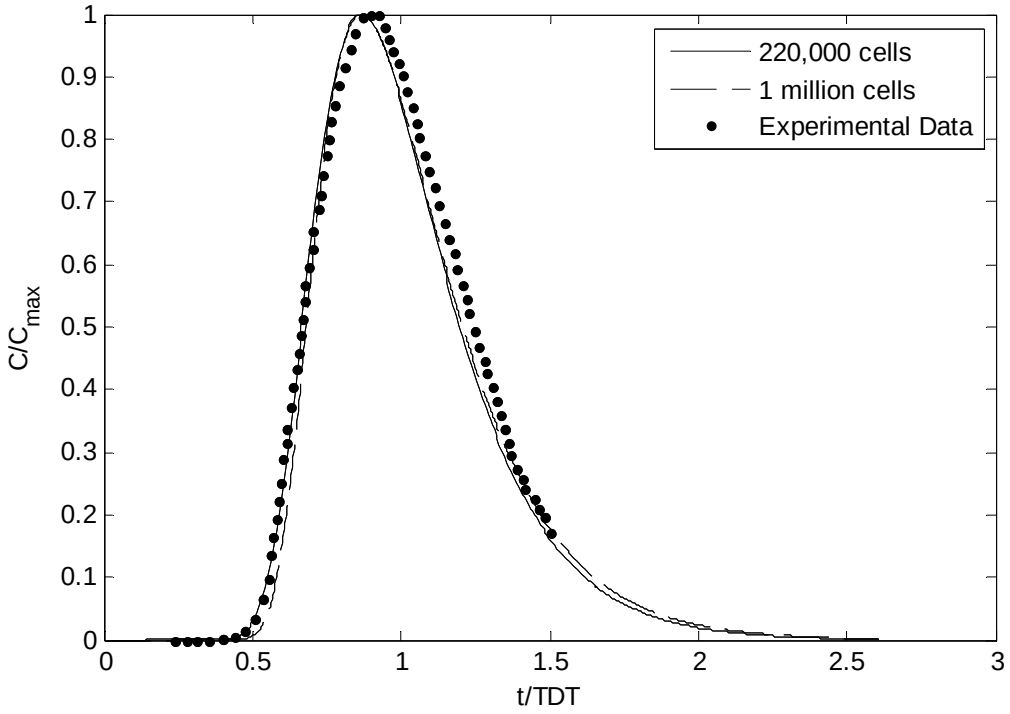

Figure 8. Comparison of FTCs generated with different mesh sizes and FTC from experimental data (Khan *et al.* 2006)

In order to optimize computational efficiency and ensure accuracy, the settings used in Workbench to develop the benchmark mesh with 220,000 cells were used to generate both the benchmark mesh and the meshes for all the modified geometries in this study.

The mesh configuration of 220,000 cells was also verified with the depth-averaged velocity profile from the experiments of Shiono *et al.* (1991). The velocity profile was measured in the fifth compartment of the tank, in the middle of the compartment in the Y-direction. The experimental data and CFD data are shown in Figure 9. The velocity in the CFD simulation deviates from the velocity in the experimental data at the left side of the cross-section because the velocity field in the CFD simulation was calculated with RANS equations, whereas the experimental data represents an instantaneous snapshot of the velocity field.

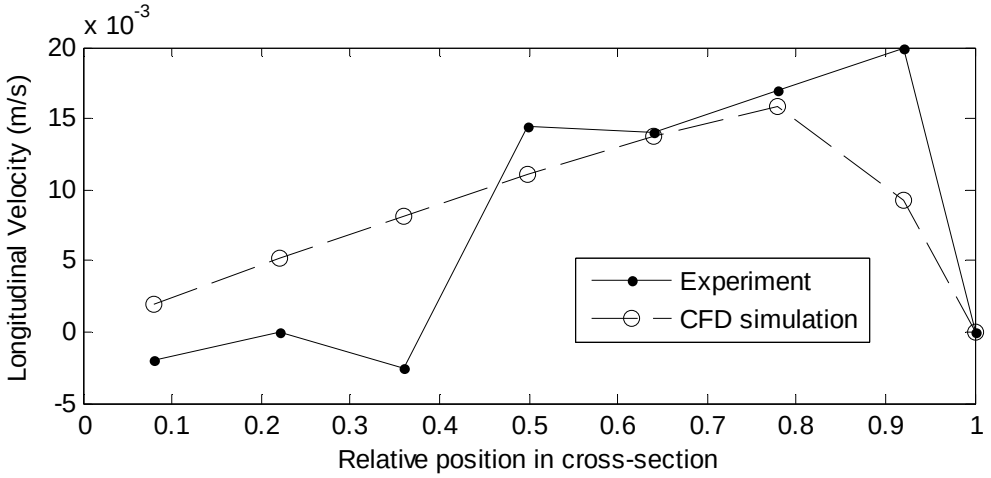

Figure 9. Comparison of computed longitudinal velocity with experimental velocity data (Wang and Falconer 1998)

3.3.3 Solution of the advection-diffusion equation

In ANSYS FLUENT 13.0, the steady state-solutions to the RANS equations were calculated until all residuals converged below 1 x 10^{-3}. The steady-state solutions to the RANS equations were then utilized in Eq. (5) to solve the time-dependent simulation of

tracer flow through the baffle tank. An area-averaged monitor of the scalar concentration at the outlet was implemented in order to create the RTD and FTC curves. A sensitivity study using time steps of 1, 2.5, and 5 seconds showed that a time step of 5 seconds yielded accurate and stable results at low computational cost (Figure 10). Combined computation time for both steps of the benchmark case where the transient solution ran for 2.5*TDT* with a time step of 5 seconds was 45 minutes using a CPU with an i7 processor and 8 GB of RAM.

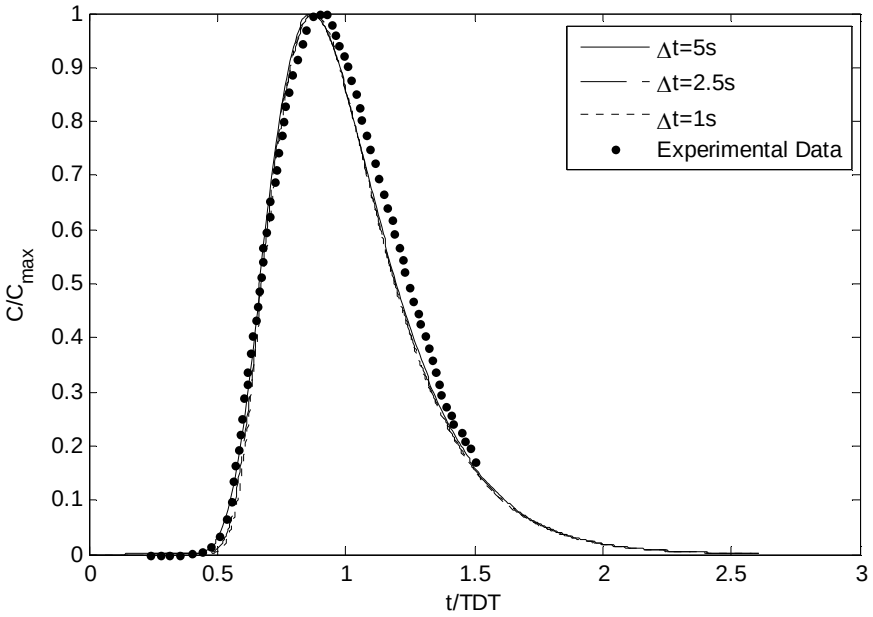

Figure 10. Comparison of FTCs generated with 5s, 2.5s, and 1s time steps and FTC from experimental data (Khan *et al.* 2006)

3.3.4 Dependence of *BF* on flow rate

The flow rate used for the benchmark geometry validation was set as the flow rate from the scaled model of Shiono *et al.* (1991). In order to ensure that the hydrodynamic characteristics in the tank were relatively independent of the flow rate, the benchmark case was modeled with flow rates of 0.5*Q*, *Q*, 2*Q*, and 4 *Q*, where $Q = 1.17\times10^{-3}$ m^3/s. The inlet velocity was set based on the flow rate, and the turbulent kinetic energy and

turbulent dissipation rate at the inlet were adjusted according to the inlet velocity. T_{10} and the length of the RTD curve increased at higher flow rates and decreased at 0.5*Q* (Figure 11), but the RTD curves normalized by *TDT*, and thus the *BF*, were relatively independent of the flow rate (Figure 12).

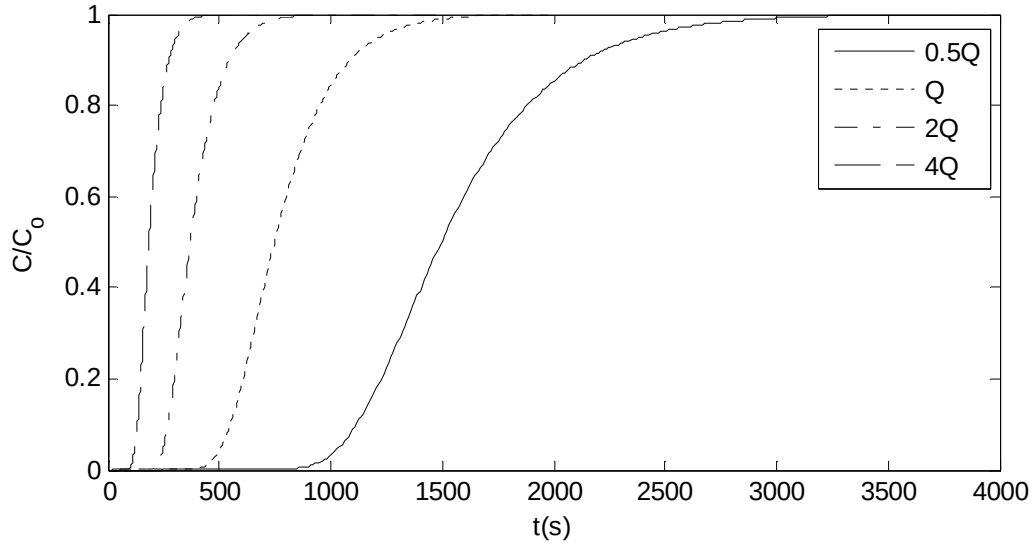

Figure 11. Comparison of RTD curves for different flow rates in the benchmark tank

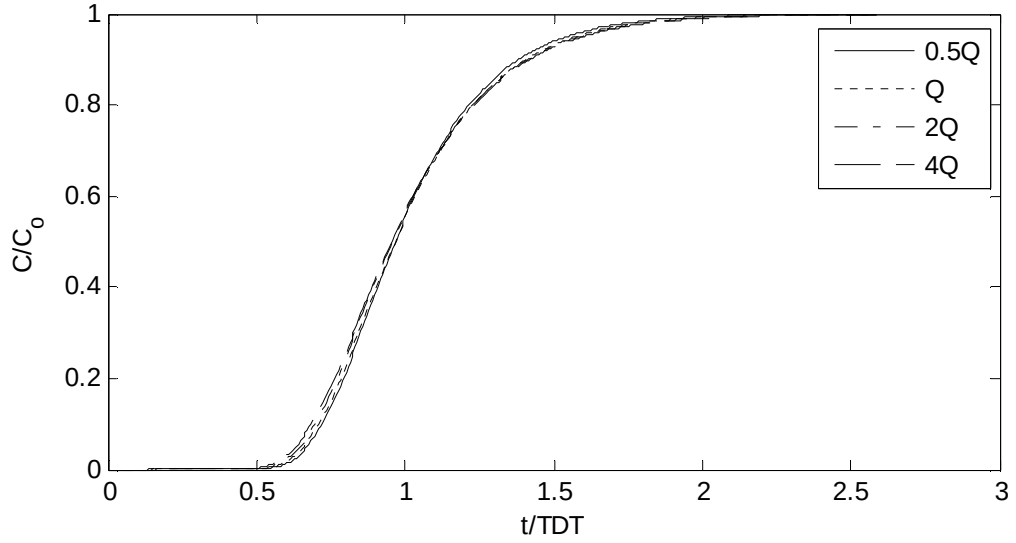

Figure 12. Comparison of RTD curves normalized by *TDT* for different flow rates in the benchmark tank

Since the flow rate of 1.17×10^{-3} m^3/s represents a realistic scaled flow rate for a disinfection system and tank efficiency does not depend on flow rate, $Q = 1.17\times10^{-3}$ m^3/s was used for all the models in the parametric study.

3.4 Parametric Study

Using CFD to study changes in *BF* caused by changes in tank configuration is more time-effective and cost-effective than building and testing physical models of new tank configurations. Now that 3-D CFD models have been convincingly validated to experimental results by Khan *et al.* (2006), Shiono and Teixeira (2000), and Wang and Falconer (1998), researchers are using CFD to attempt to optimize baffle configurations. Previous studies have analyzed only the effect of the number of baffles in the tank (Amini, 2001, Wenjun, 2007). These studies have assumed that the width of the inlet to the tank (W_{inlet}) was equal to the width of the channel (W_{ch}) and have kept the length of the baffle opening (L_{bo}) constant. In real design situations, W_{inlet} will most likely be fixed, the footprint will be governed by space considerations in the water treatment plant, and the baffle configuration will be determined by the designer. The purpose of this study was to discover general guidelines for designing contact tanks given fixed inlet and footprint configurations. We hypothesized that the optimal baffled contact tank would be defined by one or more of the following relationships: W_{inlet}/W_{ch}, L_T/W_{ch}, L_{bo}/W_{ch}, and L_{bo}/W_{inlet}. The relationship between the length of the baffle openings and the length of the tank (L_{bo}/L_T) will be discussed, but its relevance may be limited to tanks with geometries similar to the one used in this study.

In order to determine which of these relationships most affects *BF*, the length and number of the baffles in a tank were set as parameters, and a parametric study with thirty-

six configurations was performed. The plan view of the 7 baffle and 1 baffle configurations are shown without the inlet configuration in Figure 13 (a) and (b), respectively. The number of baffles was varied from 0 to 7, and L_{bo} was set at 100%, 80%, 60%, 40%, 20%, or 10% of L_T. L_T and the width of the tank (W_T) were held constant. The width of the baffle (W_{baffle}) was fixed at 0.045 m, and W_{inlet} was fixed at 0.21 m. The dependent variables in the four proposed relationships are W_{ch} and L_{bo} and are defined, respectively, as

$$W_{ch} = \frac{W_T - \#baffles * W_B}{\#baffles + 1}, \tag{7}$$

$$L_{bo} = L_T - L_B\ . \tag{8}$$

The depth of the tank and the outlet width (W_{out}) were held constant. Here we iterate that the purpose of studying tanks with different numbers of baffles was not to optimize the number of baffles for this tank, but to find relationships between geometric dimensions in this tank that depend on the number of baffles (as in Eq. (7)) such that these relationships can be applicable to other tanks.

3.5 Parametric Study Results

The results of the parametric study indicate that expansions and contractions along the direction of flow through the contact tank should be avoided, as evidenced by the non-dimensional relationships described in the following sections. The parametric study reveals new information about the dynamics of baffle tanks, especially through the relationship of L_{bo}/W_{inlet}. The 7-baffle tank performed the best, and in order to better understand the dynamics in a practical tank design, additional models were run using the 7-baffle set-up with smaller variations in L_{bo}. The design parameters and efficiencies of the thirty-six configurations tested in the parametric study are displayed in Tables 2-6.

Tables 2, 3, 4, 5, and 6 show the configurations with L_{bo}/L_T = 0.8, 0.6, 0.4, 0.2, and 0.1, respectively. The case with no baffles (case #1) is shown in Table 2.

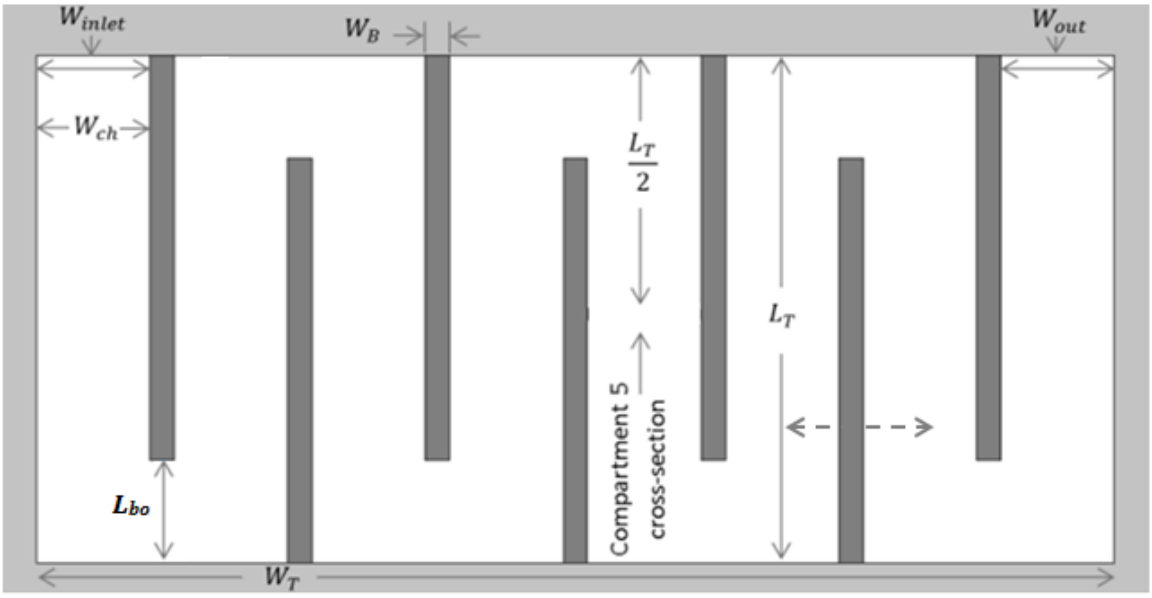

(a)

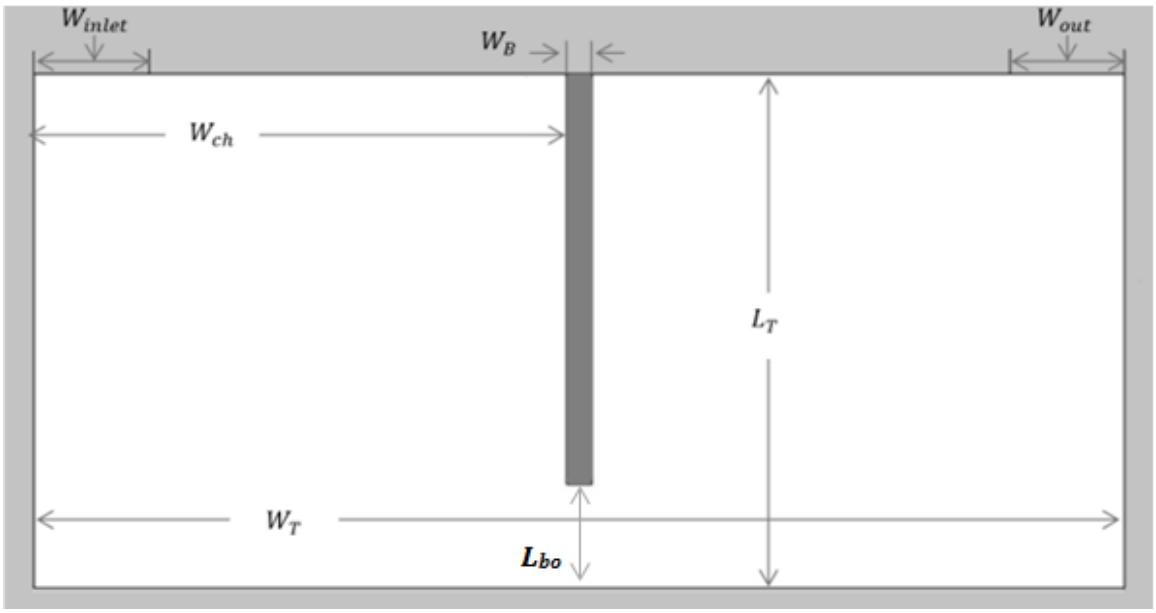

(b)

Figure 13. (a) Profile view of 7 baffle configuration and (b) profile view of 1 baffle configuration

Table 2. Design parameters and efficiency ratings of Cases 1-8

Case #	Independent Variables		Design Parameters				Efficiency					
	# baffles	L_{bo}/L_T	W_{inlet}/W_{ch}	L_T/W_{ch}	L_{bo}/W_{ch}	L_{bo}/W_{inlet}	Tank Volume (m^3)	TDT (s)	T_{10} (s)	BF	T_{90} (s)	T_{10}/T_{90}
1	0	N/A	0.11	0.47	0.47	4.48	1.03	882	321	0.36	1693	0.19
2	1	0.8	0.22	0.96	0.77	3.58	1.03	878	307	0.35	1698	0.18
3	2	0.8	0.33	1.48	1.18	3.58	1.02	874	379	0.43	1593	0.24
4	3	0.8	0.45	2.02	1.62	3.58	1.02	870	373	0.43	1599	0.23
5	4	0.8	0.58	2.59	2.07	3.58	1.01	866	392	0.45	1553	0.25
6	5	0.8	0.71	3.19	2.55	3.58	1.01	862	367	0.43	1546	0.24
7	6	0.8	0.85	3.81	3.05	3.58	1.00	859	378	0.44	1511	0.25
8	7	0.8	1.00	4.48	3.58	3.58	1.00	855	389	0.45	1530	0.25

Table 3. Design parameters and efficiency ratings of Cases 9-15

Case #	Independent Variables		Design Parameters				Efficiency					
	# baffles	L_{bo}/L_T	W_{inlet}/W_{ch}	L_T/W_{ch}	L_{bo}/W_{ch}	L_{bo}/W_{inlet}	Tank Volume (m^3)	TDT (s)	T_{10} (s)	BF	T_{90} (s)	T_{10}/T_{90}
9	1	0.6	0.22	0.96	0.58	2.69	1.02	874	334	0.38	1654	0.20
10	2	0.6	0.33	1.48	0.89	2.69	1.01	866	347	0.40	1630	0.21
11	3	0.6	0.45	2.02	1.21	2.69	1.00	859	410	0.48	1495	0.27
12	4	0.6	0.58	2.59	1.55	2.69	1.00	851	446	0.52	1404	0.32
13	5	0.6	0.71	3.19	1.91	2.69	0.99	843	501	0.59	1300	0.39
14	6	0.6	0.85	3.81	2.29	2.69	0.98	835	441	0.53	1448	0.30
15	7	0.6	1.00	4.48	2.69	2.69	0.97	828	382	0.46	1537	0.25

Table 4. Design parameters and efficiency ratings of Cases 16-22

Case #	Independent Variables		Design Parameters				Efficiency					
	# baffles	L_{bo}/L_T	W_{inlet}/W_{ch}	L_T/W_{ch}	L_{bo}/W_{ch}	L_{bo}/W_{inlet}	Tank Volume (m^3)	TDT (s)	T_{10} (s)	BF	T_{90} (s)	T_{10}/T_{90}
16	1	0.4	0.22	0.96	0.39	1.79	1.02	870	285	0.33	1786	0.16
17	2	0.4	0.33	1.48	0.59	1.79	1.00	859	327	0.38	1623	0.20
18	3	0.4	0.45	2.02	0.81	1.79	0.99	847	411	0.49	1470	0.28
19	4	0.4	0.58	2.59	1.04	1.79	0.98	835	443	0.53	1386	0.32
20	5	0.4	0.71	3.19	1.27	1.79	0.96	824	455	0.55	1318	0.34
21	6	0.4	0.85	3.81	1.53	1.79	0.95	812	473	0.58	1270	0.37
22	7	0.4	1.00	4.48	1.79	1.79	0.94	800	487	0.61	1223	0.40

Table 5. Design parameters and efficiency ratings of Cases 23-29

Case #	Independent Variables		Design Parameters				Efficiency					
	# baffles	L_{bo}/L_T	W_{inlet}/W_{ch}	L_T/W_{ch}	L_{bo}/W_{ch}	L_{bo}/W_{inlet}	Tank Volume (m^3)	TDT (s)	T_{10} (s)	BF	T_{90} (s)	T_{10}/T_{90}
23	1	0.20	0.22	0.96	0.19	0.90	1.01	866	284	0.33	1733	0.16
24	2	0.20	0.33	1.48	0.30	0.90	1.00	851	360	0.42	1568	0.23
25	3	0.20	0.45	2.02	0.41	0.90	0.98	835	409	0.49	1428	0.29
26	4	0.20	0.58	2.59	0.52	0.90	0.96	820	421	0.51	1341	0.31
27	5	0.20	0.71	3.19	0.64	0.90	0.94	805	488	0.61	1239	0.39
28	6	0.20	0.85	3.81	0.77	0.90	0.92	789	522	0.66	1158	0.45
29	7	0.20	1.00	4.48	0.90	0.90	0.91	774	550	0.71	1088	0.51

Table 6. Design parameters and efficiency ratings of Cases 30-36

Case #	Independent Variables		Design Parameters				Efficiency					
	# baffles	L_{bo}/L_T	W_{inlet}/W_{ch}	L_T/W_{ch}	L_{bo}/W_{ch}	L_{bo}/W_{inlet}	Tank Volume (m^3)	TDT (s)	T_{10} (s)	BF	T_{90} (s)	T_{10}/T_{90}
30	1	0.1	0.22	0.96	0.10	0.45	1.01	864	294	0.34	1687	0.17
31	2	0.1	0.33	1.48	0.15	0.45	0.99	847	304	0.36	1606	0.19
32	3	0.1	0.45	2.02	0.20	0.45	0.97	830	342	0.41	1481	0.23
33	4	0.1	0.58	2.59	0.26	0.45	0.95	812	403	0.50	1353	0.30
34	5	0.1	0.71	3.19	0.32	0.45	0.93	795	432	0.54	1257	0.34
35	6	0.1	0.85	3.81	0.38	0.45	0.91	777	475	0.61	1163	0.41
36	7	0.1	1.00	4.48	0.45	0.45	0.89	760	513	0.68	1077	0.48

3.5.1 Baffle opening length vs. Tank Length (L_{bo}/L_T)

The optimal L_{bo} for the 3, 5, 6, and 7 baffle tanks was 0.19 m, or $0.2L_T$, as displayed in Figure 14. The optimal L_{bo} for the 1, 2, and 4 baffle tanks was less than or equal to $0.4L_T$. For tanks with any number of baffles, $L_{bo} = 0.1L_T$ was not optimal because of flow separation caused by the sharp contractions around the baffles.

In the 7 baffle tank, there is a sharp increase in *BF* when L_{bo}/L_T decreases from 60% to 40%. In order to better illustrate the effects of different L_{bo} on the 7 baffle tank, additional models were run with $L_{bo} = 0.9L_T$, $0.7L_T$, $0.55L_T$, $0.5L_T$, and $0.3L_T$. Interestingly, the largest increase in *BF* occurs when L_{bo}/L_T decreases from 55% to 50%. The increase in *BF* when L_{bo}/L_T decreases from 55% to 50% accounts for 26% of the total increase in *BF* as L_{bo}/L_T decreases from 100% to 20%. When $L_{bo} > 0.5L_T$, the flow is not forced to change directions as it passes around the baffle, and in some cases the baffles actually create a channel that allows the flow to pass between the baffle tips, creating dead zones between the baffles, as illustrated in the mid-depth velocity contours in Figure 15.

Because the optimal L_{bo}/L_T is highly dependent on the number of baffles and L_T, it is not a desirable design variable. The merit in this variable is that it illustrates that sharp contractions around baffle tips occur when $L_{bo}/L_T = 0.1$, which causes a decrease in *BF*, and that it is important for tanks to be designed with $L_{bo}/L_T \leq 0.50$ to ensure that the flow through the tank is prevented from channeling between the baffles and creating large short circuits. In other words, it is recommended to have baffle opening lengths in the range of $0.1 \leq L_{bo}/L_T \leq 0.5$.

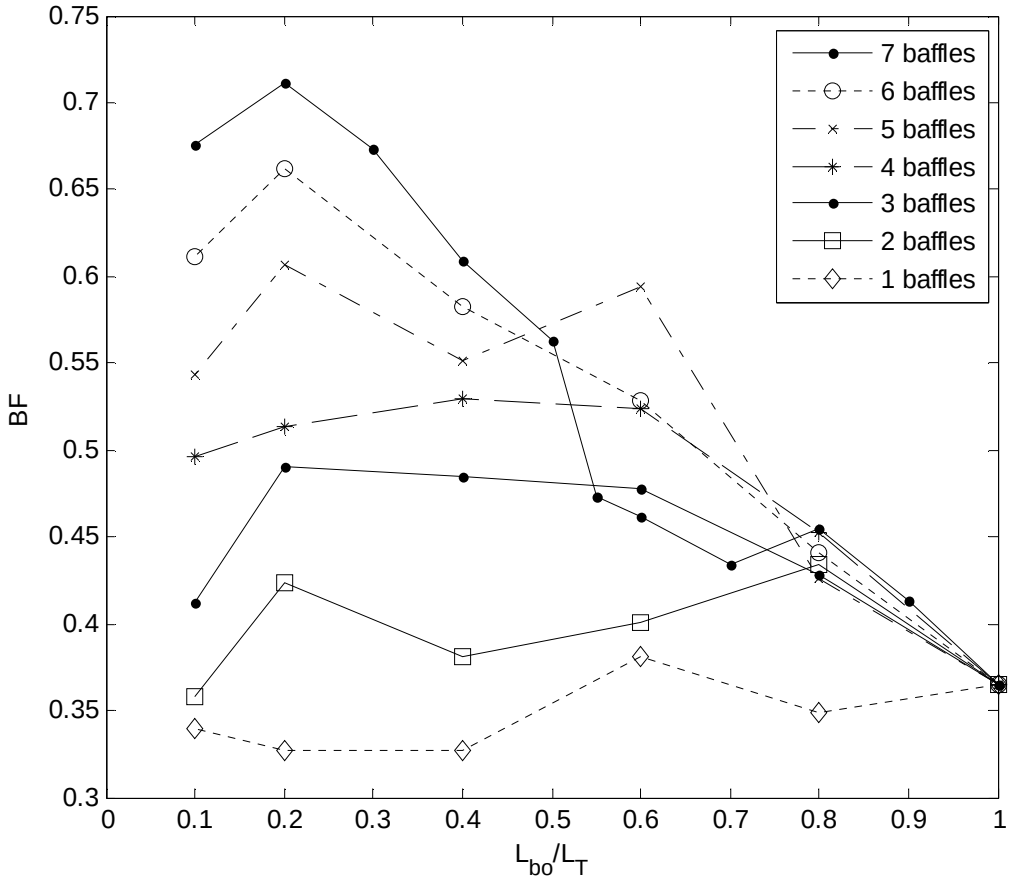

Figure 14. *BF* as a function of L_{bo}/L_T for tanks with baffle numbers from 1 to 7

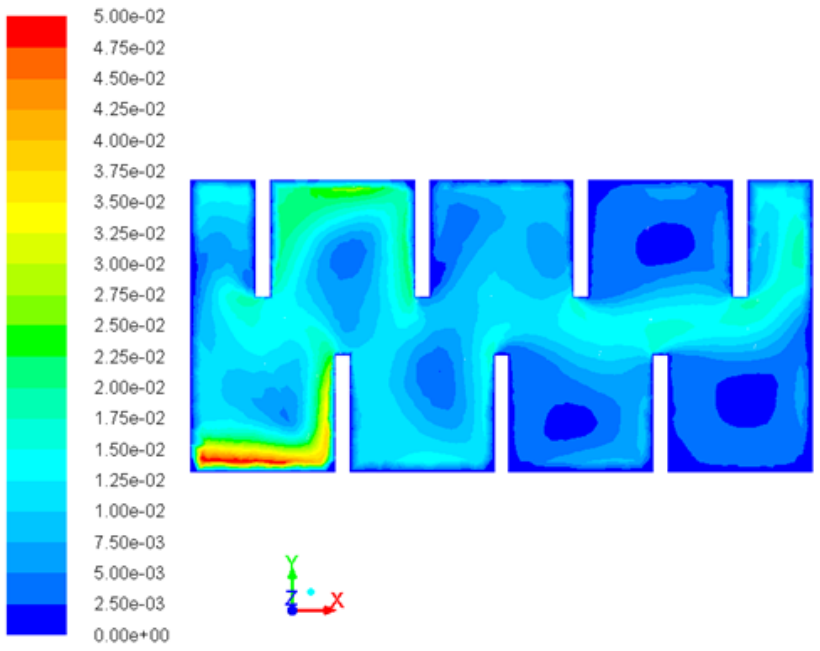

(a)

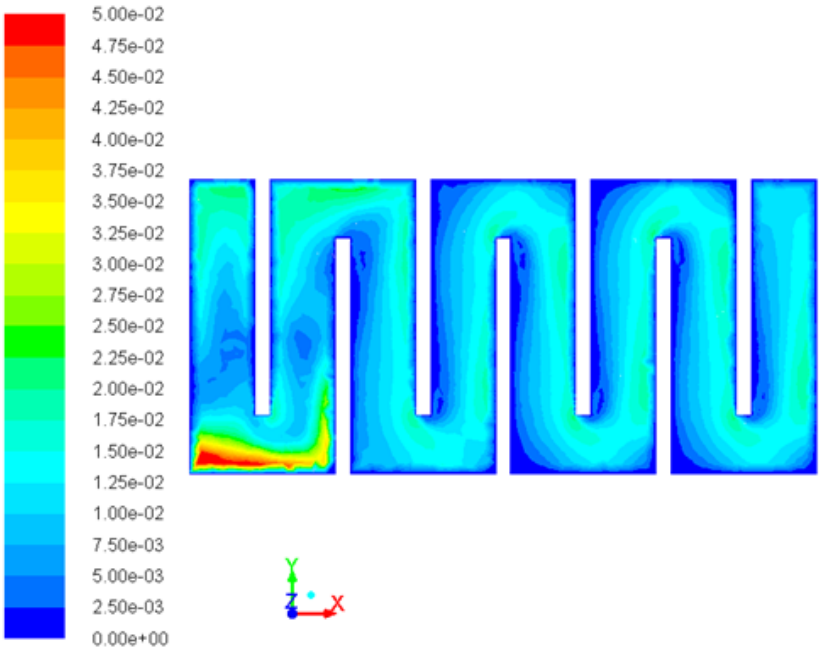

(b)

Figure 15. Velocity contours (m/s) at mid-depth of tank where (a) flow is channeled between baffle tips creating large dead zones when $L_{bo}/L_T = 0.6$ for the 7-baffle tank and (b) flow is directed for optimal use of tank volume when $L_{bo}/L_T = 0.2$ for the 7-baffle tank. Color range is limited to allow resolution near the baffles.

3.5.2 Number of Baffles and Tank Length vs. Channel Width (L_T/W_{ch})

The number of baffles in a tank is an important variable that can also be illustrated by L_T/W_{ch}, since W_{ch} is determined by the number of baffles. L_T/W_{ch} represents the length to width ratio in each compartment of the contact tank. When length to width ratio in each compartment is high, the flow in each compartment can approach plug flow before it reaches the next wall of the tank. This is the primary reason why tanks with more baffles generally perform better.

In the cases where $L_{bo} = 0.8L_T$ and $L_{bo} = 0.6L_T$, *BF* was not directly related to the number of baffles. In these cases, the large L_{bo} allowed a channel to form through the center of the tank, making the effect of the number of baffles less relevant. As shown in Figure 16, with the exceptions of $L_{bo} = 0.8L_T$ and $L_{bo} = 0.6L_T$, all baffle length configurations performed best with 7 baffles, where L_T/W_{ch}= 4.476, and *BF* increased as the ratio of L_T/W_{ch} increased. Even in the tanks where $L_{bo} = 0.1L_T$, which caused the most flow separation for any baffle length, the *BF* is best when there are 7 baffles. This indicates that the increase in flow separation caused by adding another bend is less than the decrease in flow separation caused by increasing the length to width ratio within each baffle chamber.

Figure 17 illustrates the effect of increasing the ratio of L_T/W_{ch} in the tank where $L_{bo}/L_T = 0.2$. L_T/W_{ch} is increased as the number of baffles is increased. The RTD curve is approximately the same for 0, 1, and 2 baffles. As the number of baffles is increased from 3 to 7, T_{10} is increased, T_{90} is decreased, and the shape of the RTD curve becomes closer to the square wave RTD curve seen in plug flow conditions.

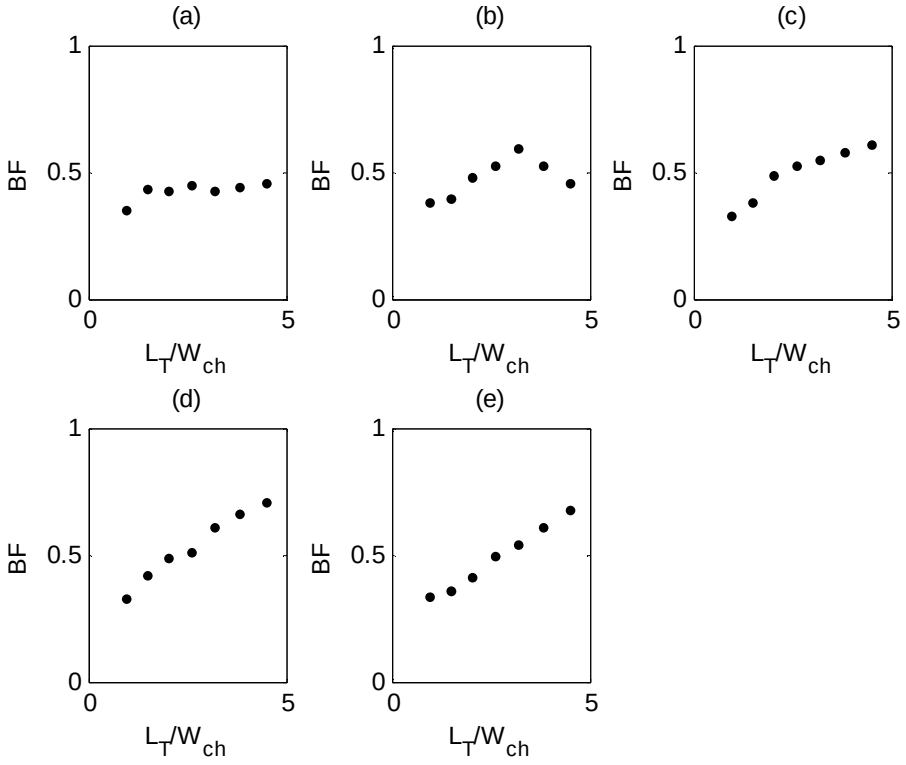

Figure 16. ***BF*** **as a function of L_T/W_{ch} for 7-baffle tank with (a) $L_{bo} = 0.8L_T$ (b) $L_{bo} = 0.6L_T$ (c) $L_{bo} = 0.4L_T$ (d) $L_{bo} = 0.2L_T$ (e) $L_{bo} = 0.1L_T$**

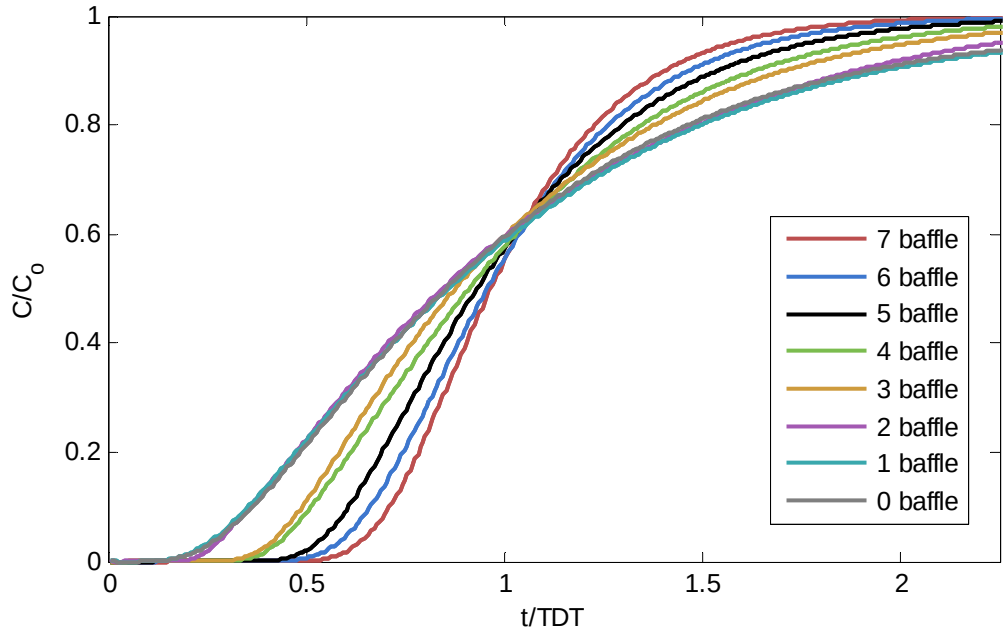

Figure 17. RTD Curves of normalized tracer concentration at the outlet with baffle numbers of 0 to 7 with $L_{bo}/L_T = 0.2$

3.5.3 Inlet Width vs. Channel Width (W_{inlet}/W_{ch})

Flow separation related to W_{inlet}/W_{ch} is caused by an expansion as the flow passes from the inlet into the first chamber of the tank. In a tank where $W_{inlet} = W_{ch}$, there will be no horizontal separation caused by the inlet expansion. Again, we see that for tanks with $L_{bo} = 0.8L_T$ and $L_{bo} = 0.6L_T$, the ratio of W_{inlet}/W_{ch} shows inconsistent patterns in relation to *BF*. These cases do not influence design criteria because tanks with $L_{bo} = 0.8L_T$ and $L_{bo} = 0.6L_T$ have been shown by this study to be poor designs because of channeling between baffle tips as seen in Figure 15(a). For the cases where $L_{bo} = 0.4L_T$, $0.2L_T$, and $0.1L_T$, Figure 18 clearly illustrates that the best tank configuration occurs when $W_{inlet}/W_{ch} = 1$.

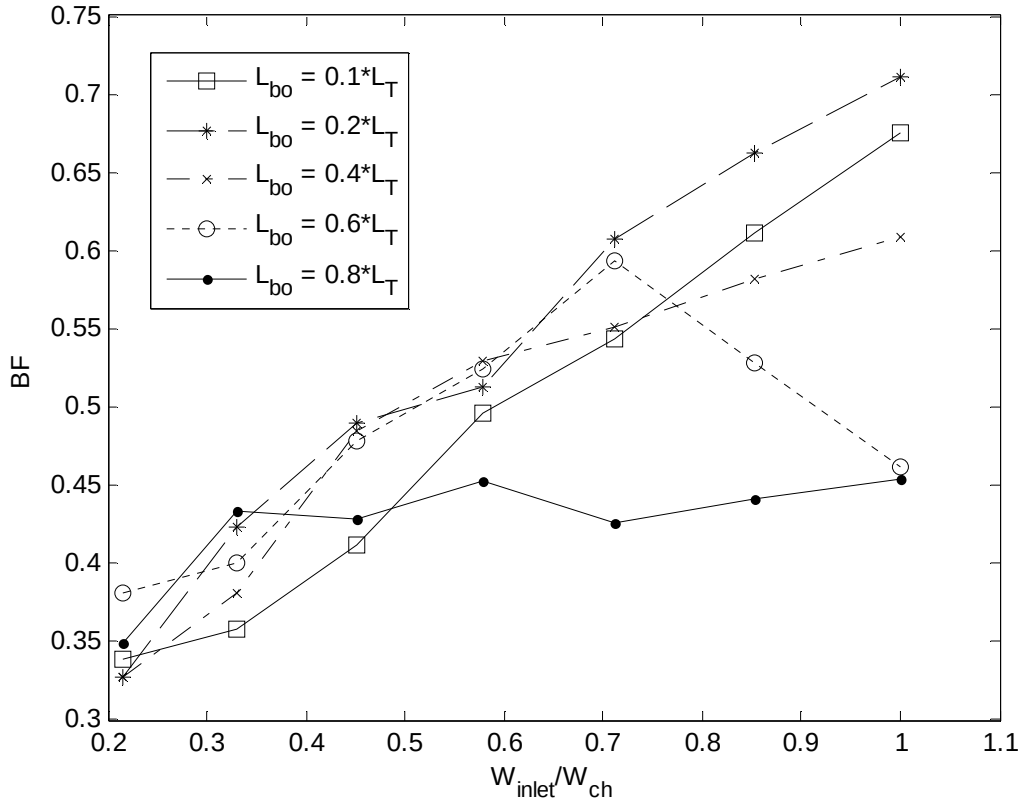

Figure 18. *BF* as a function of W_{inlet}/W_{ch} for $L_{bo}= 0.8L_T$ to $0.1L_T$

In order to approximate plug flow and maximize *BF*, designers should design tanks with $W_{inlet}/W_{ch} = 1$. This design ensures that there is no flow separation caused by expansions or contractions as the flow passes from the inlet into the first baffle chamber.

3.5.4 Length of baffle opening vs. width of channel (L_{bo}/W_{ch})

The relationship of L_{bo} and W_{ch} provides an indicator of the extent of expansion/contraction that the flow in the contact tank experiences as it passes from a channel width of W_{ch} to L_{bo} at the baffle tips. The tanks designed with 4, 5, 6, and 7 baffles achieve the best *BF* when $L_{bo}/W_{ch} \approx 1$ (Figure 19).

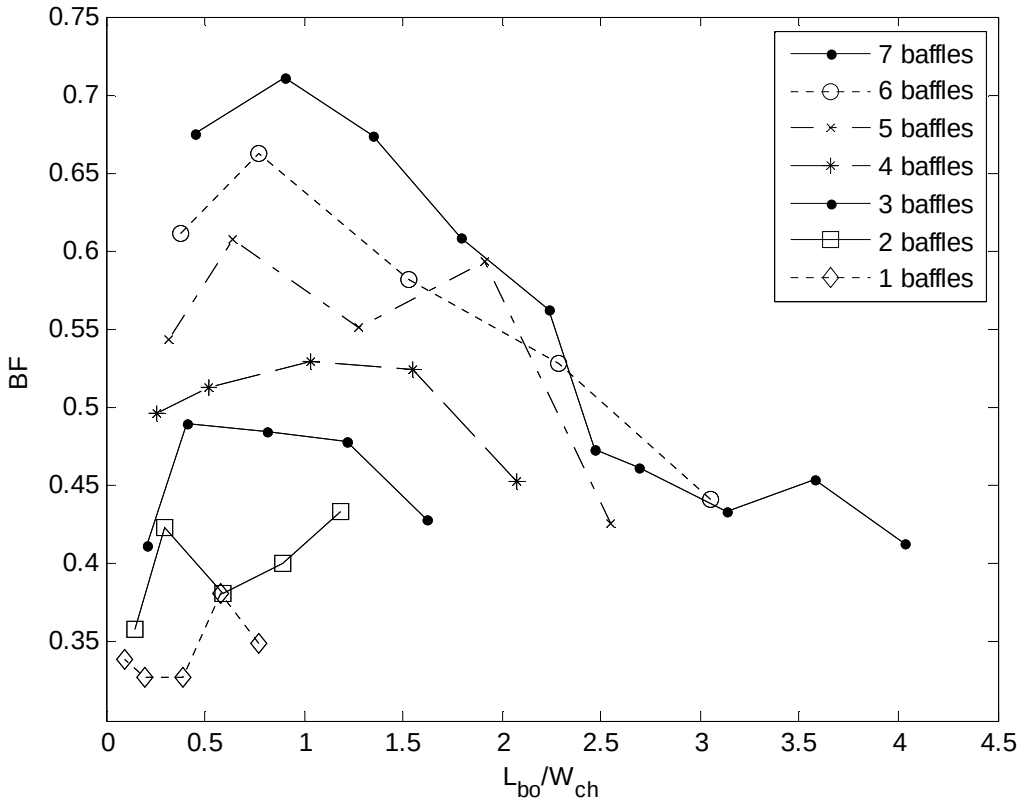

Figure 19. *BF* as a function of L_{bo}/W_{ch} with baffle numbers of 1 to 7

The tanks with 2 or 3 baffles do well, but not the best when $L_{bo}/W_{ch} \approx 1$, and the tank with 1 baffle cannot have $L_{bo}/W_{ch} = 1$. This parameter provides more insight into the hydraulic

processes in the tank than L_B/L_T because there is a pattern that holds for tanks with any number of baffles. The results of the parametric study indicate that flow separation is minimized when $W_{ch} \approx L_{bo}$, so engineers should design tanks with $W_{ch} \approx L_{bo}$ to maximize hydraulic efficiency.

3.5.5 Length of baffle opening vs. width of inlet (L_{bo}/W_{inlet})

Regardless of the flow separation caused by disparity of scales between channel and inlet widths as well as between channel width and baffle opening length, additional separation can be caused when $L_{bo} \neq W_{inlet}$. Here, we must define a difference between the width of flow in each channel, and the width of the dominant flow field. If W_{ch} is not equal to L_{bo} or W_{inlet}, there will be an expansion or contraction in the total width of the flow, but if $L_{bo} = W_{inlet}$, there will not be an expansion or contraction in the width of the dominant flow field. In the CFD models, vertical mixing in the first compartment makes it difficult to identify the dominant width of the horizontal flow field. In later compartments, however, the flow becomes primarily two-dimensional, and a dominant horizontal flow field becomes apparent. Figure 20 illustrates that the optimal ratio of $L_{bo}/W_{inlet} \approx 1$ for most cases. However, from this plot, it is not clear whether this is caused by the physics related to L_{bo}/W_{inlet} or L_B/L_T. Velocity contours taken at the mid-depth of the 3 and 7 baffle tanks illustrate that L_{bo}/W_{inlet} has an effect on the flow dynamics regardless of W_{ch} or L_B/L_T (Figure 21). Figure 21(a) shows the 7 baffle tank where $L_{bo} \approx W_{ch} \approx W_{inlet}$. The dominant flow field width in this case is approximately equal to W_{inlet}, but it is also approximately equal to W_{ch}. Figure 21(b) shows the 3 baffle tank where $L_{bo} \approx W_{inlet} \neq W_{ch}$. In this case, the dominant flow field width is approximately equal to W_{inlet}, even though $W_{ch} \approx 2W_{inlet}$. Figure 21(a) and Figure 21(b)

illustrate that L_{bo}/W_{inlet} affects flow separation regardless of W_{ch}. Figure 21(b) and Figure 21(c) show cases where $W_{inlet} \neq L_{bo}$ and the width of the dominant flow field is approximately W_{inlet}. Even in Figure 21(d), where $W_{ch} \approx L_{bo}$, the dominant flow field width in the later channels is approximately equal to W_{in}.

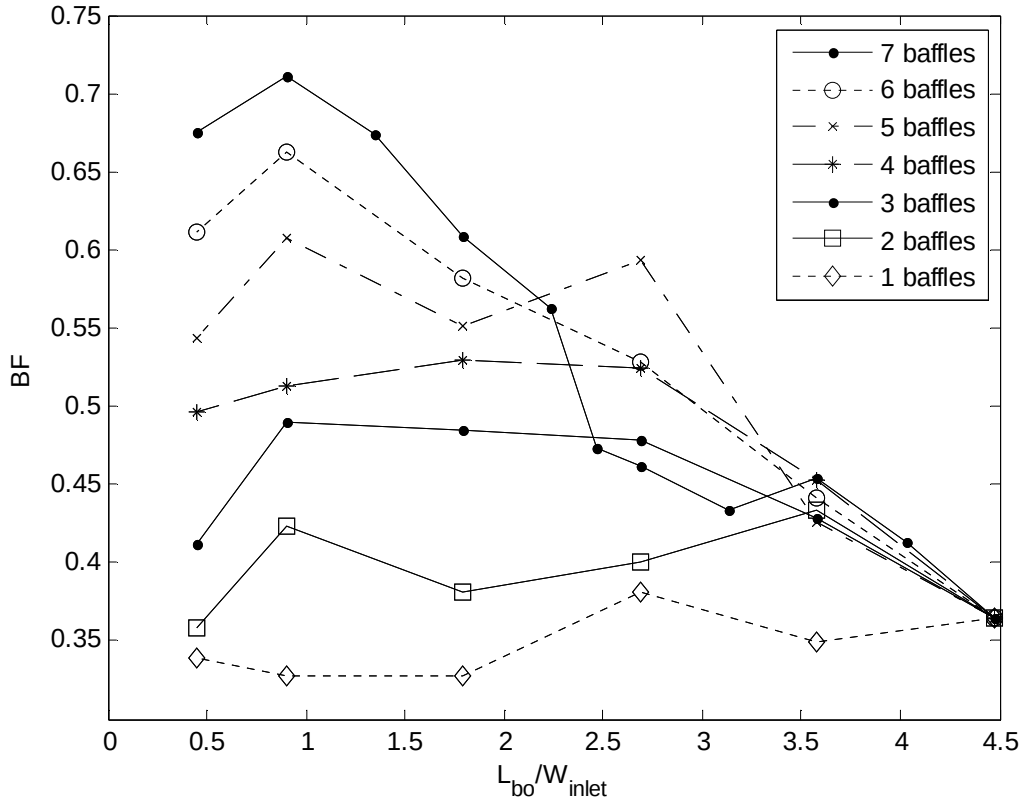

Figure 20. *BF* as a function of L_{bo}/W_{inlet} with baffle numbers from 1 to 7

This is the first study in which the relationship of L_{bo}/W_{inlet} is addressed. Intuitively, it would seem that the 3-dimensional mixing in the first several chambers of a baffle tank would eliminate the effects of W_{inlet}. However, the velocity contours in Figure 21 demonstrate that the width of flow at the inlet to the tank has a lasting effect on the dominant flow field width. Designing the tank such that L_{bo} is the same width as the dominant flow field width, i.e., W_{inlet}, will decrease separation and maximize *BF*.

The results of the parametric study show that *BF* is inversely related to the amount of flow separation in the tank. In a pipe loop, the only significant flow separation is caused by bends. In contrast, flow separation in a contact tank can be caused by: expansion from the inlet to the tank, expansions/contractions between channels and baffle openings, contraction from the tank to the outlet, and flow around bends.

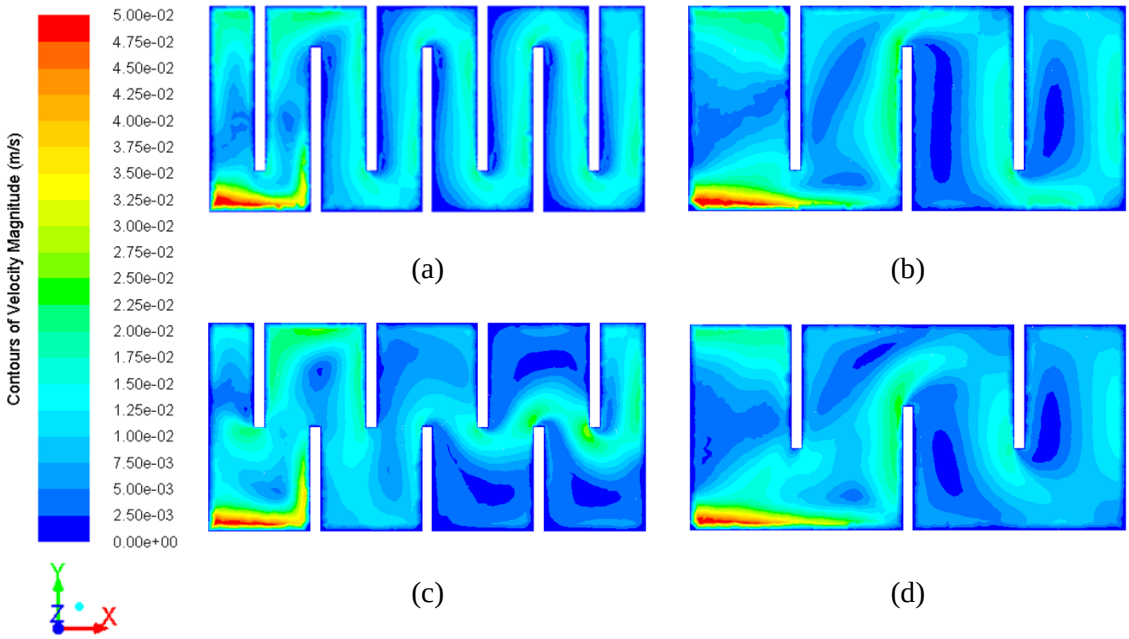

Figure 21. Dominant flow structures shown by velocity contours (m/s) at mid-depth of (a) 7 baffle tank with $L_{bo} \approx W_{ch} \approx W_{inlet}$, (b) 3 baffle tank with $L_{bo} \approx W_{inlet} \neq W_{ch}$, (c) 7 baffle tank with $W_{ch} \approx W_{inlet} \neq L_{bo}$, and (d) 3 baffle tank with $L_{bo} \approx W_{ch} \neq W_{inlet}$.

We propose that the best contact tanks will resemble pipe loops in their plan view; irrespective of L_T and W_T, the most efficient tanks will have $W_{inlet} = W_{ch} = L_{bo} = W_{out}$, so that the only flow separation will be caused by bends.

3.6 Additional Tank Configurations

The results of the parametric study have yielded some guidelines for designing baffled contact tanks with maximum hydraulic efficiency. The best configuration in the parametric study was the benchmark case, which had 7 baffles and $L_{bo} = 0.2L_T$. The *BF*

for this design was 0.71. The guidelines from the parametric study show that the optimal *BF* will be achieved when a contact tank is designed with $W_{in} \approx W_{ch} \approx L_{bo}$. The configuration of the benchmark case was consistent with these guidelines. Thus, the only way to improve upon the benchmark configuration without altering the footprint or inlet conditions would be to change the direction and/or geometry of the baffles and the configuration of the baffle turns. Four new configurations were developed, and their design parameters and efficiency ratings are displayed in Table 7.

The possibilities for baffle layout for any given tank footprint are infinite, and since the purpose of this study was to define general guidelines for baffled contact tank design, we avoided incorporating complex geometries such as spiraling or rounded baffles. Wenjun *et al.* (2007) claim that the maximum *BF* is achieved when the number of turns in a tank is minimized. In order to minimize the number of turns in a tank with the benchmark footprint, we developed the long chamber geometry shown in Figure 22. In this configuration, $W_{in} \approx W_{ch} \approx L_{bo}$, and there are three turns rather than seven as in the benchmark case. The width of the baffles was decreased by approximately half in order to keep the tank to the same footprint, and L_T/W_{ch} was increased.

Contrary to our expectations, the *BF* of the long chamber model was not significantly different than that of the benchmark case. The long chamber model had a *BF* of 0.69, which when considering the accuracy of RANS models, is not significantly different than the *BF* of 0.71 of the benchmark case. The reduction in flow separation in the long chamber model caused by the reduction in the number of turns seems to be less than the increase in separation caused by narrowing the width of the baffles, which increased the sharpness (curvature) of the turns.

Table 7. Design parameters and efficiency ratings of additional tank configurations

Case Name	Independent Variables		Design Parameters				Efficiency					
	# baffles	L_{bo}/L_T	W_{inlet} / W_{ch}	L_T/ W_{ch}	L_{bo} / W_{ch}	L_{bo} / W_{inlet}	Volume (m^3)	TDT (s)	T_{10} (s)	BF	T_{90} (s)	T_{10}/T_{90}
Long Tank	3	0.1	1.00	9.50	1.00	1.00	0.94	800	553	0.69	1157	0.48
Clubbed Baffles	6	0.2	1.00	4.48	1.00	1.00	0.85	727	570	0.78	1041	0.55
Short Pipe	0	-	1.00	4.48	-	-	0.06	54	40	0.74	71	0.56
Long Pipe	0	-	1.00	238	-	-	1.00	855	779	0.91	970	0.80

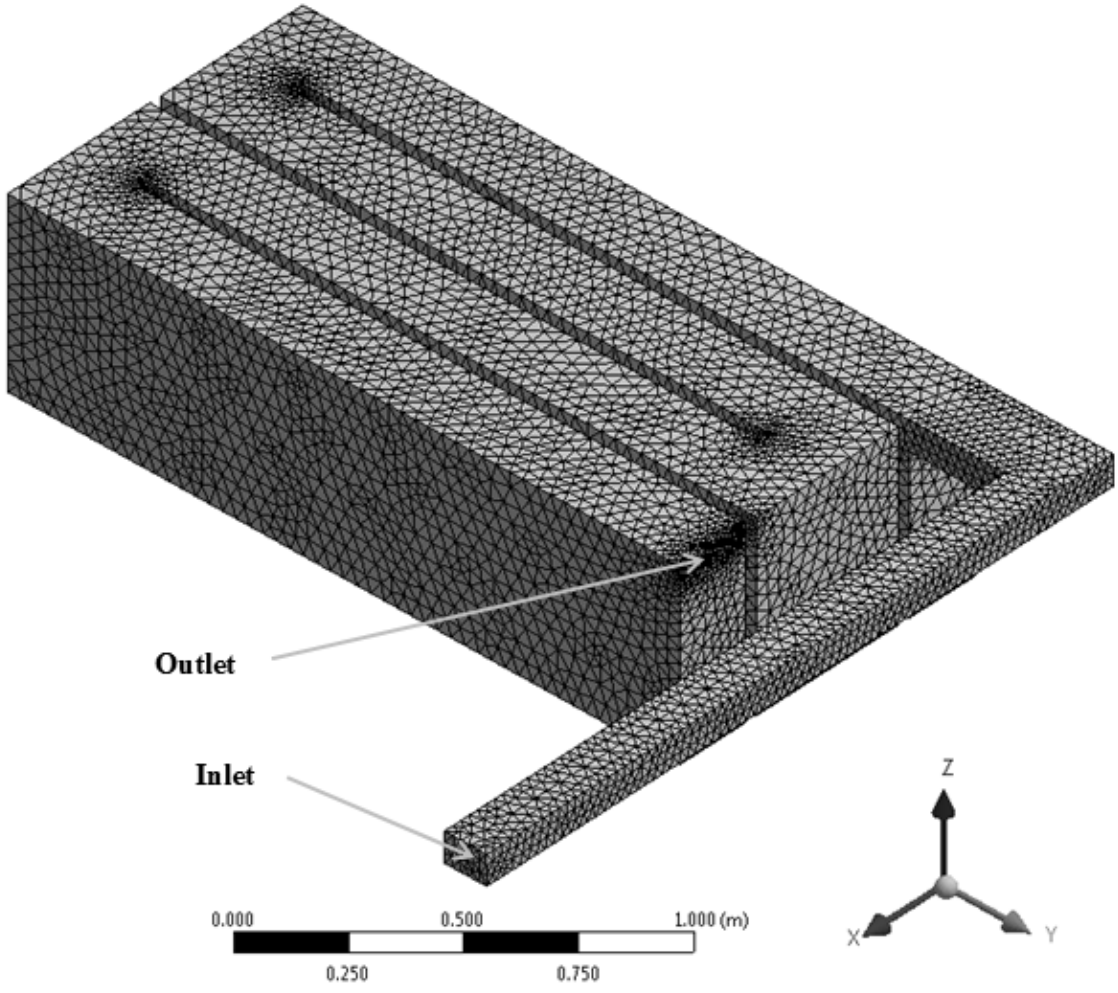

Figure 22. Long chamber model geometry and mesh

In order to explore the effect of the sharpness of turns on *BF*, we designed a tank that is illustrated in Figure 23 with "clubbed baffles." It has seventeen 90 corners as opposed to the seven 180 corners in the benchmark case. The *BF* of the configuration with clubbed baffles was 0.78, which represents a 10% increase in *BF* over the benchmark case. This demonstrates that the sharpness of turns around baffles in a contact tank can have a more significant effect than the number of turns in the tank. The "clubbed baffle" tank had the best *BF* of the tanks modeled in this study, and demonstrates the use of the design guidelines we have developed.

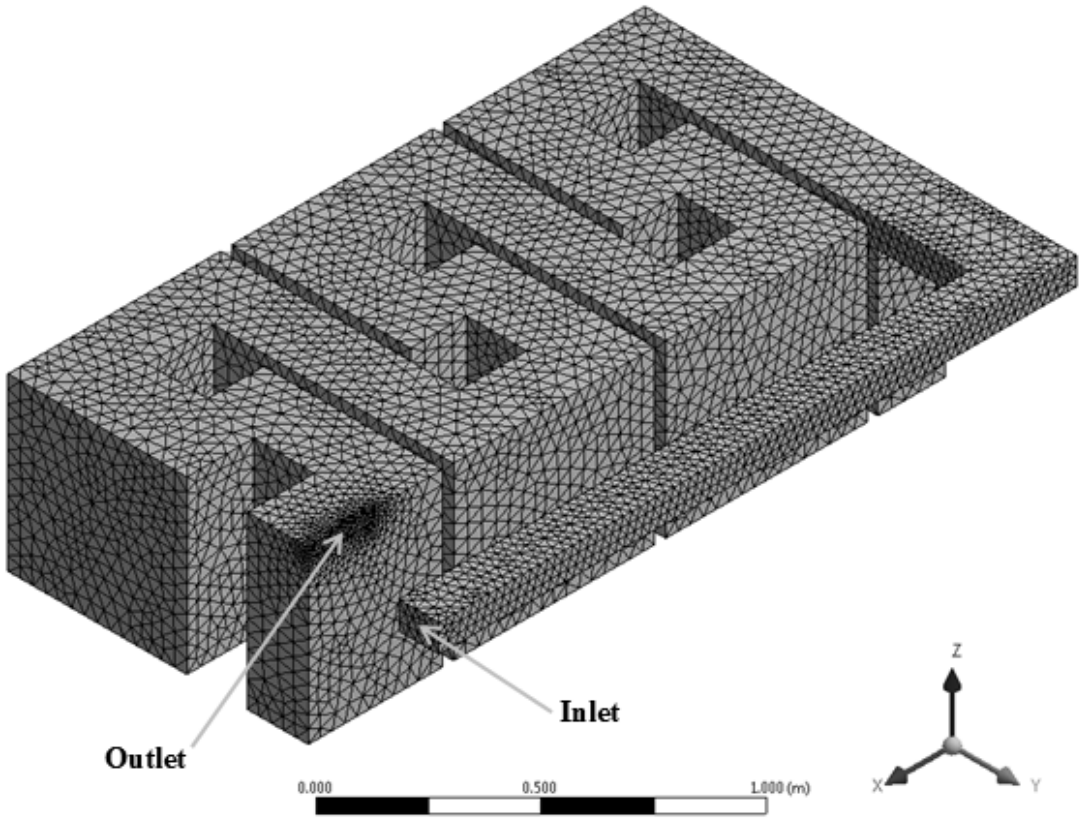

Figure 23. Clubbed baffle model geometry and mesh

3.7 Tank Efficiency

The primary quantification of tank efficiency used by water systems and regulatory systems is *BF*. In this section, we will address a quantification of efficiency based on T_{90}, which is the time it takes for 90% of a scalar concentration released at the tank inlet to reach the outlet, in addition to discussing the relationship between energy loss and hydraulic efficiency.

3.7.1 Tank Efficiency Rating

Currently, EPA guidelines regulate chlorine doses for contact tanks based on T_{10}, and the efficiency of tanks is described by *BF*. In this section, we will discuss the differences between required log-inactivation based on detention time, efficiency defined by *TDT*, and efficiency defined by the relationship between short circuiting and

recirculation. EPA concerns about tank efficiency are limited to T_{10}, while a designer or owner of a contact tank should be concerned about the behavior of the entire RTD curve. As we will illustrate, contact tanks can achieve high *BF* with low T_{10} values, high T_{10} values with low *BF*, or ideally, high *BF* and high T_{10} values. Designers should be aware of the implications of each of these possibilities. Table 8 shows the efficiency ratings of four tanks, as well the chlorine doses that would be necessary for 4-log inactivation of viruses in these tanks according to EPA guidelines for water treated at 7° C with a pH between 6 and 9. T_{90} as shown in Table 8 is the time required for 90 percent of the inlet concentration to travel through the tank to the residual sampling point, and will be introduced as a measure of efficiency.

Table 8. Tank efficiency ratings and required chlorine doses

Tank	T_{10} (s)	*TDT* (s)	T_{90} (s)	*BF*	T_{10}/T_{90}	Chlorine Dose for 4-log inactivation (mg/L)
(a.) Clubbed Baffle Tank	570	727	1041	0.78	0.55	182
(b.) Short Pipe	40	54	71	0.74	0.56	2615
(c.) Un-baffled Benchmark Tank	321	882	1693	0.36	0.19	322
(d.) Long Pipe	779	855	970	0.91	0.80	133

The tanks in Table 8 were chosen because they illustrate the extremes of efficiency in baffle tanks. The clubbed baffle tank (Figure 23) has the best *BF* of the tanks in this study that fit in the benchmark footprint. The "short pipe" tank (Figure 24) represents a tank in which the second section of the inlet configuration is extended for 1.995 m across the long dimension of the benchmark footprint. The un-baffled benchmark tank is simply the benchmark tank without any baffles. The "long pipe" tank is the only tank from Table 8 that does not fit in the benchmark footprint. The "long pipe"

tank represents a configuration in which the "short pipe" tank is extended 50 m such that the tank volume is similar to the tank volumes in this study (≈1m^3).

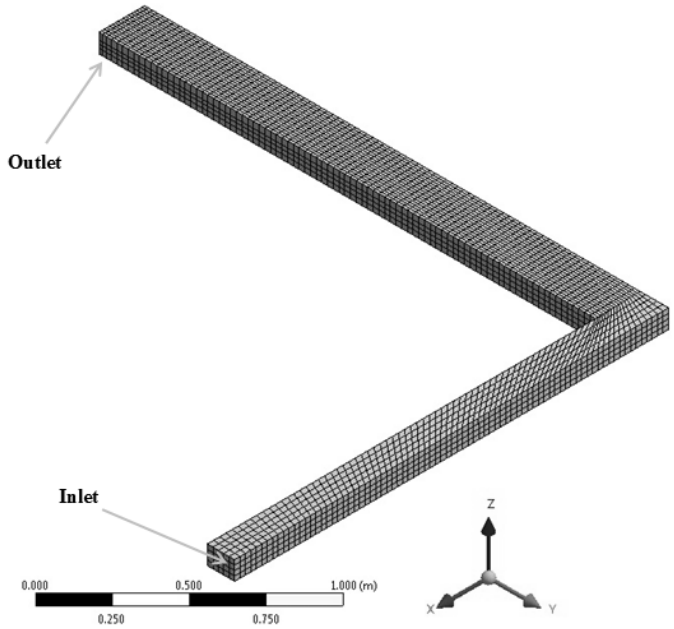

Figure 24. "Short Pipe" model geometry and mesh

Clearly, from a disinfection standpoint, the "long pipe" tank would be the best choice because it has the highest T_{10}, the highest *BF*, the highest ratio of T_{10} to T_{90}, and the lowest required chlorine dose, which corresponds to the lowest DBP risk. However, when you consider that the model is 1:8 scale, it becomes clear that the "long pipe" tank is an impractical choice because if built in full scale it would be 0.4 km long. The best practical configuration for disinfection is the clubbed baffle tank because it requires the lowest chlorine dose of the tanks that could be built practically. It is also has the best *BF* of the tanks that fit in the benchmark footprint. The "short pipe" configuration, shown in Figure 24, fits in the benchmark footprint and was modeled to show that adding too much baffling can decrease the disinfection capabilities of a tank by decreasing T_{10}, even while making the *BF* increase. The un-baffled benchmark case has a lower *BF* than

the “short pipe” tank, but a higher T_{10}, which shows that a lower chlorine dose can in some cases be used for tanks with lower *BF*.

T_{10}/T_{90} is an efficiency rating introduced by Wilson and Venayagamoorthy (2010) to illustrate the total efficiency of the tank. T_{10}/TDT is a good efficiency rating when considering disinfection, but since it does not reflect the upper half of the RTD curve, it neglects the full hydrodynamic behavior of the tank. T_{10}/TDT can be seen as a measure of short-circuiting because it shows the relationship between the times it takes the first 10% of fluid to pass through the tank compared to the amount of time ideal plug flow would take to travel through the tank. In the same light, T_{90}/TDT can be seen as a measure of recirculation. T_{10}/T_{90}, then, is an indicator of both short circuiting and recirculation, which is useful for designers and operators. According to USEPA, two tanks with the same T_{10} should be treated with the same dose of chlorine. The USEPA regulations are designed for disinfection, not for operational cost and hydrodynamic efficiency. If one of the tanks with identical T_{10} has a much higher T_{90}, the last 10% of treated water on the RTD curve in that tank will have a much higher log-inactivation than needed. This costly inefficiency is not apparent from the *BF*, so we suggest that T_{10}/T_{90} be used along with T_{10}/TDT to show the efficiency of contact tanks.

To illustrate the relationships between T_{10}, *TDT*, and T_{90} and their influence on *BF* and T_{10}/T_{90}, RTD curves were generated where the transient scalar transport was monitored in the benchmark 7-baffle model at each of the baffle openings, which are illustrated in white in Figure 25. The RTD curves measured at the baffle openings are shown in Figure 26. As the flow passes through each chamber in the 7-baffle tank, the time it takes to reach T_{10}, *TDT*, and T_{90} increases in consecutive baffles, as demonstrated

in Figure 27. *TDT* increases linearly throughout the compartments because it is a theoretical value based on the volume of the tank and the flow rate. Increases in T_{10} through consecutive compartments of the tank are accompanied by even greater increases in T_{90} (Figure 28). This explains why the increases in T_{10} plateau and the increases in *BF* flatten out in later compartments, as shown in Figure 29. The velocity contour in Figure 15 (b) shows that in early compartments the velocity profiles are not uniform and there are few areas of recirculation. In later compartments, dominant flow structures develop along with large recirculating areas represented by dead zones. The volume taken by these dead zones reduces the useable volume in each compartment and creates an upper limit for the *BF* of the tank.

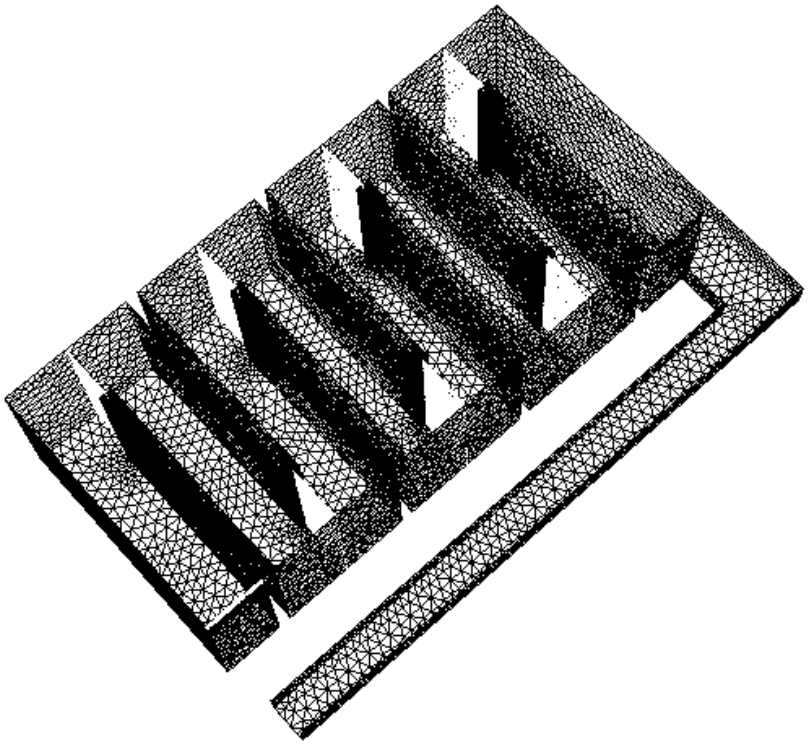

Figure 25. 7 baffle tank with baffle openings illustrated in white

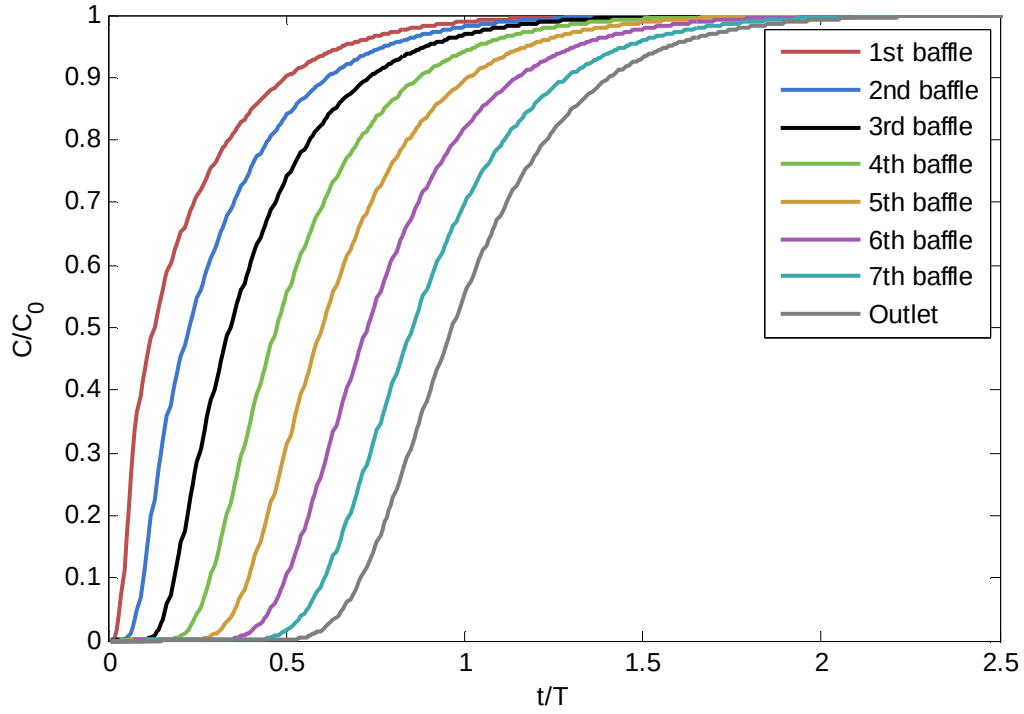

Figure 26. RTD curves measured at baffle compartment openings in 7 baffle tank

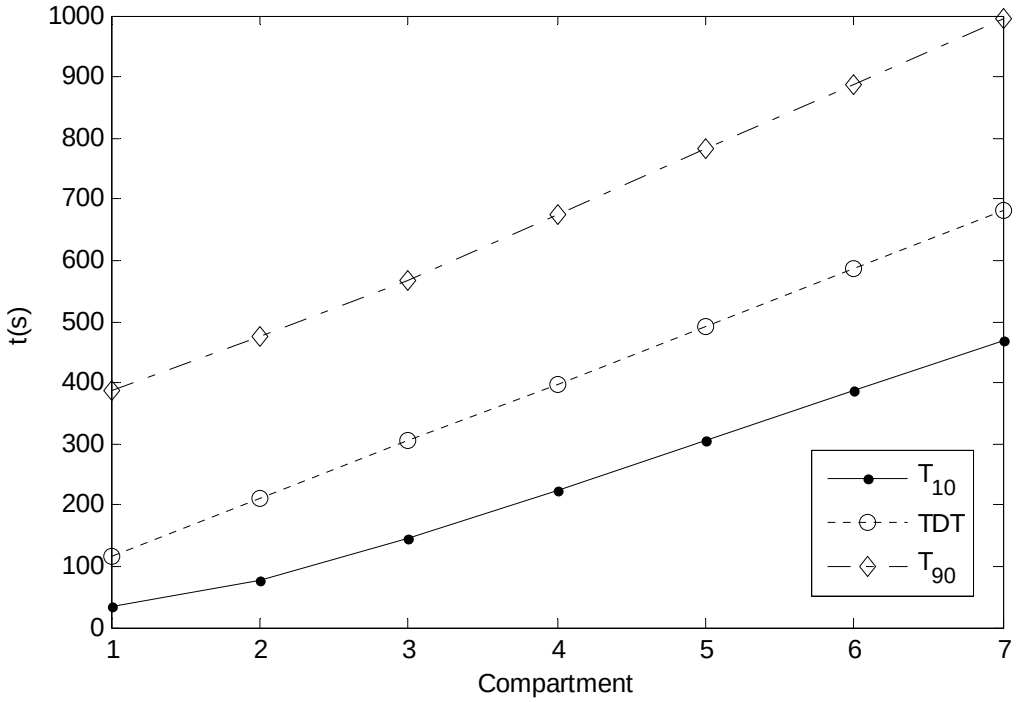

Figure 27. Comparison of T_{10}, *TDT, and* T_{90} measured at compartment openings

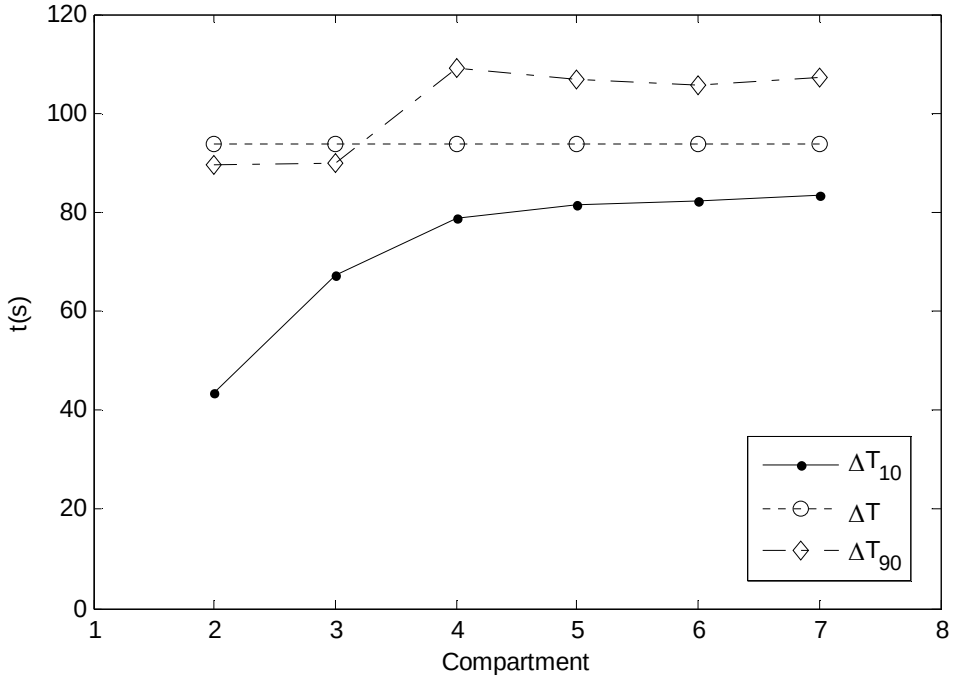

Figure 28. Comparison of ΔT_{10}, Δ TDT, and ΔT_{90} measured between consecutive compartment openings

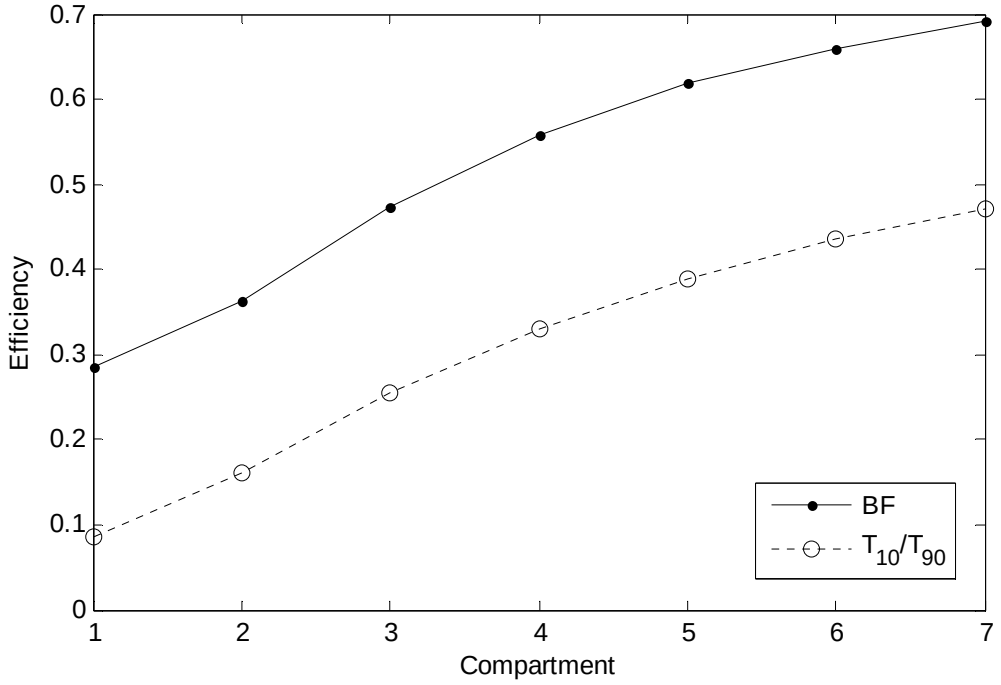

Figure 29. Comparison of *BF* and T_{10}/T_{90} as efficiency ratings at compartment openings

3.7.2 Energy Loss

The energy losses in a baffled contact tank will be primarily caused by contractions, expansions, bends, and friction losses. It seems that adding baffles to a tank will cause increases in energy loss due to friction and turns, and that the most efficient tanks will have high energy losses. In reality, adding baffles to an unbaffled tank will increase losses from bends and friction, but also decrease losses from expansions and contractions from the inlet to the first baffle chamber and from the last baffle chamber to the outlet. We find that there is no relationship between minimizing or maximizing energy loss and minimizing or maximizing *BF*. As illustrated in Figure 30, energy loss, represented by total pressure loss between the inlet and outlet of the tank, is actually minimized for the 7 baffle tank when L_{bo}/L_T = 0.3, where *BF* is good, but not at the maximum. Our results do not clearly indicate a direct relationship between *BF* and energy loss.

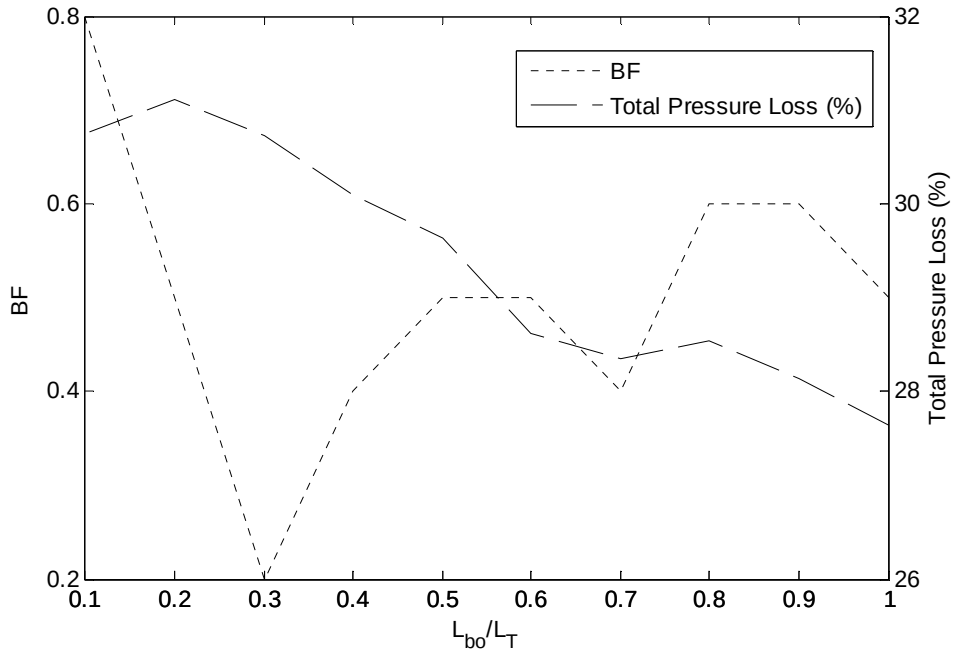

Figure 30. *BF* and total pressure loss as functions of L_{bo}/L_T for the 7-baffle tank

3.8 Conclusion

We have presented results from highly resolved three-dimensional CFD simulations of the flow dynamics and passive scalar transport in baffled disinfection contact tanks. The model of the benchmark tank configuration was verified using a FTC and a depth-averaged cross-sectional velocity profile from physical experiments. Our results indicate that the physical phenomena by which the flow in contact tanks deviates from plug flow are short circuiting, recirculation, and dead zones, and that these phenomena are caused by flow separation. The purpose of this study was to identify the characteristics of the most hydraulically efficient baffle tanks and define guidelines based on dimensional relationships for the design of the most efficient baffle tank configuration given a fixed inlet size and a fixed footprint.

The results of our parametric study show that the major causes of flow separation in contact tanks are the turns around the baffles and the expansions/contractions occurring at the inlet, baffle openings, and outlet. The dimensional relationships from this study that most affected hydraulic efficiency were W_{inlet}/W_{ch}, L_{bo}/W_{inlet}, and L_{bo}/W_{ch}, and these relationships were approximately equal to one in the most efficient tanks. Tanks with higher baffle numbers had higher *BF*s, which can be attributed to the higher length to width ratio of baffle chambers in tanks with higher numbers of baffles. *BF* was shown to increase as flow passed through each compartment of the 7 baffle tank. In later compartments of the 7 baffle tank, *BF* showed diminished increases, suggesting an upper limit to *BF* that will be dependent on tank configuration. The optimum value of L_{bo}/L_T will depend on the footprint of the tank and W_{inlet}, but for any serpentine baffle tank, L_{bo}/L_T should be less than 0.5 to prevent large dead zones between baffles. Our results

show that tank dimensions should be designed to satisfy $W_{inlet} = W_{ch} = L_{bo}$, so that expansions and contractions in the direction of flow will be minimized and plug flow conditions will be approximated. Baffle geometry should be designed to achieve an optimum balance between the sharpness and the number of turns. We have presented a new baffle tank design with "clubbed baffles" that is based on the guidelines developed from this study. The "clubbed baffle" tank fits in the benchmark footprint and has a *BF* of 0.78, which is 10% greater than the *BF* of the scaled model of the Embsay Chlorine Contact Tank.

Additional research concerning the size and orientation of inlets and outlets to baffle tanks and appropriate baffle configurations for cylindrical and other non-rectangular cuboid tanks is needed in order to more fully define the characteristics of optimal baffle tank design. Inlet configuration and the hydraulic efficiency of cylindrical tanks will be investigated in Chapter 4.

CHAPTER 4. MODIFIED STORAGE TANKS

4.1 Introduction

Chapter 3 showed that serpentine baffle tanks with the proper configuration can achieve *BFs* of 0.7. Serpentine baffle tanks are more economical than pipe loops, but they are usually still expensive. The cheapest contact tanks are off-the-shelf water storage tanks. They are usually only used by very small water systems because their *BFs* are on the order of 0.1. The purpose of the research in this chapter is to propose and test modifications for storage tanks that significantly increase *BF* by altering the inlet conditions so that the flow in the tank is approximately uniform. We seek the configuration that optimizes the area of flow such that the flow becomes uniform early on in the tank, i.e., close to the bottom. Uniform flow occurs when there is no separation or recirculation. The proposed modifications must be relatively inexpensive and easy to implement.

In serpentine baffled contact tanks, hydraulic efficiency is ensured by dividing the tank into compartments, where the tank is configured so that plug flow is approximated in each chamber of the tank. In this chapter, we use storage tanks modified to serve as contact tanks to illustrate that inlet conditions can be configured such that velocity profiles near the inlet are close to uniform. Since there are no obstructions in the tank, uniform flow at the bottom of the tank will lead to uniform flow throughout the tank. Thus, inlet modifications can serve as an alternative to baffles. We propose two types of modified inlets: diffusers and manifolds.

The storage tank used in this analysis is shown in Figure 31. The inlet is located in the sidewall of the tank, close to the bottom. The tank outlet is the pipe oriented in the

negative *x*-direction at the top of the tank. The general direction of flow in the tank, then, is upwards (in the positive *z*-direction). The problem with the standard single inlet is that it creates large recirculating flows in the tank that lead to short-circuiting and dead zones. The goal of the inlet manifold and inlet diffuser is to spread the momentum of the water coming from the inlets across the horizontal plane of the tank, and to ensure that the velocity distributions across horizontal cross-sections at all heights in the tank are more uniform than the horizontal velocity distribution measured at the inlet height.

The design parameters for the inlet diffuser and inlet manifold will be the number of inlets, the distribution of the inlets, and the height of the inlets (H_I) compared to the height of the water in the tank (H_T). H_I and H_T are illustrated in Figure 31, where the inlet has been pointed down and extended to the center of the tank. Tanks will be tested with 1, 4, 8, and 16 inlets at $H_I = 0.05H_T$, $0.1H_T$, $0.2H_T$, $0.4H_T$, and $0.75H_T$. These configurations will be tested at several flow rates in order to ensure that inlet design configurations can distribute flow evenly regardless of flow rate.

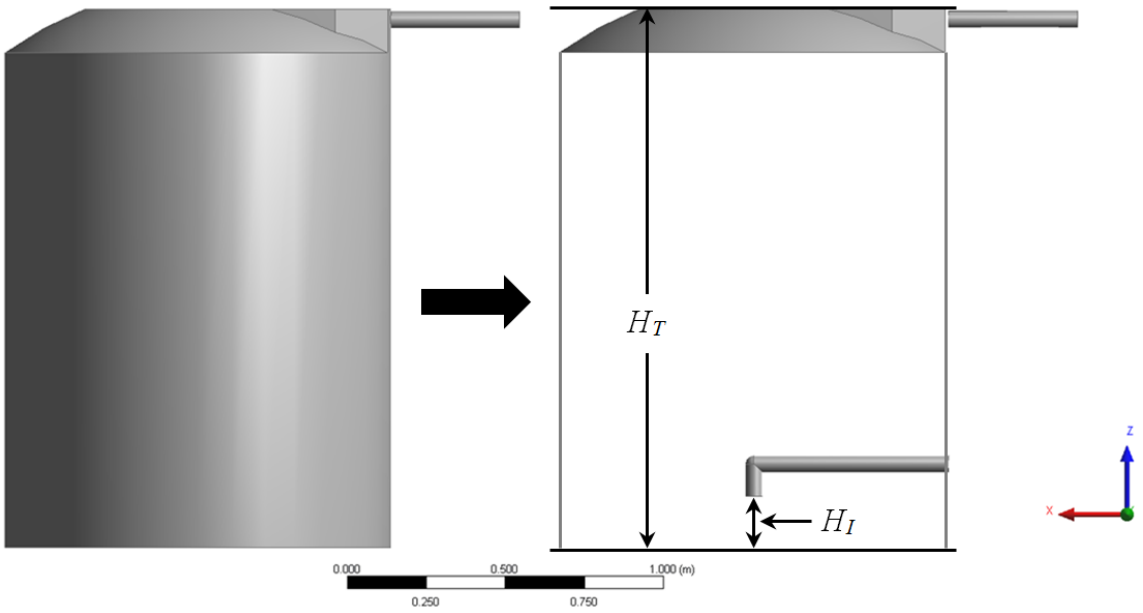

Figure 31. Tank geometry and definitions of height dimensions

The inlet diffuser and inlet manifold concepts are illustrated in Figure 32(a) and Figure 32(b), respectively. The layout of this chapter is as follows: Section 4.2 describes the CFD model development and validation for the study and the numerical methods used, Section 4.3 explains the configurations of the various tank designs, Section 4.4 illustrates the results of the parametric study of inlet configurations, Section 4.5 describes the effects of flow rate on hydraulic efficiency in modified storage tanks, and Section 4.6 summarizes the findings.

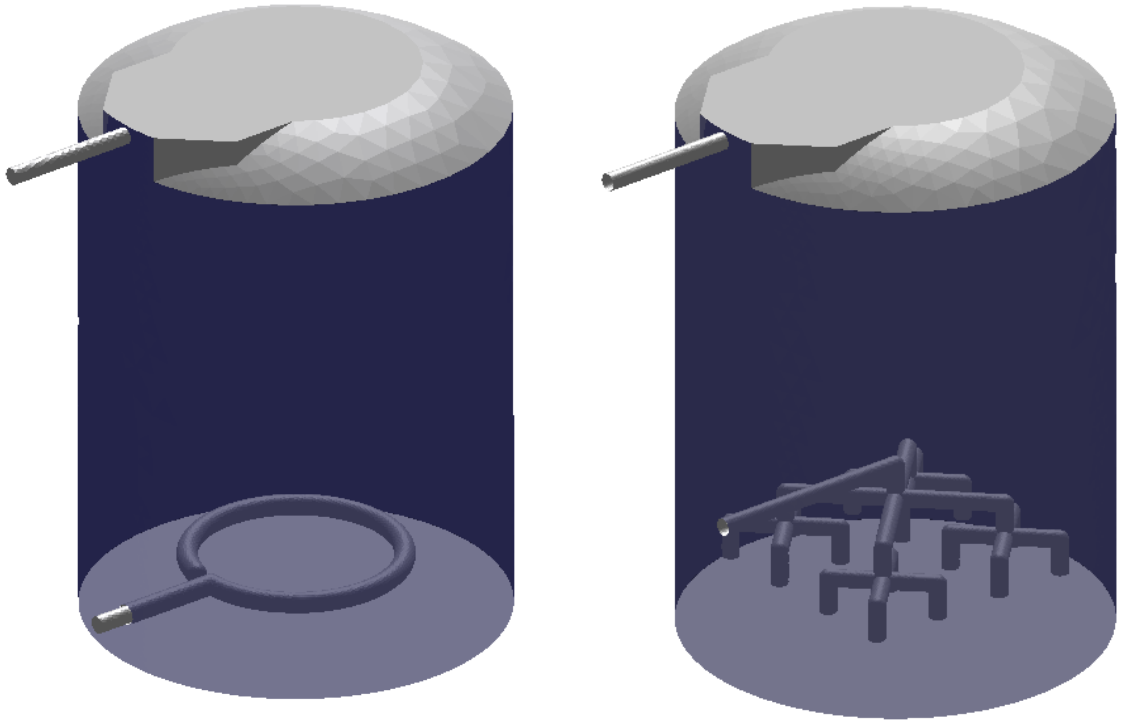

(a) (b)

Figure 32. (a) Inlet diffuser, where flow enters the tank through holes drilled in the bottom of the circular pipe, and (b) 16-inlet manifold

4.2 Model Development and Numerical Methodology

4.2.1 Numerical Methodology

The setup in ANSYS FLUENT used to model the serpentine baffle tanks (see Chapter 3) was also used to model the modified storage tanks. The only difference was that the κ-ε RNG turbulence model was used to model the turbulence in the modified storage tanks. The κ-ε RNG turbulence model was chosen based on a parametric study of turbulence models. It was chosen because it had the fastest solution time of the models that provided solutions that matched the validation study.

4.2.2 Single-Phase Modeling vs. Multi-Phase Modeling

Although there is a free-surface in the storage tank because the outlet pipe is below the top of the tank, the parametric study of inlet manifolds was done using a single-phase model with a wall boundary condition representing the free-surface of the water. An accurate multi-phase model for the momentum in the tank was developed for the study, but the scalar transport solution time was 100 times longer for the multi-phase model than for the single-phase models and was inaccurate, so the multi-phase model was not used to calculate scalar transport. The multi-phase model was used without scalar transport to calculate the height of the free-surface of the water in the tank at the modeled flow rate. The free-surface height from the multi-phase model was then used to delineate the free-surface in the single-phase model using a wall boundary condition, as shown in Figure 33 (a) and (b). The calculated free-surface height of the water in the tank was 1.7 m. Validations showed that the steady-state velocity fields calculated using the multi-phase model, a single-phase model with a wall boundary condition for the free-surface, and a single-phase model with a symmetry boundary condition for the free-surface were

all very similar. The solvers in FLUENT converged more quickly with the wall boundary condition than with the symmetry boundary condition, so the wall boundary condition was used in the parametric study of inlet configurations.

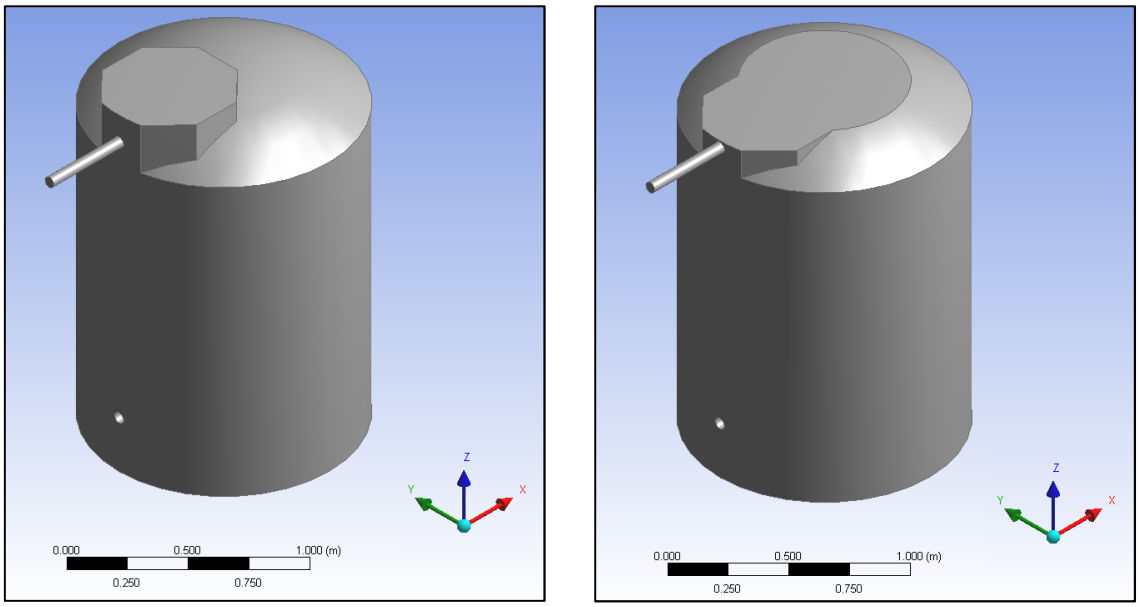

(a) **(b)**

Figure 33. (a) Modified tank configuration (b) modified tank configuration with free-surface set as a rigid-lid.

4.2.3 Geometry and Grid Generation

The validation case used in this study was based on the physical geometry of the vertical cylindrical modified storage tank modeled by Wilson and Venayagamoorthy (2010). The diameter of the validation tank was 1.22 m and the height of the tank, H_T, was 1.83 m. The center of the inlet pipe was 0.11 m above the bottom of the tank. The inlet pipe extended 10 cm into the tank, turned 45 degrees downwards, and then extended 10 cm. The center of the outlet pipe was 1.67 m above the bottom of the tank. The validation tank, which hereafter will be referred to as the benchmark tank because it represents a typical inlet configuration for tanks currently in use, is shown in Figure 34.

The side wall of the tank, shown in blue, is shown as transparent so that the inlet is visible.

The geometry of the benchmark case was used for the walls and outlet of all cases in the parametric study of tank designs. Variations in H_I and the number of inlet manifolds were the only changes made to the benchmark geometry.

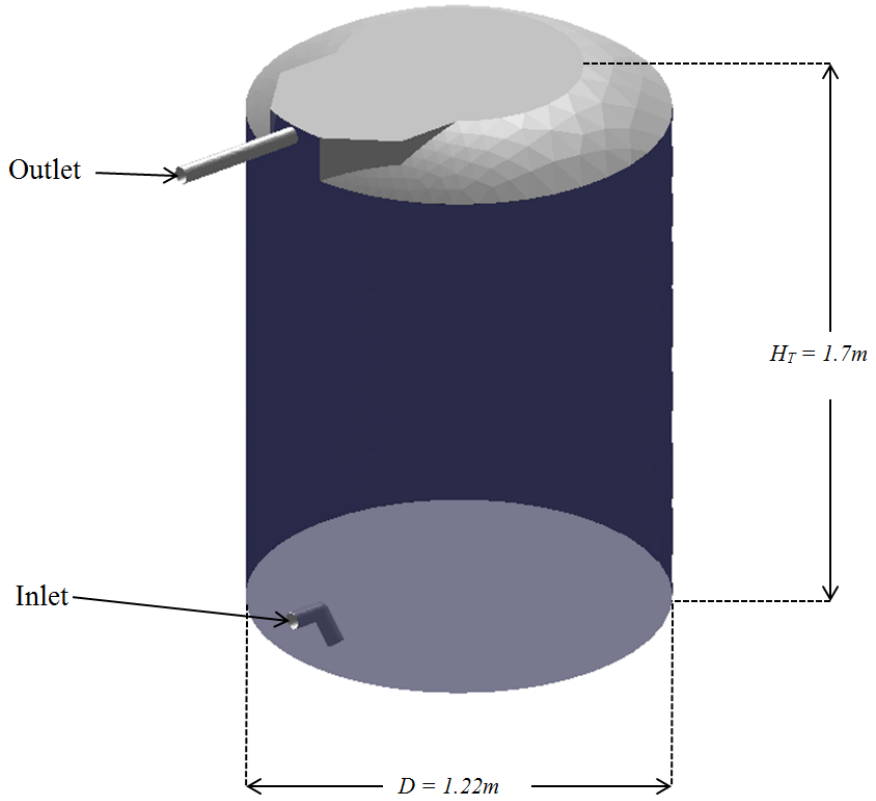

Figure 34. Tank geometry for validation (benchmark) case

4.2.4 Time Step Selection

Implicit solvers, which are computationally stable at any time step, were used in FLUENT to simulate the modified storage tanks. The time step selection then had no effect on the stability of the solutions, but only affected the temporal resolution of the transient scalar transport. A parametric study of time steps for the verification CFD case was performed using time steps of 0.1, 1, and 10 seconds. All time steps performed well,

but the 10-second time step skipped over some of the small variations in scalar concentration measured at the outlet. The 0.1 and 1-second time steps both showed sufficient resolution of the scalar variation at the outlet. Since computational time was a constraint in this study, and the 1-second time step took $1/10^{th}$ as long as the 0.1-second time step to compute the solution, the 1-second time step was chosen for the study.

4.2.5 Mesh Development and y^+

Since the parametric study of inlet configurations involved many different geometries, it was important to discover a mesh setup that would yield appropriate skewness, orthogonal quality, and y^+ values for the meshes of all of the geometries. The enhanced wall function was used in FLUENT, so the y^+ values needed to be less than 5. Inflation layers were used in ANSYS Mesh to place points very close to the walls. The first inflation layer was 1 mm thick. There were a total of 5 inflation layers with a growth rate of 1.1. Meshes ranged in size from 260,000 cells for the validation case to 2.5 million cells for the 16-inlet configuration. The inflation layers ensured that appropriate y^+ values were seen in all cases.

4.2.6 Model Validation

The model was validated using experimental data from Wilson and Venayagamoorthy (2010). The steady-state velocity field in the geometry of the validation case was modeled at a flow rate of 0.000946 m^3/s (15 gpm). Once the solution of the steady-state velocity field converged, a scalar concentration of 1 was introduced at the inlet and the outlet concentration was monitored. The model was run for 10,000 seconds. The *TDT* of the tank at the modeled flow rate was 2050 seconds. T_{10} was measured as 324 seconds, yielding a *BF* of 0.16. As seen in Figure 35, the RTD curve of

the physical model and the validation CFD model match very closely. Velocity measurements were not used in this validation because there are no available velocity data from the physical experiment.

Mesh refinement was not possible because of computational restrictions and was not necessary due to the very low y^+ values at the walls. Mesh independence was tested using a coarser mesh with no inflation layers. The CFD model run with the coarse mesh yielded an RTD curve that almost exactly matches the CFD model with the inflated mesh (Figure 35). Computational time could have been decreased by using the mesh without inflation layers, but because the inlet configuration was altered significantly in the parametric study of inlet manifolds, we deemed it prudent to keep the inflation layers to avoid any numerical errors caused by inappropriate y^+ values in cases where the inlet configuration changed the velocity magnitude near the walls.

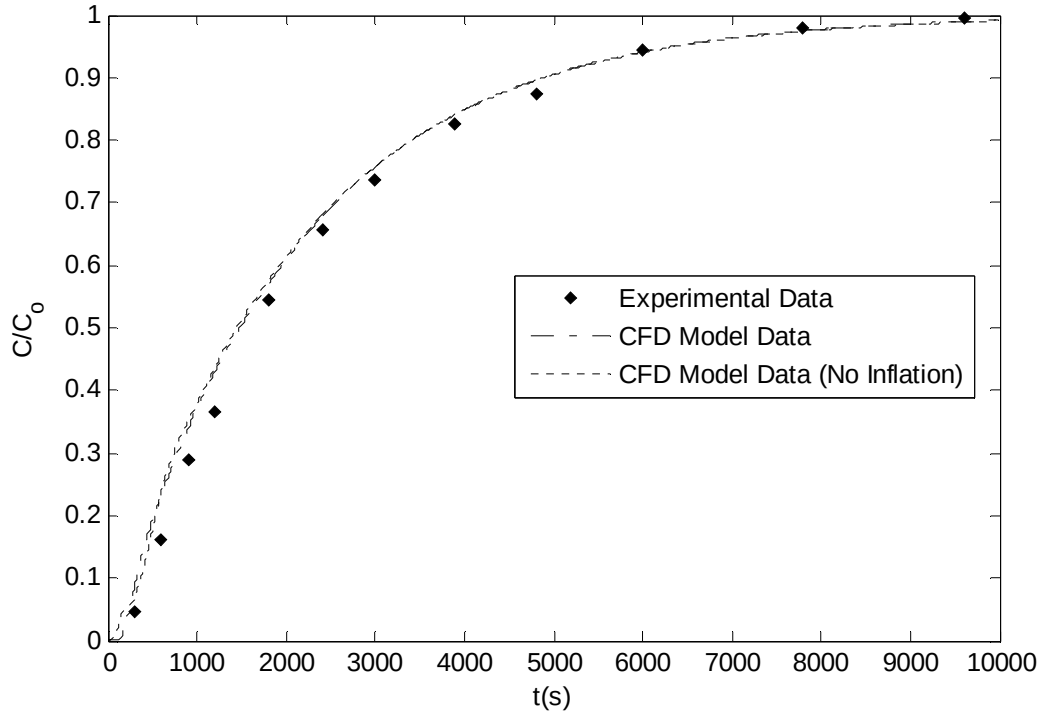

Figure 35. RTD curves of physical and CFD models of the validation case

4.3 Tank Design

The goal of contact tank design for any system is to create plug flow. In pipe loops, this is achieved by ensuring that the pipe length between turns is significantly larger than the pipe diameter. In serpentine baffle tanks, plug flow is approached when the length to width ratio in each baffle chamber is much greater than 1 and when contractions and expansions are minimized by setting the inlet width, the baffle opening length, and the width of the baffle chambers to the same dimension.

The approach we will take to create plug flow in the storage tanks is to modify the inlet conditions so that the velocity distribution is close to uniform across the entire diameter of the tank as soon as the flow leaves the inlet(s). In order to illustrate the conditions we are trying to create at the inlet of the tank, we present a design that could be utilized to create near perfect plug flow at the inlet. This design is impractical, and only serves to represent the conditions we are trying to create.

A typical water supply pipe used for the tank sizes we are investigating is 5 cm in diameter. The tank diameter is 1.2 m. To create conditions in which the flow would be truly uniform at the tank inlet, pipe expansions could be used to expand the 5 cm pipe to 1.2 m in diameter. This would require a large number of expansions. The 1.2 m inlet pipe would then have to be long enough to allow the turbulent mixing caused by the expansions to subside. The uniform flow in the 1.2 m pipe could then be introduced into the contact tank through the tank bottom, which would serve at the inlet. The top of the tank would serve as the outlet and release into another pipe that is 1.2 m in diameter. The diameter of this pipe would then be contracted from 1.2 m to 5 cm.

The expansion joints, contraction joints, and length of extra pipe required for this setup would cost many times the cost of the actual tank, making this design totally impractical. The idea of this setup is not a consideration for an actual design, but it serves to show the configuration of an idealized modified storage tank because it allows plug flow at the inlet of the tank. This setup was modeled in FLUENT in order to show the best possible scenario for a modified storage tank. The expansions and contractions were not necessary in the model because the bottom of the tank was set as an inlet with uniform velocity distribution and the top of the tank was set as an outlet, as shown in Figure 36. The *BF* was 0.78, which shows that even with ideal inlet conditions, the low length to width ratio of the storage tank limits the hydraulic efficiency.

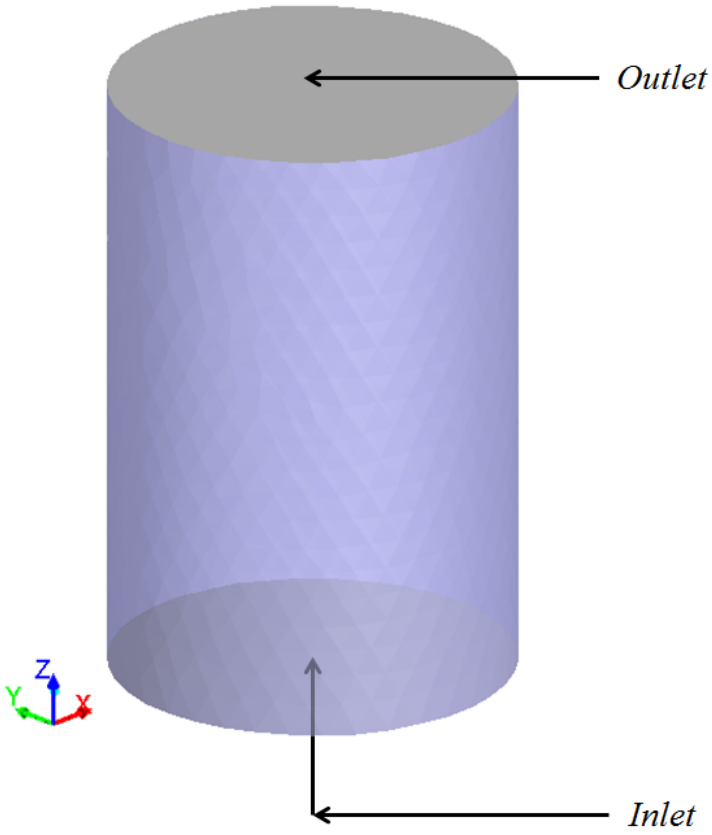

Figure 36. Ideal configuration, *BF* = 0.78

We suggest that the practical approach to attempt to recreate the conditions in the idealized tank is to use many inlets to the tank at the bottom of the tank. We hypothesize that outlet conditions will be less critical to plug flow than the inlet conditions, so the outlet used in our study will be the same as the one used in the benchmark case. In order to set a benchmark for the best possible inlet configuration, we tested a tank with the inlet set as the bottom of the tank with uniform velocity and the outlet set the same as the benchmark tank. The *BF* for this configuration was 0.63, which serves as the practical limit of the hydraulic efficiency of the benchmark tank with inlet modifications. The addition of the benchmark outlet to the idealized configuration decreased *BF* by 0.15, which is significant. However, the addition of the benchmark inlet and outlet to the idealized configuration decreased the *BF* by 0.62, showing that inlet conditions have a greater effect on *BF*. Outlet conditions are important and present a subject for further research, but were outside the scope of this work.

Two methods will be used to separate the flow from the inlet pipe so that it comes into the tank through many different inlets. First, a diffuser will be designed and modeled based on sewage outfall manifolds. The diffuser will be a pipe that is the same diameter as the supply pipe and that has holes drilled into it. The water will flow into the tank through this pipe and enter the interior of the tank through the holes in the pipe. A design criterion will be followed such that the same magnitude of flow comes through each hole in the pipe. The second design technique will utilize an inlet manifold. The inlet manifold will create multiple inlets by using T-joints and/or 4-way junctions inside the modified storage tank to divide the flow from the water supply pipe into multiple inlet pipes. The diameter of the supply pipe and the inlet pipes in the manifolds will be 5 cm.

4.3.1 Inlet Diffuser

A prototype design for an inlet diffuser was developed with 8 inlet ports. The inlet height was 0.11 m. In order to ensure that the same flow rate came from each of the 8 holes in the pipe, the holes had to be 1 cm in diameter (please consult Roberson *et al.* (1998) for the design protocol used to determine that 1cm holes would create equal flow rates from the 8 inlet ports at the modeled flow rate). This design caused the velocity of the water leaving each of the holes to be very high (1.7 m/s), which led to short circuiting in the tank. The *BF* of the prototype design tested in FLUENT was 0.13, which was lower than that of the benchmark case.

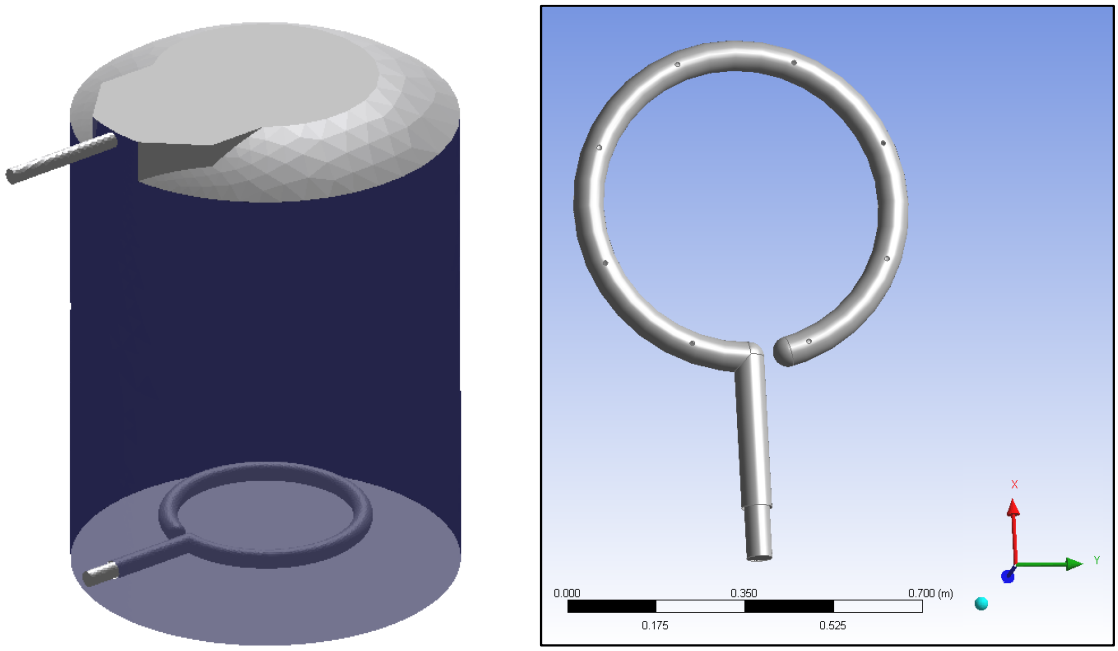

(a) (b)

Figure 37. Inlet diffuser (a) shown through the side wall of the tank and (b) shown from underneath

The inlet diffuser worked as designed because equal flow rates came out of each hole in the pipe, as seen in Figure 38, but the high velocities at the inlets caused the inlet

diffuser design to be inefficient even though the inlet locations were fairly evenly spread throughout the tank. The inlet diffuser design was not refined or tested further because of its poor performance in comparison with successful initial testing of the inlet manifolds. In hindsight, this is not surprising, since such diffusers enhance/promote more mixing. On the other hand, the use of inlet manifolds with dividing flows will serve to reduce the turbulent mixing and promote plug flow.

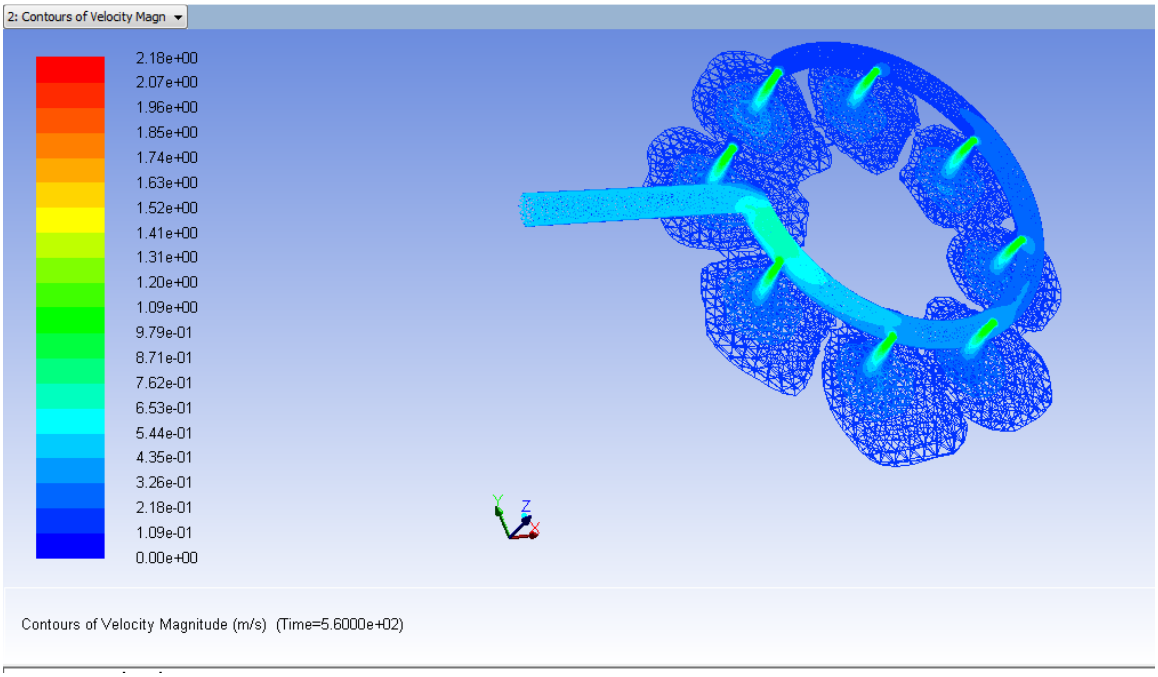

Figure 38. Equal flow entering tank from each of 8 inlets

4.3.2 Inlet Manifold

We hypothesize that two parameters, number of inlets and H_I, will control the efficiency of scalar transport in a tank with an inlet manifold.

4.3.2.1 Number of Inlets

The number of inlets was set to 1, 4, 8, and 16. The purpose of the inlet manifold is to reduce the cross-sectional average velocity at the inlet. The inlet diameter and pipe diameter throughout the manifold were kept constant so that the number of inlets and the

inlet velocity at each inlet would be inversely related. The distribution of the inlets across the horizontal plane of the tank was accomplished with a different inlet manifold configuration for each number of inlets.

4.3.2.2 Flow Rate

In the serpentine contact tank benchmark case discussed in Chapter 3, the *BF* was independent of flow rate. We hypothesize that in the modified storage tanks, flow rate will affect *BF* because the inlet diameter(s) are much smaller than the tank diameter and the momentum at the inlet will affect the flow patterns in the tank. In order to test how large the effect of flow rate on *BF* will be, two flow rates will be used in this study; one flow rate will be a typical flow rate and the other will be a higher flow rate. The validation tank has a volume of two cubic meters (approximately 500 gallons). A typical flow rate through a tank this size is 0.000946 m^3/s (15 gpm). The high-end flow rate seen in a tank this size is 0.001892 m^3/s (30 gpm). The flow rates (Q_{total}) used in the study of inlet manifolds will be Q = 0.000946 m^3/s and $2Q$ = 0.001892 m^3/s.

4.3.2.3 Inlet Boundary Conditions

The turbulent kinetic energy (κ) and turbulent dissipation (ε) are specified at the inlet based on the turbulence intensity (I) and turbulence length scale (l). I is calculated as

$$I = 0.16 * Re^{-1/8}, \qquad (9)$$

where $Re = V_{inlet} * D_{inlet} / v_{water}$, D_{inlet} = inlet diameter = 5 cm, v_{water} = 10^{-6} m^2/s, and $Vinlet$ is calculated as

$$V_{inlet} = \frac{Q}{A} = \frac{Q_{total}}{A_{inlet} * \#inlets}. \qquad (10)$$

Turbulence length scale is calculated as

$$l = 0.07 * D_{inlet} . \quad (11)$$

κ is calculated as

$$\kappa = \frac{3}{2}(V_{inlet} * I)^2. \quad (12)$$

ε is calculated as

$$\epsilon = C_{\mu}^{3/4} * \frac{\kappa^{3/2}}{l} . \quad (13)$$

The inlet velocities and turbulent kinetic energy and dissipation specified at the inlet for each manifold configuration for flow rates of *Q* and 2*Q* are shown in Table 9 and Table 10, respectively. The equations used to calculate the turbulence kinetic energy, turbulence dissipation, turbulence intensity, and turbulence length scale are from ANSYS Inc. (2010).

Table 9. Inlet variables for models run at *Q* (Q_{total} = 0.000946 m3/s)

# Inlets	V (m/s)	κ (m^2/s^2)	ε (m^2/s^3)
1	0.4688	0.0006796	0.0008202
4	0.1172	6.007E-05	2.155E-05
8	0.0586	1.786E-05	3.494E-06
16	0.0293	5.309E-06	5.664E-07

Table 10. Inlet variables for models run at *2Q* (Q_{total} = 0.001892 m3/s)

# Inlets	V (m/s)	κ (m^2/s^2)	ε (m^2/s^3)
1	0.9375	0.0022858	0.0050598
4	0.2344	2.020E-04	1.330E-04
8	0.1172	6.007E-05	2.155E-05
16	0.0586	1.786E-05	3.494E-06

4.3.2.4 Inlet Manifold Configurations

We hypothesized that the hydraulic efficiency of the modified storage tank would be best when the inlet or inlet manifold was pointed down and was centered in the tank. For each number of inlets, the distribution of the inlets across the horizontal plane of the

tank needed to be different in order to maximize the distribution of flow from the inlets across the tank. The approach taken in this study to ensure that the same flow rate came out of each inlet in the manifold was to ensure that the distance traveled between the water supply pipe and the inlet at the end of every manifold was the same, and that the number of pipe bends and the distances between pipe bends along the path traveled through each section of the manifold was the same.

For the case with 1 inlet, the inlet was placed in the center of the tank, as shown in Figure 39. For the case with 4 inlets, a four-way junction was added to the 1-inlet configuration. The pipes that led radially outwards from the junction were half the radius of the tank in length. At the end of these pipes, there was a 90 degree downwards bend that led into a 10 cm section of pipe that opened into the tank. The 4-inlet configuration is shown in Figure 40.

The goal of the inlet manifold was to spread the flow from the inlet around the diameter of the tank so that the flow approaches plug flow. For the 1-inlet and 4-inlet configurations, the optimal distribution of the inlets across the x-y plane was fairly self-suggestive, but the ideal distribution of inlets for the 8-inlet configuration was more difficult to design.

The design that was chosen for the 8-inlet configuration meets both of the design criteria in that equal flow should come from all inlets and spatial distribution is maximized. As seen in Figure 41, if the jets coming from each inlet section spread equally, the distance between each jet and the closest obstruction to it, be it another jet or a wall, will be equal. The 8-inlet manifold design was generated by adding two-way branches to each of the outlets of the 4-inlet manifold. The two-way branches were

rotated 45 degrees in the x-y plane. The pipes coming out of each of the four two-way branches were 16.3 cm long.

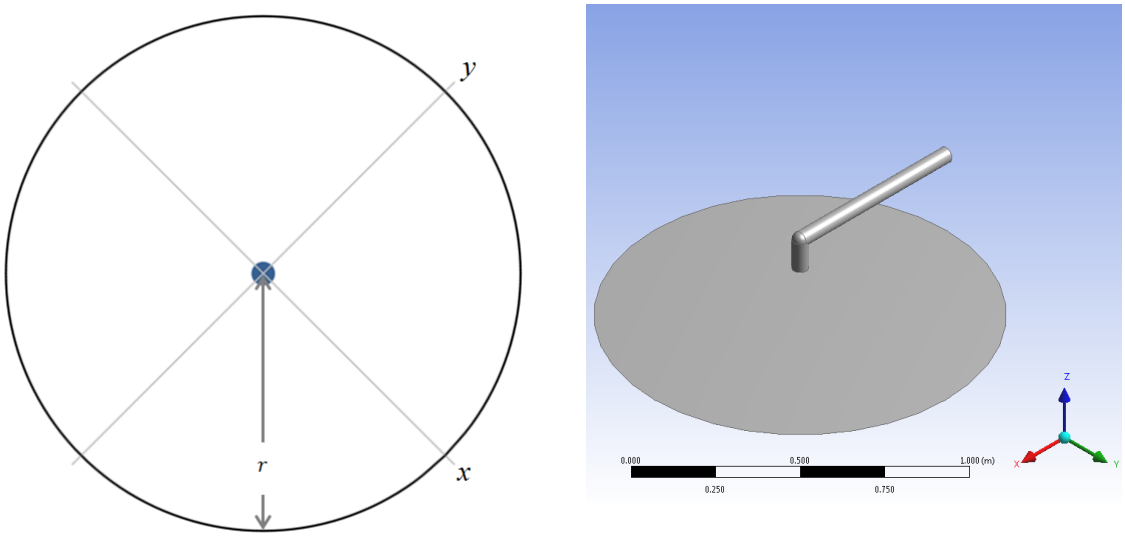

(a) (b)

Figure 39. 1 inlet configuration (a) top view with inlet in blue (b) view of inlet with the side wall of the tank hidden

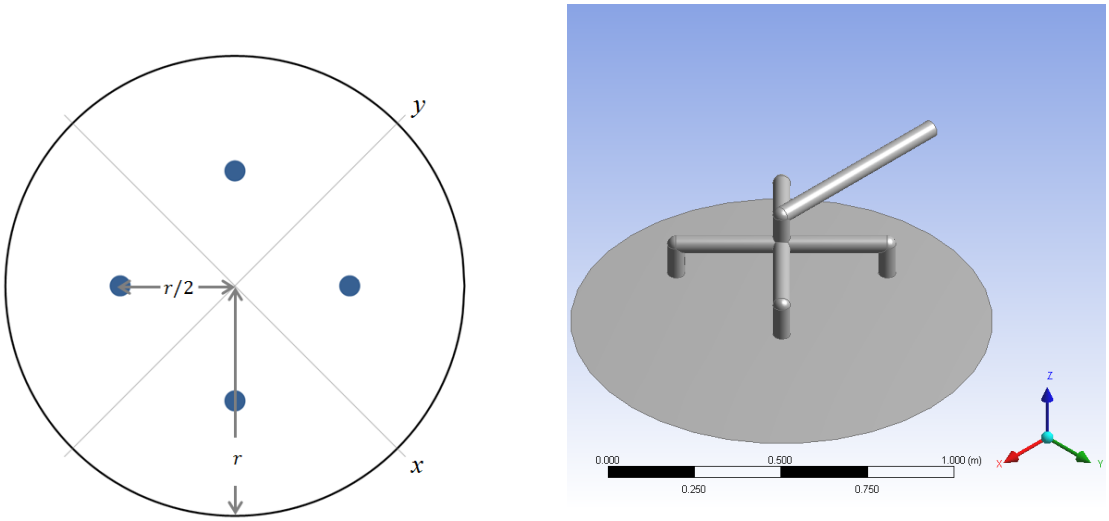

(a) (b)

Figure 40. 4 inlet configuration (a) top view with inlets in blue (b) view of manifold with the side wall of the tank hidden

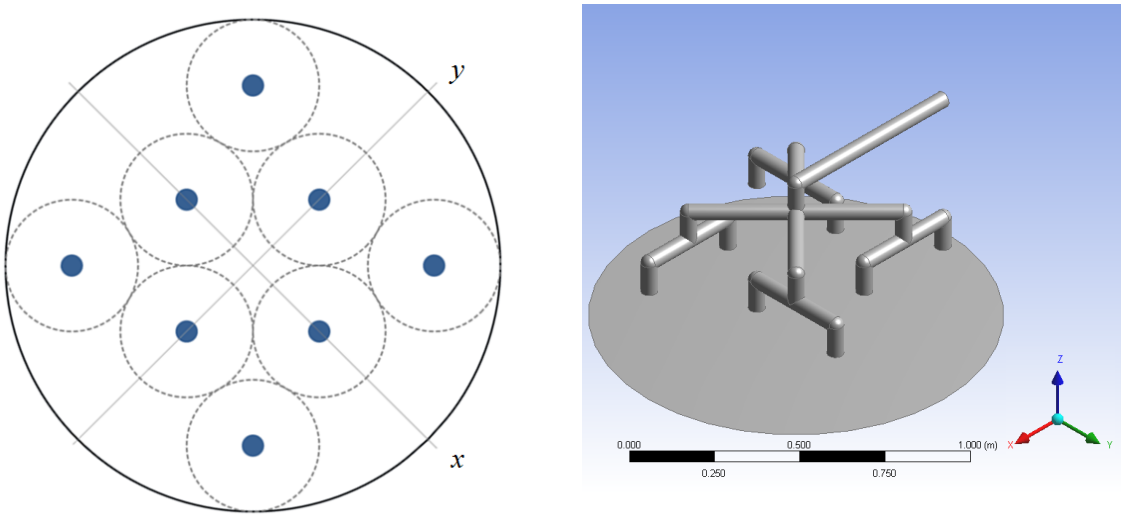

(a) (b)

Figure 41. 8 inlet configuration (a) top view with inlets in blue (b) view of manifold with the side wall of the tank hidden

The coordinates of the center of each of the inlets in the 8-inlet configuration in the x-y plane are shown in Table 11.

Table 11. Coordinates of the center of the inlets in the x-y plane for the 8-inlet configuration

Inlet	x(m)	y(m)
1	-0.446	0.000
2	-0.163	-0.163
3	-0.163	0.163
4	0.000	0.446
5	0.000	-0.446
6	0.163	-0.163
7	0.163	0.163
8	0.446	0.000

The 16-inlet manifold, displayed in Figure 42, was generated by adding 4-way branches to each of the outlets of the 4-inlet manifold. The pipes attached to the 4-way branches were one quarter of the radius of the tank in length. A 90 degree downward

bend at the end of each of these pipes led to a 10 cm pipe that discharged into the main volume of the tank.

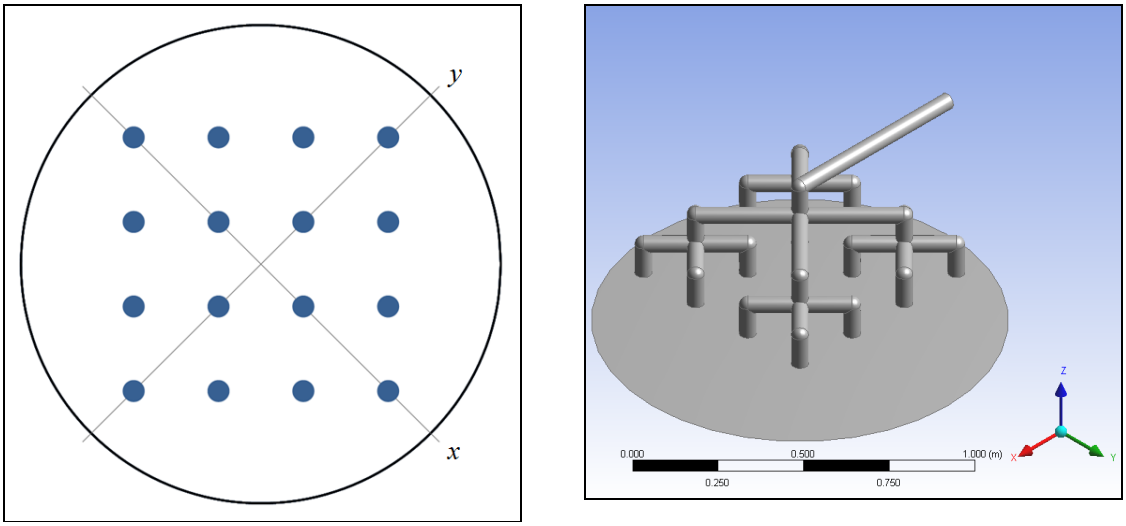

(a) (b)

Figure 42. 16 inlet configuration (a) top view with inlets in blue (b) view of inlets with the side wall of the tank hidden

The coordinates of the center of each of the inlets in the 16-inlet configuration in the x-y plane are shown in Table 12.

Table 12. Coordinates of the center of the inlets in the x-y plane for the 16-inlet configuration

Inlet	x(m)	y(m)	Inlet	x(m)	y(m)
1	-0.457	0.000	9	0.000	-0.152
2	-0.305	-0.152	10	0.000	-0.457
3	-0.305	0.152	11	0.152	0.000
4	-0.152	0.000	12	0.152	-0.305
5	-0.152	-0.305	13	0.152	0.305
6	-0.152	0.305	14	0.305	-0.152
7	0.000	0.457	15	0.305	0.152
8	0.000	0.152	16	0.457	0.000

4.3.2.5 Height of Inlet(s)(H_I)

The height of the inlet in the tank should affect how far the jet coming from the inlet can spread horizontally before it hits the bottom of the tank. We hypothesize that there will be an ideal inlet height that allows the jets coming from the inlet manifold to spread laterally until they intersect adjacent jets or approach the sidewall of the tank just as they reach the bottom of the tank. H_I will be modeled at five locations: 5%, 10%, 20%, 40%, and 75% H_T.

4.4 Inlet Manifold Parametric Study Results

The results of the parametric study show that at the normal and high operating flow rates, *Q and 2Q*, the *BF* of the modified storage tank was best with the 16-inlet configuration. At both the normal and high flow rates, *Q* and *2Q*, the *BF* is best when H_I is between $0.1H_T$ and $0.2H_T$. As predicted, the *BF* was dependent on flow rate, but in most cases the difference between *BFs* at different flow rates was less than 0.1.

4.4.1 Results at $Q_{total} = Q$

The contact tank modeled with a 16-inlet manifold configuration with the outlets located at $H_I/H_T = 0.1$ had a *BF* of 0.51, which was the highest *BF* measured in the study when $Q_{total} = Q$, and was 220% more efficient than the benchmark case. For the 1-inlet configuration, the *BF* when $H_I = 0.2H_T$ was 42% higher than the *BF* for the benchmark case. This validates our assumption that moving the inlet to the center of the tank and pointing it downwards causes more hydraulically efficient flow patterns in the tank than the setup of the benchmark case. The *BFs* for all cases are shown in Table 13.

Table 13. *BFs* for $Q_{total} = Q$

BF (Q = 0.000946 m3/s)				
H_I/H_T(%)	1 Inlet	4 Inlets	8 Inlets	16 Inlets
5	0.21	0.18	0.19	0.37
10	0.18	0.26	0.17	0.51
20	0.23	0.17	0.34	0.37
40	0.10	0.12	0.27	0.29
75	0.15	0.22	0.15	0.11

The *BFs* for all cases are also plotted in Figure 43. The *BF* of the validation case with the standard inlet (*BF* = 0.16) and the idealized case with the optimal but impossible-to-construct inlet condition (*BF* = 0.63) are shown as benchmarks in Figure 43. The results of the models run at $Q_{total} = Q$ show that an inlet manifold with 16 inlets can create flow conditions that yield a *BF* that is close to that of an idealized inlet.

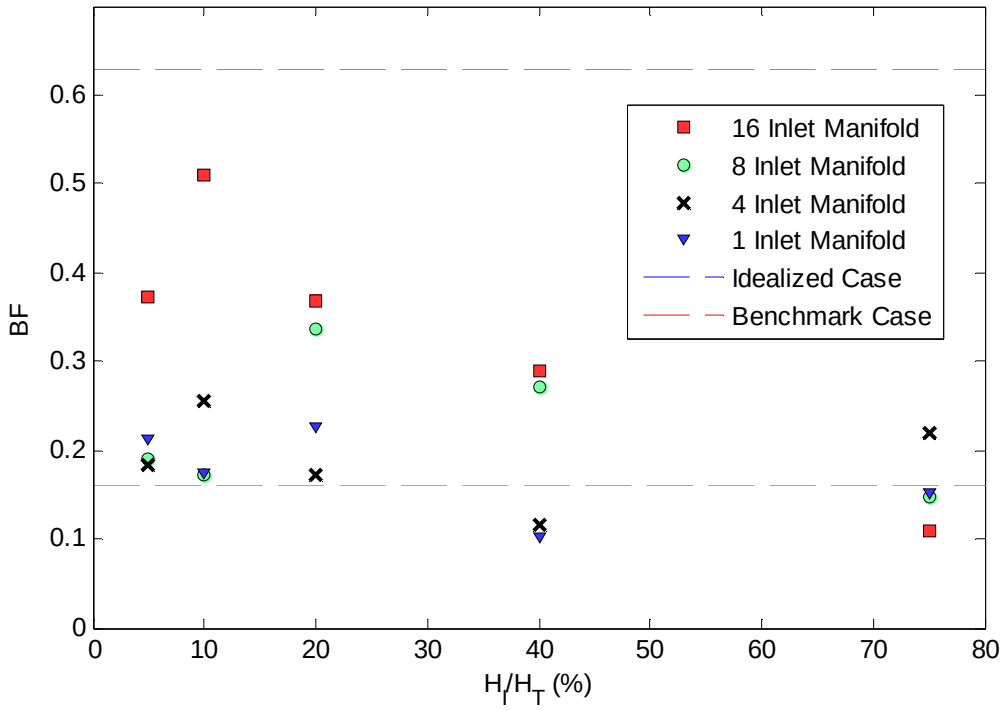

Figure 43. *BF* for *Q* (Q_{total} = 0.000946 m3/s)

When the inlet manifold has 16 inlets, and $H_I = 0.1H_T$, the *BF* is 0.51, which is 81% as efficient as the case with the idealized inlet where *BF* is 0.63. For each inlet configuration tested, there was an inlet height at which the *BF* was worse than the *BF* of the benchmark case, as illustrated in Figure 43 by the cases with *BF*s below the line showing the *BF* of the benchmark case.

4.4.1.1 H_I/H_T at $Q_{total} = Q$

As shown in Table 14, the *BF* for each manifold configuration is best when H_I is between $0.1H_T$ and $0.2H_T$. The 1-inlet and 8-inlet manifold configurations perform best at $H_I = 0.2H_T$, whereas the 4-inlet and 16-inlet manifold configurations perform best at $H_I = 0.1H_T$. The 8-inlet and 16-inlet manifold configurations perform worst at $H_I = 0.75H_T$. The 1-inlet and 4-inlet manifold configurations perform worst at $H_I = 0.4H_T$. The degree of uniformity of flow in the modified storage tanks with different numbers of inlets is highly dependent on H_I. The results of this study show that at $Q_{total} = Q$, the ideal inlet height is between $0.1H_T$ to $0.2H_T$ for all inlet configurations.

Table 14. Optimal *BF* and H_I

# Inlets	Best *BF*	H_I at Best *BF* (%H_T)
1	0.227	20
4	0.255	10
8	0.337	20
16	0.510	10

Similar changes in flow pattern were seen in the 1-inlet and 4-inlet tanks at different H_I. The flow patterns that develop in tanks with 1-inlet at different inlet heights are shown in Figure 44 (a)-(e). As seen for the 1-inlet tank in Figure 44, when the inlet is located below the ideal inlet height, dead zones are induced at the top of the tank. At H_I

= 0.4H_T there is short-circuiting in the middle of the tank, which decreases hydraulic efficiency and lowers *BF*. When H_I = 0.75H_T, there is enough momentum from the inlet to push most of the flow to the bottom of the tank before it circulates back to the top. This essentially makes the distance of the average flow path in the tank longer in the tank with H_I = 0.75H_T than in the tank with H_I = 0.4H_T.

Flow is far from uniform when H_I = 0.75H_T, but the flow separation actually serves to increase hydraulic efficiency because it causes the flow patterns in the tank to represent those that might be created by a baffle. The short circuiting in the middle of the tank at H_I = 0.4H_T is visible in Figure 44 (d). Figure 44 (e) shows the jet that creates a longer flow path when H_I = 0.75H_T. The general pattern shown by the results of the tanks with 8 and 16 inlets is that when the inlets are located below the ideal inlet height, dead zones are induced at the top of the tank. When the inlets are located above the ideal inlet height, there is short-circuiting at the top of the tank and dead zones form at the bottom of the tank. Unlike the tanks with 1 and 4 inlet(s), the tanks with 8 and 16 inlets do not have higher *BF*s at H_I = 0.75H_T than at H_I = 0.4H_T. Rather, the *BFs* of the tanks with 8 and 16 inlets decrease as H_I is raised above the ideal inlet height.

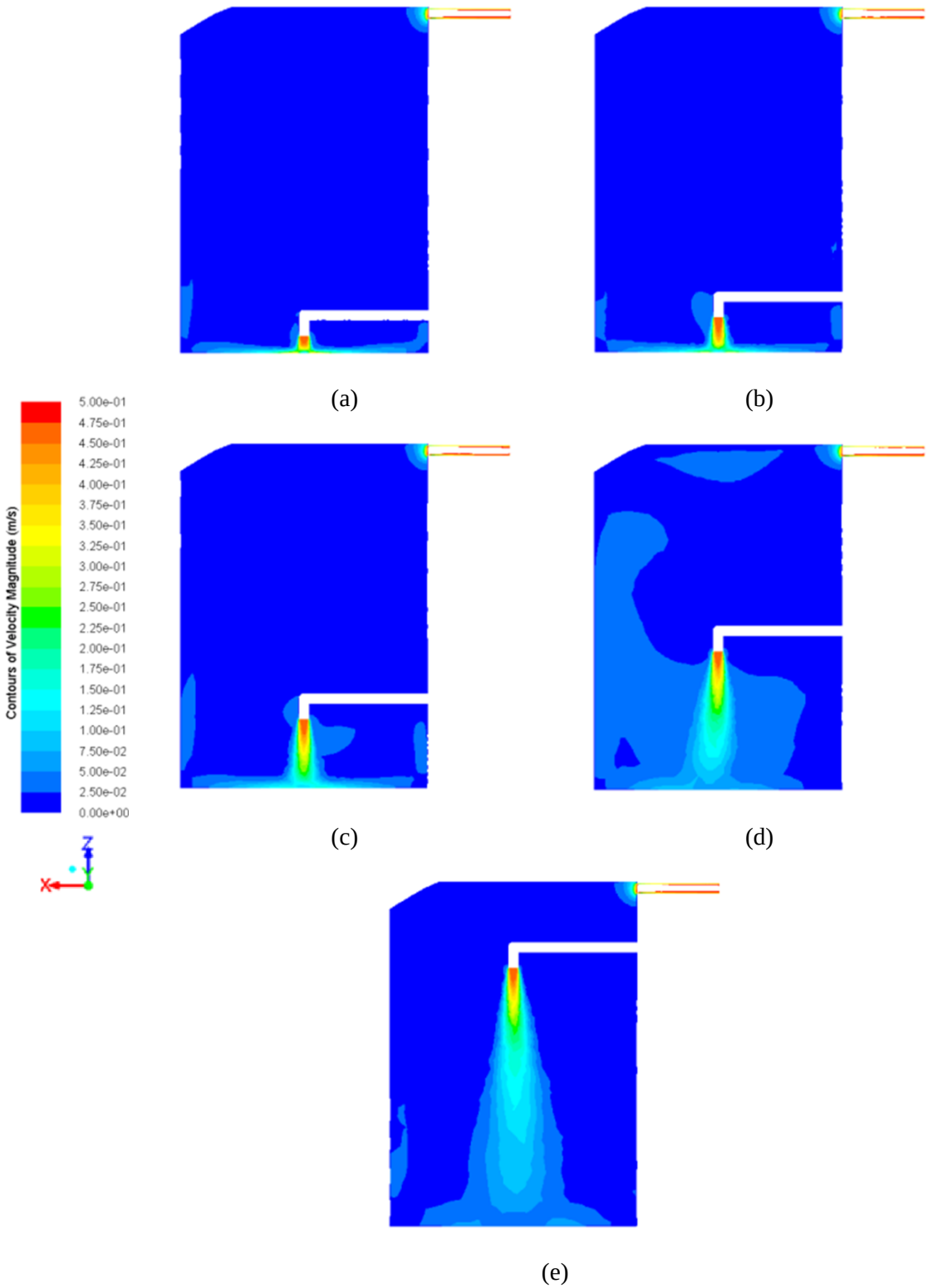

Figure 44. Velocity contours showing flow patterns in modified storage tanks at $Q_{total} = Q$ for 1-inlet configurations with (a) $H_I = 0.05H_T$, (b) $H_I = 0.1H_T$, (c) $H_I = 0.2H_T$, (d) $H_I = 0.4H_T$, and (e) $H_I = 0.75H_T$

The flow patterns that develop in tanks with 16 inlets at different H_I are shown in Figure 45 (a)-(e). In Figure 45 (a), there is a visible dead zone at the top left of the tank when $H_I = 0.05H_T$. In Figure 45 (b), which shows the case where $H_I = 0.1H_T$ and where *BF* is maximized, flow velocity is relatively uniform throughout the tank. In Figure 45 (c), which shows the case where $H_I = 0.2H_T$, the velocity is relatively uniform above the inlets, but dead zones form at the bottom of the tank. In Figure 45 (d) and (e), which show the cases where $H_I = 0.4H_T$ and $H_I = 0.75H_T$, respectively, short circuiting at the top of the tank and dead zones at the bottom of the tank cause large deviations from uniform flow. The high degree of short circuiting when $H_I = 0.75\ H_T$ illustrates why the tank with 16 inlets can have a lower *BF* than the benchmark case.

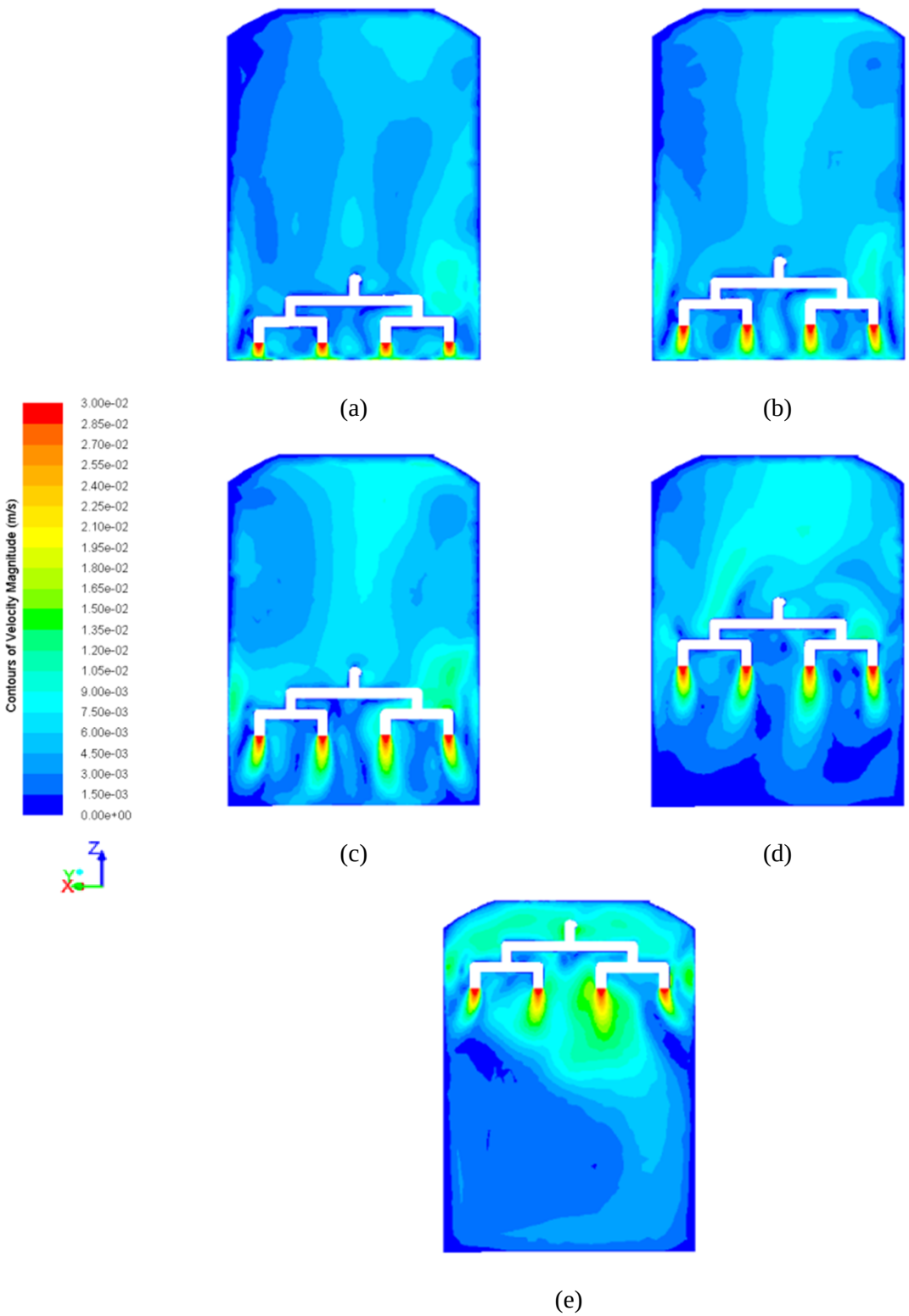

Figure 45. Velocity contours showing flow patterns in modified storage tanks at $Q_{total} = Q$ for 16-inlet configurations with (a) $H_I = 0.05H_T$, (b) $H_I = 0.1H_T$, (c) $H_I = 0.2H_T$, (d) $H_I = 0.4H_T$, and (e) $H_I = 0.75H_T$

Confirmation of the design technique used for the 8-inlet manifold and for the soundness of the use of inlet manifolds to create a more uniform flow condition in the modified storage tank is displayed in Figure 46. Figure 46 (c) shows a cross-section of velocity magnitude taken at $0.2H_T$, which is the height of the inlet. At the inlet locations, the velocity is downwards and is the magnitude of the inlet velocity. Around the inlets, the velocity is predominantly upwards and of much lower magnitude than at the inlets. The cross-sections taken at $0.1H_T$ and $0.05H_T$ show progressively more uniform velocity distributions and illustrate that the jets created by the downwards facing inlets spread in a fairly uniform fashion. At $0.5H_T$, the velocity distribution is very uniform compared with the velocity distribution at the other locations. Since the velocity distributions in the bottom and middle of the tank are more uniform than the distribution at the inlet, the inlet configuration has successfully spread the momentum of the water from the inlet across the horizontal plane of the tank.

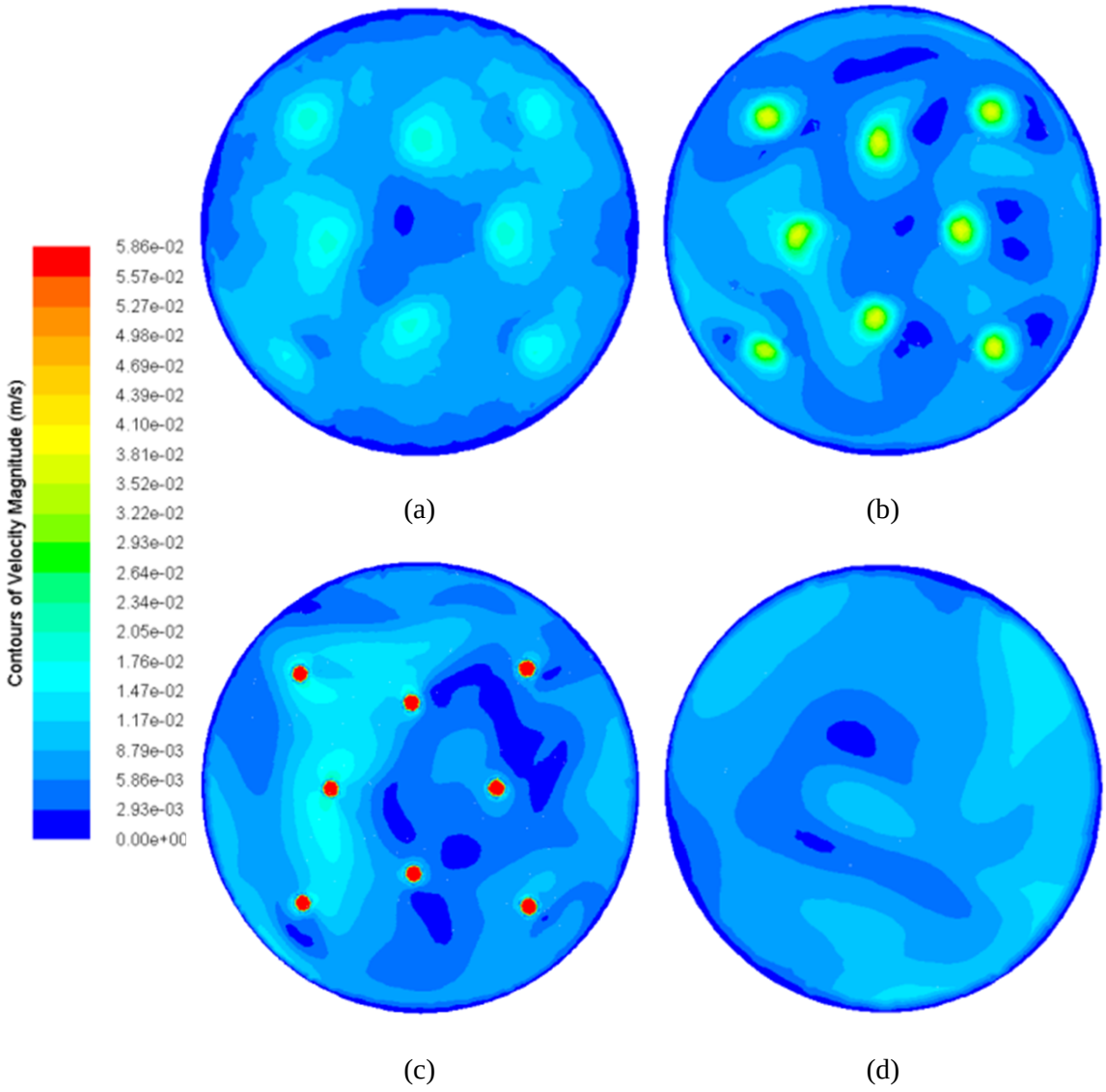

Figure 46. Velocity contours of the tank with 8-inlets and $H_I = 0.2H_T$ at horizontal cross-sections taken at heights of (a) $0.05H_T$, (b) $0.1H_T$, (c) $0.2H_T$, and (d) $0.5H_T$

4.4.1.2 Number of Inlets

In general, increasing the number of inlets to the tank created flow patterns in the tank that were closer to plug flow. As shown in Table 14, the *BF*s of the tanks with 1, 4, 8, and 16 inlets at their respective ideal inlet heights increased as the number of inlets increased. The relationship between the increase in the number of inlets and the increase in *BF* is nearly linear, as displayed in Figure 47.

The maximum limit of *BF* for a modified storage tank with height to diameter ratio and outlet conditions used in this study is 0.63, based on the tank tested with the idealized inlet condition. We hypothesize that increasing the number of inlets beyond the numbers tested would eventually lead to decreasing returns, and that the *BFs* of tanks with increasing numbers of inlets would approach the maximum possible value asymptotically rather than linearly. The equation of the fit line shown in Figure 47 indicates that *BF* would reach 0.63 if 23 inlets were used. We acknowledge that this is probably unreasonable and that the linear increase in *BF* in relation to the number of inlets probably only applies to a certain range of inlet numbers.

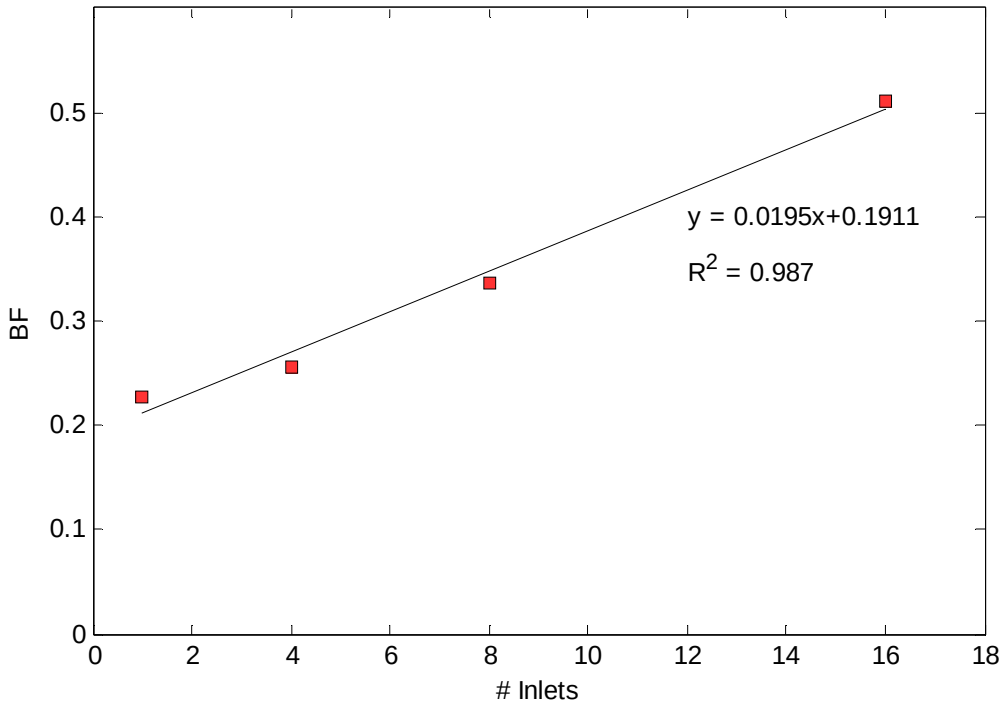

Figure 47. Relation of *BF* and number of inlets at Q_{total} = Q

4.4.2 Results at $Q_{total} = 2Q$

The contact tank tested at $Q_{total} = 2Q$ with a 16-inlet manifold configuration with the inlets located at $H_I/H_T = 0.1$ had a *BF* of 0.61, which was the highest *BF* measured in

the study when $Q_{total} = 2Q$ and was 280% more efficient than the benchmark case. The *BFs* for all cases at $Q_{total} = 2Q$ are shown in Table 15. Due to computational time constraints, the 8-inlet configuration was not tested at $Q_{total} = 2Q$.

Table 15. *BFs* for $Q_{total} = 2Q$

BF (Q = 0.001892 m3/s)			
H_I/H_T(%)	1 Inlet	4 Inlets	16 Inlets
5	0.15	0.16	0.42
10	0.21	0.15	0.61
20	0.15	0.14	0.34
40	0.12	0.15	0.41
75	0.19	0.23	0.14

The *BFs* for all cases at $Q_{total} = 2Q$ are plotted in Figure 48.

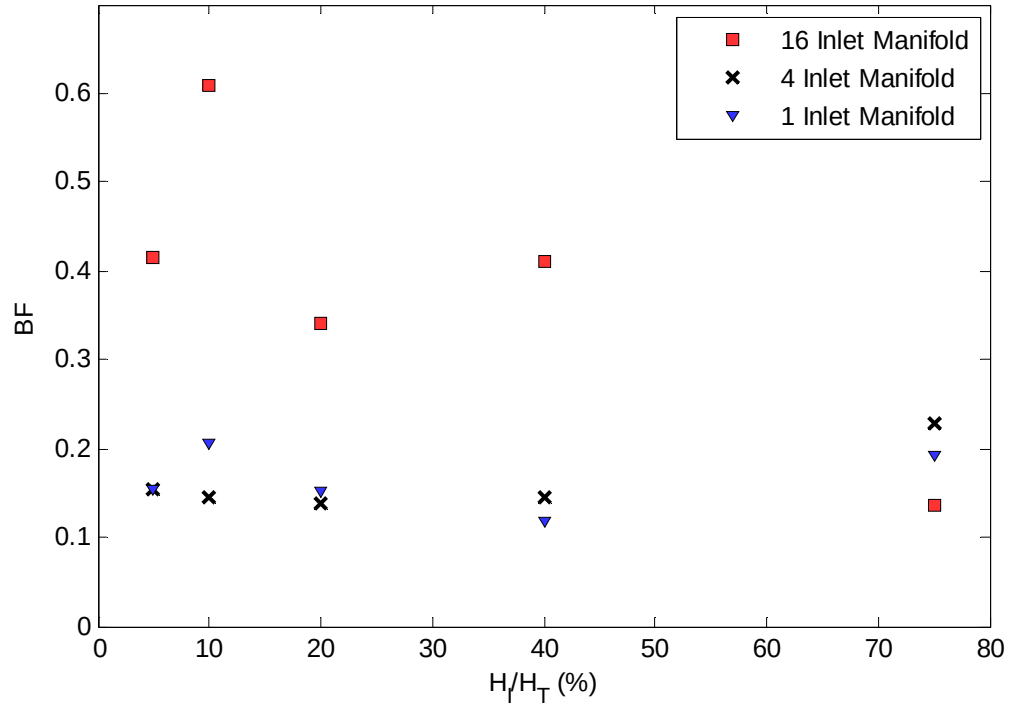

Figure 48. *BF* for *2Q* (Q_{total} = 0.001892 m3/s)

4.4.2.1 H_I/H_T at $Q_{total} = 2Q$

The *BF* for the 1-inlet and 16-inlet manifold configurations tested at $Q_{total} = 2Q$ was best when $H_I = 0.1H_T$, as shown in Table 16. The 4-inlet manifold configuration had the best *BF* when $H_I = 0.75H_T$. The fact that the highest *BF* tested for the 4-inlet configuration tested at any H_I for $Q_{total} = 2Q$ was near the top of the tank is interesting because it shows that the internal hydraulics of the tank are dependent on H_I and the number of inlets. However, the fact that the 4-inlet manifold yielded the highest *BF* at $H_I = 0.75H_T$ does not indicate that H_I should be set above $0.2H_T$ for certain cases. The difference in the best and worst *BFs* at different heights for the 4-inlet configuration is small (0.08) when compared to the difference in the best and worst *BFs* at different heights for the 16-inlet configuration (0.48). Like the *BFs* of the models tested at $Q_{total} = Q$, the *BF*s of the models tested at $Q_{total} = 2Q$ show that, in general, the optimum H_I for the tested tank is between $0.1H_T$ and $0.2H_T$.

Table 16. Optimal *BF* and H_I

# Inlets	Best *BF*	H_I at Best *BF* ($\%H_T$)
1	0.207	10
4	0.229	75
16	0.608	10

4.4.2.1 Number of Inlets

The increase in *BF* is linearly related to the increase in the number of inlets, as displayed in Figure 49. We recognize that 3 points is not a sufficient number to indicate a linear relationship; the line and r-square value are simply used to show that for the configurations tested, *BF* increased relatively linearly with an increase in the number of

inlets. This increase is similar to that seen is the models tested at $Q_{total} = Q$. This shows that increasing the number of inlets can increase the *BF* in a tank regardless of flow rate.

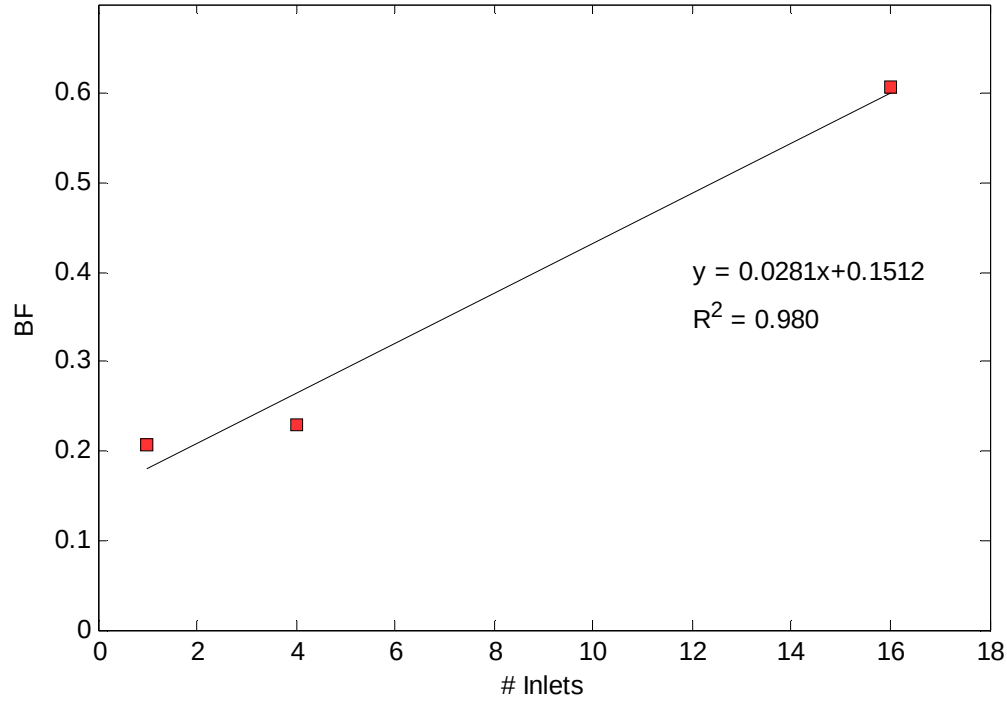

Figure 49. Relation of *BF* and number of inlets at $Q_{total} = 2Q$

4.5 The Effect of Flow Rate on *BF*

As predicted, the flow rate affected the *BF* in the modified storage tanks. The change in *BF* caused by doubling the flow rate (ΔBF) was significant, but for all of the geometries tested, $\Delta BF < 0.12$. Table 17 and Table 18 show ΔBF directly and as a percentage, respectively, for all the tested cases. The maximum decrease in *BF* when Q was increased to 2Q was -0.11 and was seen in the 4-inlet manifold at $H_I=0.1H_T$. The maximum increase in *BF* when Q was increased to 2Q was 0.12 and was seen in the 16-inlet manifold at $H_I=0.4H_T$.

Table 17. Change in *BF* when Q_{total} is increased from *Q* to *2Q*

ΔBF from *Q* to *2Q*			
$H_I/H_T(\%)$	1 Inlet	4 Inlets	16 Inlets
5	-0.06	-0.03	0.04
10	0.03	-0.11	0.10
20	-0.07	-0.03	-0.03
40	0.02	0.03	0.12
75	0.04	0.01	0.03

Table 18. Percent change in *BF* when Q_{total} is increased from *Q* to *2Q*

% change in *BF* from *Q* to *2Q*			
$H_I/H_T(\%)$	1 Inlet	4 Inlets	16 Inlets
5	-28%	-15%	12%
10	18%	-43%	19%
20	-33%	-19%	-7%
40	15%	25%	42%
75	26%	5%	24%

4.6 Conclusion

In this study, we have developed designs for inlet manifolds that drastically increase the hydraulic efficiency of modified storage tanks. The hydraulic efficiency, which was quantified by *BF*, was increased by utilizing multiple inlets across the horizontal plane of the tank. Inlet manifolds had 1, 4, 8, or 16 inlets and H_I was tested at $0.05H_T$, $0.1H_T$, $0.2H_T$, $0.4H_T$, and $0.75H_T$. The optimum H_I was found to be between $0.1H_T$ and $0.2H_T$, and the *BF* was found to be approximately linearly related to the number of inlets in the models tested.

The 16-inlet configuration tested at $H_I = 0.1H_T$ had a *BF* of 0.51, which is 81% as efficient as the ideal modified contact tank. This design increased *BF* in the modified tank by 220% in comparison to tanks utilizing standard inlets. Increasing the number of

inlets further beyond 16 would result in meshes too large for accurate CFD modeling. Increasing the number of inlets would also result in an inlet manifold that would be more difficult and costly to build. We propose that the 16-inlet manifold is the best practical inlet design configuration for the modified storage tank tested.

Water systems that use modified storage tanks as contact tanks should be aware of the changes in *BF* caused by changes in flow rate. *BF* was dependent on flow rate in the models run for this study, but the changes in *BF* at different flow rates were much smaller than the changes in *BF* that occurred by modifying the inlet configuration.

CHAPTER 5. CONCLUSION

5.1 Summary of Research

The literature review performed in this thesis illustrated that although there have been many publications about hydraulic efficiency in serpentine baffle tanks, there were none that universally modeled the independent and aggregate effects of variations in baffle number and baffle length in tanks with fixed footprints. The literature review also showed that small water systems currently use storage tanks as contact tanks, and that these storage tanks have very low hydraulic efficiency.

Chapter 3 of this thesis presented a parametric study of baffle configurations in serpentine baffled contact tanks. The parametric study included highly resolved 3-D CFD model studies of forty serpentine baffle tank configurations. Chapter 4 presented original designs for inlet manifolds that increase hydraulic efficiency in modified storage tanks to the level seen in typical serpentine baffled contact tanks. Thirty-six different inlet manifold configurations were tested using highly resolved 3-D CFD models. The results provide new insights into the effects on hydraulic efficiency of inlet number and vertical and horizontal inlet placement in storage tanks.

5.2 Major Conclusions

We find that in a serpentine baffled contact tank with a fixed inlet configuration and footprint, the hydraulic efficiency is maximized when the length to width ratio in each baffle compartment is maximized and when the inlet width, the channel width, and the baffle opening length have the same dimension. Flow separation will occur at the turns around the baffles in the tank, but the degree of flow separation is a function of both the angle and width of the turn. A “clubbed baffle” configuration was introduced to

modify the benchmark serpentine baffle tank. The “clubbed baffles” decreased the angle of the turns in the tank from 180 degrees to 90 degrees and increased the number of turns from seven to seventeen. The addition of the “clubbed baffles” increased the *BF* by 10%, illustrating that the cumulative flow separation caused by turns around baffles can be decreased when the angle of the turns is decreased, even when the number of turns is more than doubled.

The inlet manifolds designed to modify vertical storage tanks for use as contact tanks increased the hydraulic efficiency of the tanks by 220%. This was achieved by spreading the inlets from the manifold evenly across the horizontal plane of the tank and setting the height of the inlets such that when the flow left the inlets, there was minimal short-circuiting and dead zones at the top and bottom of the tank. The inlet pipe size for all manifold configurations was kept constant, so the total inlet area was proportional to the number of inlets. The relationship between the number of inlets and the *BF* was linear.

The height to width ratio of the tank modeled was low, which prohibits plug flow even with ideal inlet and outlet conditions. To provide a realistic upper limit of hydraulic efficiency for the benchmark tank, an idealized case was modeled with the bottom of the tank set as the inlet with uniform velocity. The *BF* observed in the tank modified with the 16–inlet manifold was 81% of the *BF* seen in the idealized case, which shows that practical inlet manifolds can be used to increase *BF* in storage tanks to values close to the *BF* seen in idealized tanks that represent the limit of plug flow.

5.3 Recommendations for Further Work

The contact tanks in this study were modeled as steady single-phase systems. In real operating conditions, outlet flow rates can be variable and free-surface elevations are not fixed in time. In order to capture the real-time disinfection efficiency in a tank with varied outlet flow rates and variable free-surface elevations, multi-phase models need to be utilized in conjunction with scalar transport models.

WORKS CITED

Amini, R., Taghipour, R. and Mirgolbabaei, H. (2011), *Numerical assessment of hydrodynamic characteristics in chlorine contact tanks*. International Journal for Numerical Methods in Fluids. doi: 10.1002/fld.2394

Anderson, John D, JR. *Computational Fluid Dynamics – The Basics With Applications*; McGraw Hill; New York, 1995.

ANSYS, Inc.. (2010). ANSYS FLUENT User's Guide. Canonsburg, PA.

ANSYS, Inc.. (2011). ANSYS FLUENT Theory Guide. Canonsburg, PA.

Crozes, G.F., Hagstrom, J.P., Clark, M.M., Ducoste, J., Burns, C. (1999). Improving clearwell design for CT compliance, *AWWARF & AWWA*, Denver, Colorado: 154.

COMSOL Inc. (2010). *COMSOL Multiphysics User's Guide*. Burlington, MA.

Davis, M.L., Cornwell, D.A. *Introduction to Environmental Engineering*; McGraw Hill; New York, 2008.

Hannoun, I.A., Boulos, P.F. List, E.J. (1998). Using hydraulic modeling to optimize contact time. *Journal of America Water Works Association (AWWA)*, August: 77-78.

Khan, L.A. , Wicklein, E.A. , Teixeira, E.C. (2006), *Validation of a three-dimensional computational fluid dynamics model of a contact tank, J. Hydraul. Eng.* **132** (7):741–746.

Launder, B. E., Spalding, D. B. *Lectures in Mathematical Models of Turbulence*. Academic Press, London, England. 1972.

Launder, B. E., Spalding, D. B. (1974). Numerical computation of turbulent flows. *Comput. Methods Appl. Mech. Eng.*, 3(2): 269–289.

Pope, Stephen B. *Turbulent Flows*; Cambridge University Press; Cambridge, 2000.

Roberson, J.A., Cassidy, J.J., Chaudhry, M.H. *Hydraulic Engineering*; Wiley, 1998.

Shiono, K.E., Teixiera, E.C. & Falconer, R.A. (1991). Turbulent measurements in chlorine contact tank. *First international conference on water pollution: Modeling, measuring and predicting, Southampton, UK*: 519–531.

Shiono, K. & Teixeira, E.C. (2000). Turbulent characteristics in a baffled contact tank. *Journal of Hydraulic Research (JHR)*, 38(6): 403-416.

US EPA. (1999). Disinfection profiling and benchmarking guidance manual. *EPA 815-R-99-013*, Office of Water, Washington, D.C.

US EPA. (2003). LT1ESWTR Disinfection Profiling and Benchmarking Guidance Manual., Office of Water, Washington, D.C.

US EPA. (2009). National Primary Drinking Water Regulations. EPA 816-F-09-004, Office of Water, Washington, DC.

US EPA. (1998). Revisions to Primacy Requirements. EPA 63 FR 23362, Office of Water, Washington, DC.

US EPA. (2004). Understanding the Safe Drinking Water Act. EPA 816-F-04-030, Office of Water, Washington, DC.

Venayagamoorthy, S.K., Stretch, D.D. (2010). On the turbulent Prandtl number in homogeneous stably stratified turbulence. *Journal of Fluid Mechanics*, 644: 359-369.

Wang, H., Falconer, R.A. (1998a), Numerical Modeling of Flow in Chlorine Disinfection Tanks. *Journal of Hydraulic Engineering*, September, 1998, 918-931.

Wang, H., Falconer, R.A. (1998b), Simulating Disinfection Processes in Chlorine Contact Tanks Using Various Turbulence Models and High-Order Accurate Difference Schemes. *Wat. Res.*, 32(5):1529-1543.

Wenjun, L., Zhipeng, D., Junwei, J. (2007), Optimizing the configuration of a clearwell by integrating pilot and full-scale tracer testing. *Front. Environ. Sci. Engin. China*, 1(3): 270-275.

Wilson, Jordan M., Venayagamoorthy, Subhas K. (2010) Evaluation of Hydraulic Efficiency of Disinfection Systems Based on Residence Time Distribution Curves. Environ. Sci. Technol. Vol 44, 9377-9382.

APPENDIX I. USER DEFINED FUNCTION FOR DIFFUSIVITY

The user defined diffusivity was solved using the code shown in Figure 50. The code was written in the C language.

```
#include "udf.h"
DEFINE_DIFFUSIVITY(diff_coeff,c,t,i)
{
return C_MU_T(c,t) / 0.7+0.001;
}
```

Figure 50. User defined function for diffusivity

The molecular diffusivity used in the user defined function is the molecular diffusivity of water.